A STUDY OF STEADY-STATE HEAT CONDUCTION AND DEFORMATIONS ON MODEL CONCRETE AND COMPOSITE BRIDGES

by

Yaroslav B. Symko

A thesis submitted to the School of Graduate Studies at the University of Ottawa, in partial fulfillment of the requirements for the degree of Master of Applied Science in Civil Engineering.

Ottawa, Canada

December, 1971

Table of Contents

SYNOPSIS

An experimental and analytical investigation has been carried out on the thermal behaviour of concrete and composite bridge models. Their cross sections were composed of a reinforced concrete slab monolithic with either a steel beam or a reinforced concrete beam. The upper and lower surfaces of the simple span bridge member models have been exposed to different steady temperatures and a two-dimensional temperature field has been produced in the plane of the beam cross section. The beams were free from external restraints and stresses were induced by temperature changes.

In the laboratory, various temperature conditions have been applied to the simply supported beams. The outer surface was heated by means of an electric heater or alternately was cooled by the use of melting ice. The temperatures within the beam were measured with copper-constantan thermocouples and the longitudinal deformations with linear transducers, Hewlett-Packard model type 7DCDT-100. The beams were immersed in water until tested with melting ice and were completely dried prior to being heated. In this manner, the analysis of the temperature field was limited to use the thermal conductivity of fully saturated concrete and completely dry concrete.

The finite element method has been used to determine the temperature field within the cross section and the elastic deformations and stresses it produced. In the analysis, the beam cross section was represented by an assemblage of rectangular and alternately of triangular elements. A linear temperature variation within each element was assumed. In the stress analysis, a linear strain variation within the elements was used due to the linear temperature distribution. A solution to the thermoelastic problem of the unrestrained beams was obtained using linear strain rectangular elements. The derivation of a linear strain triangular element with six nodes was also presented. The resulting system of the finite element equations has produced a symmetric, positive-definite matrix which was stored in band form in the computer. Cholesky's square root method was used for the solution of the system of equations.

The solution of the thermoelasticity problem of the unrestrained beams has been obtained by the plane strain formulation. The beams were initially considered to be fully restrained at its ends. The resultants of these end restraints and the stresses due to restraints and to the two-dimensional temperature variation as well were computed. The restraining stresses produced solely by these end restraints were computed and were superposed on the previous results. The final stresses were those of the simply supported beams subjected to a steady temperature variation. Under the condition that the tensile strength of the concrete has not been exceeded, the section of the beams was considered to be uncracked in the analysis.

The restraining stresses were obtained as the solution of nonthermal plane strain problems. These problems were formulated by assuming either a uniform longitudinal strain or a linear strain such that the resultants of the restraints, required at the ends to maintain a state of plane strain, were equal to those in the thermally restrained problem.

The effects of variations in the Poisson's ratio and in the coefficient of expansion of the concrete have been presented in the computed stresses and strains.

List of Figures in Appendix B

List of Tables in Appendix C

List of Computer Flow Charts in Appendix D

CHAPTER I

INTRODUCTION

1.1 Object

The object of the investigation was to determine experimentally and analytically the steady two-dimensional temperature distribution produced in a cross-sectional plane of the composite simple span bridges when their upper and lower surfaces were exposed to different temperatures. In addition, the temperature effects on the strength of the structure were studied on a short term basis. Two typical members of the bridges were modelled and their details are shown in Figures 1 and 1a. The composite steel-concrete beam consisted of a reinforced concrete slab acting compositely with a steel beam. The reinforced concrete T-beam was composed of the same reinforced concrete slab cast monolithically with a reinforced concrete beam.

The analytical study was separated into two parts. First, using the theory of heat transfer in solids, the temperature distribution was predicted. Second, with the knowledge of the existing temperature field, stresses and deformations were computed away from the ends of the beams. The stress analysis was restricted to the linear thermoelasticity theory and the material properties such as the thermal conductivity,

the coefficient of expansion, the modulus of elasticity, and Poisson's ratio were considered to be uniform. Both the temperature and the thermoelasticity problem were solved by means of the finite element method.

1.2 Nature of the Problem

It is known that changes in temperature cause bodies to expand or contract. If all the elements in a body are free to deform, no stresses are produced. The thermal stresses are produced when these natural deformations of the elements are prevented either by external forces or by the adjacent elements having different deformations.

Since the natural thermal deformations depend on the temperature and on the coefficient of expansion, the elements will tend to deform in different amounts as a result of a nonuniform temperature distribution or of a uniform temperature change in a composite structure made of materials having different coefficient of expansion. Such deformations in a body free of external constraints cannot proceed according to the local temperature rise and they must interfere with each other in order to enable the body to remain continuous.

In stress analysis, the continuity of the deformable body under the conditions of the linear, small-displacement theory is assured by the compatibility equations. For bodies which are long in comparison with cross-sectional dimension and for sections relatively far from the ends, the assumption that plane sections remain plane is made in place of the compatibility equations.

Stresses in an unrestrained composite beam will not be zero unless the temperature variation is such as to produce a uniform or linear displacement distribution throughout the cross-sectional plane without any interference with the displacements of adjacent elements. For such a temperature field the plane cross sections remain plane and no internal forces are produced by adjacent elements to maintain that plane section during the expansion or contraction of the beam. If a temperature field tends to cause throughout the plane a nonlinear distribution of displacements, then the elements will interact and exert on each other internal forces in order to prevent the plane cross section from warping out of plane. These internal forces give rise to thermal stresses. The T-beam or the composite steel-concrete beams of exposed bridge sections are subjected to various temperature distributions and it is with thermal stresses produced by different temperature variations that this investigation is concerned.

The thermal stresses in the unrestrained beams in this investigation result from the nonuniform two-dimensional temperature distributions and due to the different coefficient of expansion of concrete and steel. Since the section of the T-beam and the composite steel-concrete beam is geometrically symmetric, the temperature field, which is a function of the spatial coordinates, will have across the width symmmetric variations about the center line of these sections.

These temperature variations tend to split the sections into halves by the bending action that the nonuniform temperature variations produce about the vertical axis passing through the centroid of the half sections. These half sections mutually prevent each other from bending and thus give rise to thermal bending stresses about these vertical axes. Such stresses can be produced by steady temperature variations as well as under transient conditions.

This investigation is restricted to steady temperature variations. It is felt that an understanding of the behaviour of the beams in steady temperature condition is necessary before dealing with the transient temperatures. The thermal stresses, determined by the transient temperature distributions as a result of gradual changes in environment temperatures, are little different from those computed from the same temperature distribution in steady state. Before steady temperature condition prevails, the beams will experience greater thermal stresses due to higher temperature gradients occurring through the cross-sectional area of the beams. These transient temperatures are distributed nonlinearly and it is the nonlinearity in the temperatures that causes stresses in a homogeneous body free of external restraints.

In steady condition, the temperature variation over the cross sections can be considered in two parts, one within the slab and the other in the beam. The temperature, in the slab, varies almost linearly through the thickness. The heat transfer in the beam is analogous to that in a fin which is attached to a surface of a structure for the

express purpose of increasing the surface heat transfer. Its temperature profile through the depth is nonlinear. The beam and slab, each tends to have different curvatures due to its temperature variation, interact in order to satisfy the requirement of plane cross section and thus thermal stresses are introduced.

The behaviour of the sections becomes more complicated especially when the sections are composed of dissimilar materials such as steel and concrete. The temperature gradients, in the steel which has a higher thermal conductivity, are not as large as those occurring in concrete. With these abrupt changes in temperature gradients throughout the section made of concrete and steel, each having different coefficient of expansion, the possibility of the unrestrained beams to undergo temperature changes without producing stresses is very unlikely to occur.

Various temperature differentials are produced between the upper and lower surfaces of the exposed bridges to seasonal temperatures. These temperature differentials could be caused by solar radiation, wind convection, rainfall, snow, or by a sudden warm or cold wave that changes the ambient air temperature. The temperatures in the structure undoubtedly do not reach steady state due to the low thermal conductivity of concrete and to the continuous variation of the surrounding air temperature with time.

The magnitude of the temperature differential depends largely on the rate of heat transfer by conduction in steel and concrete. The entire steel beam, having a higher thermal conductivity than the concrete, reacts more rapidly to the surrounding air temperature while the concrete slab undergoes a more gradual adjustment towards the air temperature. The largest temperature differential occurs in the bridge at early stages of a sudden change of the surface temperature.

The thermal stresses become more severe as the temperature differentials are increased. These stresses may either increase the stresses that already exist in the bridge due to dead load, live load, creep, and shrinkage or they may partially relieve the structure from its stresses. The concrete has a very low tensile strength which is in the order of a few hundred pounds per square inch. To cause failure in the tensile zone of concrete, the magnitude of the thermal stresses need not be very large.

Thermal stresses may be significant enough to affect the strength of the exposed bridges to daily temperature fluctuation by fatigue rather than by overstressing the structure. Temperature fluctuation is typical in North American climate. In summer the sun can heat the upper surface of the bridge to as much as 140° F and in winter temperature drops to a low of -40° F.

Thermal fatigue rarely causes failure by complete separation of material in one particular region. Cracks are usually scattered throughout the sections. Under repeated thermal loading, failure of the material is first initiated in one or many locations wherever large stresses occur. These cracks do not propagate throughout the sections under repeated thermal load as is the case under mechanical loading.

The thermal stresses in these yielded regions are lowered and large stresses, which may cause failure, are developed in other regions. Whenever the thermal loadings are repeated, new cracks are formed elsewhere and thus, the strength of the bridge is reduced so that it can no longer sustain the load it carried.

1.3 Review of Previous Research

The thermal analysis of composite bridges involves solutions of problems related to heat transfer, stress analysis and material properties.

The formulation for closed-form solutions of thermoelastic problems, dealing with plates and beams having uniform cross section made of homogeneous and isotropic material, can be found in the standard works of Timoshenko and Goodier (1), Gatewood (2), and Boley and Weiner (3). The fundamental principles of theory of thermal stresses have been used in the analysis of bridge members subjected to steady two-dimensional temperatures such that a solution can be obtained by finite element method.

Zuk (4 and 5) has obtained a closed-form solution of one-dimensional thermal stress problem for simply supported composite bridge beams. These beams were composed of homogeneous and isotropic concrete slab and steel beam. The concrete slab was restrained transversely against deformation due to the effect of adjacent beams that formed the bridge cross section and the longitudinal stresses were computed due to a simplified nonuniform temperature distribution that varied only through the depth of the section. Berwanger (6) has extended Zuk's approach for simple beams to continuous-span bridges and has presented a solution to such problems that are involved in

satisfying the compatibility conditions at interior supports. In addition, Berwanger has considered symmetrical as well as unsymmetrical steel reinforcement in the concrete slabs that experience nonuniform temperature distributions.

The problem for determining the two-dimensional temperature field and the corresponding stresses within the simply supported beams of complex cross section as shown in Figures 1 and 1a is entirely intractable by classical methods. A numerical approach such as the finite element method can easily handle the complex geometry of the cross sections composed of dissimilar materials.

At the present time, there are a large number of research papers available on the development of finite elements and its applications to structural analysis. Only references relevant to this work have been cited. The finite element method was proposed by Turner, Clough, Martin, and Topp (7) and it was applied to plane stress problem. Gallagher, Padlog, and Bijlaard (8) have extended finite element analysis to solve problems such as heated homogeneous plates having across the width a parabolic variation of temperature and thickness or having a centrally located hole. The plate of nonuniform thickness was idealized by an assemblage of rectangular elements, each of constant thickness and linear thermal strain distribution. Weber (9) has demonstrated the use of the finite element method in thermoelastic plate problems. As an illustrative example, Weber has given a solution to the nonuniform thickness plate problem in reference (8) by using a linear strain rectangular element of linear thickness. In the present study, the derivation of the rectangular and triangular element for the

temperature and stress problem has followed the procedure outlined by Cowper, Kosko, Lindberg, and Olson (10).

The finite element method is applicable to problems that can be formulated in variational form. Zienkiewicz and Cheung(11) have applied finite elements to solve general steady heat conduction problems dealing with several types of boundary conditions including convection, specified surface temperatures, and specified heat flux. In their textbook, the formulation of triangular and quadrilateral elements both having linear temperature variation is given. The applications of finite elements have been extended to transient heat conduction problems and Wilson and Nickell (12) have presented a finite element formulation of transient heat conduction problem.

The accuracy of the results obtained in the analysis of temperatures and stresses in the beams can be seriously disrupted by incomplete knowledge of the properties of steel and concrete. The steel thermal properties of interest in this investigation are well known. It is difficult to predict the required thermal properties of concrete since the concrete is a nonhomogeneous and anisotropic material. The major factors influencing these properties are the mix proportions, the type of cement, the type of aggregates, volume of air voids present, the moisture content of the concrete, the temperature, and the concrete age. The coefficient of expansion and the dynamic modulus for the concrete of the same mix proportion that was used in this investigation, were measured experimentally by Sarkar (13). These properties were measured at different temperatures, at different

contents of water absorbed in concrete, and at different ages such that the results can be used in this analytical computation of thermal stresses for the concrete that was fully saturated and alternately completely dry when tested at various temperature distributions. The investigation carried out by Sarkar is an extension of the study reported by Berwanger (14).

The studies conducted on the thermal conductivity of concrete by Lenzt and Monfore (15), by Campbell-Allen and Thorne (16), and by Thompson (17) have shown that the content of water present in concrete is a significant factor. Lentz and Monfore have shown that the variation of the thermal conductivity of concrete is very small within the temperature range of $0^{o}F$ to $75^{o}F$. In this investigation, the conductivity of concrete at tempratures within the range of $32^{o}F$ to $126^{o}F$ can be considered to be uniform without introducing significant error. Brewer (18) has correlated the conductivity with the unit weight for concretes varying from oven-dry to fully saturated. In this respect, an approximate value of the conductivity of the concrete can be selected according to its unit weight and to its water content.

1.4 Scope of Present Investigation

This investigation is concerned with the analysis of stresses and strains resulting from steady two-dimensional temperature distributions produced throughout the cross-sectional area of the beams shown in Figures 1 and 1a. The two bridge beam models were simply supported at the ends. These beams were exposed on the upper and lower surfaces to ambient air at different uniform temperatures or their outer surfaces were maintained at a uniform temperature.

Experimentally, the sections were subjected to four different types of temperature distributions. The upper or lower surface of the beams was alternately cooled with melting ice while the other surface was exposed to the laboratory room temperature. During the cooling tests, the concrete was considered to be fully saturated as the beams were completely immersed in water prior to testing. The concrete was then dried and the experimental investigation was extended to heated structures. The air, above the reinforced concrete slabs, was electrically heated to various temperatures. Similarly heating tests were also carried out on the beams having its lower surfaces exposed to various ambient air temperatures. In addition, as the ambient air temperature underneath the sections was increased, the tests were extended to a forced convective system as the upper surface of the composite steel-concrete beam was cooled by a cross flow of air produced by electric fans. The temperatures within the beam were measured with copper-constantan thermocouples and the longitudinal deformations with linear transducers, Hewlett-Packard model type 7DCDT-100.

To compute analytically the stresses and strains, the temperature field over the cross section must first be known. The two-dimensional temperature distributions, to which the beams were subjected in the experimental investigation, were obtained by means of the finite element method. The resulting temperatures were determined from two different element models. Rectangular and triangular elements, both having a linear temperature variation were employed. Based on the linear temperature variation, the rectangular and triangular elements having a linear strain distribution were considered in the stress analysis.

The thermal stresses and strains were obtained using a uniform rectangular element idealization in which the reinforcing wires were considered. The beams in the finite element idealization behaved as a linear elastic structure. The expressions, for the stresses and strains in the unrestrained beams subjected to temperature changes, were developed only for uncracked section since the tensile strength of concrete has not been exceeded.

The thermoelasticity problem was solved in three stages. The beams were initially considered to be fully restrained at their ends by the plane strain formulation. The solution of the problem yielded the stresses, produced by the two-dimensional temperature distributions and by the artificial end restraints, and in addition, the resultant force and moment of these restraints which were required to maintain the state of plane strain. This problem will be consistently referred to in this investigation as the thermally restrained problem. The stresses and strains solely due to these end restraints were computed and then these results were superposed on the previous solution in order to obtain the solution of the unrestrained beams. The restraining stresses due to the resultant force and due to the resultant moment were considered separately and were obtained as the solution of a nonthermal elasticity problems. The solutions of these nonthermal problems were formulated by the two-dimensional theory of plane strain. In the formulations, a uniform and alternately a linear longitudinal strain distribution was inserted into the stress-strain equation that only relates the longitudinal strain to the normal stresses. The resulting stresses, strains, and the resultant force and moment acting

on the ends were determined by the finite element method in terms of the assumed strains. These strains were computed by equating the resultant restraints of the nonthermal problem to those in the restrained thermal problem.

In the finite element method, the resulting system of linear equations produces a sparsely populated coefficient matrix, which is symmetric and positive-definite. This matrix, which is stored in band form in the computer program, will be consistently referred to in the temperature problem and in the stress problem as the stiffness matrix of the structure. These equations are solved by means of Cholesky's square root method.

1.5 Acknowledgements

The present study was carried out under the direction of Professor Carl Berwanger. The author wishes to thank him for his guidance during this investigation.

The project was financially supported by research grant of the Ontario Department of University Affairs and through grants held by Professor Berwanger.

In addition, the author is indebted to Dr. G.R. Cowper, Dr. G.M. Lindberg, and Dr. M.D. Olson of the National Research Council of Canada for valuable discussions and suggestions concerning the finite element analysis of the elasticity problems.

The Computing Centre of the University of Ottawa is to be thanked for providing their facilities.

1.6 Notations

A list of symbols used and their general meaning is summarized below. The notation distinguishes matrices which are denoted by straight brackets from vectors or columns which are indicated by braces

Latin Letters

a, b, c	Element dimensions
a_i, b_i	Coefficients of assumed polynomials
{A}	Column of coefficients a_i
{C}	Column of polynomial distribution
d	Depth of steel beam
d_c	Thickness of reinforced concrete slab
D	Rigidity for plane strain problem
E	Modulus of elasticity of material
F(m,n)	Modified Euler's beta function
{F}	Load vector or known column matrix
$\{F_A\}$	Element load vector that results from ε_A
$\{F_B\}$	Element load vector that results from $Y\varepsilon_B$
$\{F_e\}$	Subscript e indicates load vector or known column of element
$\{F_t\}$	Subscript t denotes element load vector due to temperature
g	Thermal conductivity of material
h	Unit surface conductance or convection heat transfer coefficient
h_v	Unit surface conductance for vertical surface

I	Functional
I'	Electric current passing in heating element
J	Number of generalized coordinates of finite element
$[k]$	Stiffness matrix of finite element relative to vector $\{A\}$
$[K]$	Stiffness matrix of structure
$[K_c]$	Convective stiffness matrix of finite element
$[K_e]$	Stiffness matrix of finite element with respect to global coordinate system
$[K_L]$	Stiffness matrix of finite element with respect to local coordinate system
$[L]$	Upper band factor matrix of symmetric structure stiffness matrix K
ℓ	Typical distance between nodes
m_i, n_i, p_i, q_i, r_i, s_i	Exponents of ζ, η or x,y in i^{th} term of polynomial expression
M	Resultant moment of end restraints in restrained thermal problem
M_B	Resultant moment of end restraints in nonthermal problem
N	Number of equation in resulting system of linear equation in finite element method
NUBW	Half band width of matrix [K]
O	Truncation error
P	Resultant force of end restraints in restrained thermal problem
P_A	Resultant force of end restraints in nonthermal problem
q	Heat transfer
Q	Heat supplied or heat lost for half beam per foot length
$[R]$	Rotation matrix
s	Boundary surface

$[S]$	Stress matrix
t	Temperature
t_g	Ambient temperature
t_s	Surface temperature
$[T]$	Temperature transformation matrix
$[T_1]$	Displacement transformation matrix
$[T_d]$	Strain transformation matrix
u,v	Global displacements in x,y directions. Subscript indicates first derivative
$\bar{u},\bar{v}$	Local displacements in ζ, η directions. Subscript indicates first derivative
U	Strain Energy
U_A	Represents part of strain energy that results from ε_A
U_B	Represents part of strain energy that results from $Y\varepsilon_B$
U_t	Strain energy dealing only with thermal effect
V	Potential energy of external load
V'	Voltage supplied to electric heater
x,y,z	Global coordinates
$\{X\}$	Unknown column vector or scalar
y_b	Distance from centroid uncracked section to base of finite element
y_c	Distance from base of finite element to centroid of stress volume
Y	Distance from centroid of uncracked section to any point within section
w	Thickness of web in structural steel section

Greek Letters

α	Coefficient of thermal expansion of material
ε_A	Uniform strain in z-direction produced by resultant force of end restraints
ε_B	Linear strain in z-direction produced by resultant moment of end restraints
ε_x, ε_y, ε_z,	Strains in x,y, and z directions
ε_ζ, ε_η	Strains in ζ and η directions
γ_{xy}, $\gamma_{\zeta,\eta}$	Shear strain
ζ ,η	Local coordinates
θ	Angle between global and local coordinate axes
ν	Poisson's ratio
σ_x,σ_y,σ_z	Normal components of stress parallel to x,y, and z axes
σ_z', σ_z''	Normal components of stress parallel to z axis in nonthermal problems
σ_ζ ,σ_η	Normal components of stress parallel to ζ and η axes
τ_{xy}	Shear stress
Π	Total potential energy

CHAPTER 2

Experimental Investigation

2.1 Outline of Tests

The experimental program consisted of measuring the deformations and the temperatures of a heated and cooled simply supported composite steel-concrete beam and reinforced concrete T-beam. The main features of the two sections are shown in Figures 1 and 1a.

The cooling tests were carried out by placing melting ice on either the top or bottom surface of the beam. The other surface was exposed to an ambient temperature at room temperature.

Tests on heated structures were conducted by means of an electric heater. The heater, placed either above or underneath the sections, was used to raise the ambient air temperature in varying increments. While the lower surface of the composite steel-concrete beam was heated, the experimental program was extended to a forced convective system. The upper surface of the reinforced concrete slab was chilled by a cross flow of air produced by electric fans.

2.2 Specimens

The cross section of the composite steel-concrete beam used in this investigation was modeled on the bridge that spans the Assiniboine River at Brandon, Manitoba. The scale factor for the model beam cross section shown in Figure 1 was 0.35395. Of the steel sections listed in

the manual of American Institute of Steel Construction (19), the 10 X 4 B15 section of ASTM A36 grade steel was selected as the section whose dimensions are the closest to the scaled dimensions of the prototype steel beam 30 WF 108. To have the flange width equal to the scaled prototype width, the steel flange was machined to the required width of 3.68 inches.

To investigate the thermal behaviour between the composite steel-concrete beam and reinforced concrete T-beam, the choice of the cross-sectional dimensions of the reinforced concrete T-beam shown in Figure 1a, was based on the composite beam model dimensions. The concrete T-beam was constructed of the same reinforced concrete slab and of a reinforced concrete beam. The reinforced concrete beam was designed so that the concrete T-beam would have the same elastic moment capacity as the composite beam model.

The beam models of 62 inches simple span were reinforced with 75 ksi U.S.S. deformed steel wire conforming to ASTM A 496 specifications (20). The concrete had a water-cement ratio of 0.672. The mix proportions of a cubic yard of concrete consisted of 477 lbs. of normal Type 1 Portland cement, 317 lbs of water, 1610 lbs. of fine quartz aggregates and 1610 lbs. of coarse limestone aggregates. A 3/4 inch maximum size aggregate was used and the aggregates were graded according to the Standard Specifications for Concrete Aggregates (CSA A 23.1). In the tests made in accordance with ASTM C 39 specifications (21), the concrete at 28 days for the composite steel-concrete beam and for the reinforced concrete T-beam had a compressive cylinder strength of 4100 and 4300 psi respectively.

2.3 Apparatus

Temperature Measuring Devices

Temperatures were measured by means of butt-welded copper-constantan thermocouples. The thermocouple lead wires were both # 20 gauge. The thermocouple potentials, based on an ice-bath reference junction, were measured with a manual Honeywell potentiometer readable to 0.001 millivolt.

Displacement Measuring Devices

A schematic diagram of the equipment, used for measuring deformations at the surfaces of the sections, is given in Figure 2. A general view of the apparatus is shown in Figure 3.

A D.C. power supply unit, Hewlett Packard model 6204 B was used to supply constant voltage to the transducers. The voltage required was 6 volts. The output of the transducers was monitored on the Frequency Counter model 5221 A as the output voltage from the transducers by a Voltage Frequency Converter of Hewlett Packard model 2212 A. All twelve transducers were connected to the readout device by two Switching Units, BLH model 220.

The deformations were measured with displacement transducers of the Hewlett Packard Sanborn 7 DCDT-100. The DCDT senses surface deformation by means of a movable magnetic core. Whenever the specimen contracts or expands, this core is displaced along the axis of the bore in the coil assembly as shown in a simplified functional diagram of the transducer in Figure 3. The setup of the DCDT's each having a 10 inch gauge length is shown on the upper surface of the concrete slab in Figures 4, 8, and 9. The transducers were mounted on aluminium blocks

which were glued to the surfaces of the beams. The transducer core was fixed at the end of an aluminium rod and was positioned inside the transducer by connecting the other end of the 10 inch aluminium rod to another aluminium block. The longitudinal contractions or expansions of the beams within the 10 inch gauge length will cause the core to displace from its initial position.

The effect of the heat on the aluminium bars of a high coefficient of expansion has an appreciable influence on the surface displacement measurements. The aluminium rods were subjected to various changes in temperature and the expansion or contraction of the bars were taken into consideration in the calculations of the required surface deformations.

The contraction of the aluminium bars due to the temperature change from room temperature to melting ice temperature was measured experimentally. A cardboard was placed between the ice cubes and the concrete surface in order to prevent change in temperature of the concrete surface during the very short period that was required for the aluminium rods to reach the melting ice temperature. From the thermocouple readings taken along the concrete surface, it was found that the temperature of the concrete surface remained unchanged during that period. In this way, only the aluminium bars were permitted to react to the sudden change in temperature. The frequency readings of the transducers were recorded as the contraction of the bars. From these readings, the coefficient of expansion was calculated for each bar exposed to the ice cubes. The cardboard was then removed and, after the temperature field within the beams has reached steady-state, the following set of readings was registered as the surface thermal deformations of the beams.

In tests in which the aluminium rods were exposed to ambient air, the temperature change of each rod resulting from its proximity to the warm or cool surface was measured by means of a copper-constantan thermocouple glued to the surface. Using the measured coefficient of expansion pertaining to each aluminium rod, the expansions or contractions of the rods were computed and, thus the surface thermal deformations of the beams were obtained.

Heating Elements

The heating elements were arranged to electrically heat the air above or below the beams. The elements consisted of a nichrome strip with a resistance of 0.416 ohms per lineal foot. An A.C. voltage of 110 volts was supplied to the heater. The current was controlled by three Jagabi resistors of 9 ohms and 12 amperes, shown in Figure 3. The rate of electrical heat supplied per foot length of half of the beam is given by

$$Q = (I'V' \; 3.413) \frac{1}{2} \left(\frac{12}{62}\right) \qquad \text{BTU/hr-ft.} \qquad 2.1$$

where I' denotes the measured current in amps through the heating element and V' is the potential drop across the heating elements in volts.

These nichrome strips were mounted on a dexion angle frame which was placed either above, as shown in Figure 4, or below the beam. The frame was then enclosed by 2 inch thick styrofoam slabs to form a chamber.

2.4 Preparation of the Test Specimen

The beams of 62 inches in length were simply supported at the ends so that the beams were free to rotate about the supports and to deform in the longitudinal direction when temperature changes occurred. The temperature variations and the resulting deformations were measured at mid-span in the beams by an arrangements of thermocouples and transducers shown in Figures 5 and 5a.

The edges of the slab were insulated with 2 inch thick styrofoam against heat exchange since in the bridge the horizontal temperature gradients throughout the section between adjacent slabs is zero. The effectiveness of the insulation was checked by means of a thermocouple placed between the concrete surface and the styrofoam as shown in Figure 5.

The end surfaces of the beams were also insulated with styrofoam against heat exchange with the surrounding air so that a uniform temperature over its full length is maintained. A series of thermocouples was placed at $10\frac{1}{2}$ and $23\frac{1}{2}$ inches from the ends to verify the uniformity of the spanwise temperatures.

2.5 Test Procedure

Thermocouples and transducers readings were recorded after 2 days of the onset of temperature conditions. The four distinct temperature conditions imposed on the beams are given as follows:

1) The upper surface of the concrete slab was cooled to a uniform temperature of melting ice. The bottom of the slab was exposed

to an ambient air temperature in the laboratory, as shown in Figure 6.

2) The temperature conditions were reversed, as the melting ice was placed underneath the slab and the upper surface of the slab was subjected to the ambient air temperature.

3) The temperature of the air above the slab was controlled by an electric heater while the bottom surfaces of the beam were exposed to laboratory air temperature. A view of the interior of the styrofoam chamber with the heater placed on top of the slab is shown in Figure 4. The complete chamber is shown in Figure 7. The quantity of heat supplied was increased in three or four increments. The increase of air temperature in the chamber was limited since the particular model of the transducer used in this experiment, was design to a temperature range of $-65^{o}F$ to $140^{o}F$.

4) The general procedure outlined in step 3 was followed, except that the temperature conditions were reversed. The heater was placed under the beam whose top surface was exposed to ambient air temperature in the laboratory. This temperature condition was extended to a forced convection system for only the composite steel-concrete beam. As the air below the beam was heated to various temperatures, the top surface was chilled by a cross flow of air produced by three electric fans. A general view of this system is shown in Figure 9.

The variation of the thermal conductivity of concrete, due to the water content absorbed in the concrete, was controlled in order to facilitate the analytical formulation. The concrete, in the T-beam, was maintained fully saturated from casting till the tests with

melting ice were completed. The composite beam was submerged in water for a period of one month prior to testing. In the tests in which the beams were heated, the concrete was considered to be complete dry. Prior to the test, initial transducers readings were taken at uniform temperature within the dried beams in order to avoid the shrinkage effect of concrete.

The T-beam and the composite beam were tested after a period of 6 and 9 months respectively.

CHAPTER 3

Analysis of Heat Conduction Problems by Finite Elements

3.1 General

The composite steel-concrete beam and the reinforced concrete T-beam are subjected to a steady two-dimensional temperature field which is a function of the x and y coordinates in the cross-sectional plane as given in Figures 10 and 10a. With the z-axis in the longitudinal direction of the beams, the temperature over the cross sections away from its ends is uniform. A slight variation in the longitudinal temperature near the ends still exists even for insulated ends. The end effects are neglected and this study considers the temperature to be uniform over the full length. The temperature field t(x,y) within the beams made of materials of uniform thermal conductivity g, must satisfy the heat conduction equation

$$\frac{\partial}{\partial x}\left(g\,\frac{\partial t}{\partial x}\right) + \frac{\partial}{\partial y}\left(g\,\frac{\partial t}{\partial y}\right) = 0 \qquad 3.1$$

subject to the following boundary conditions

a) For a specified surface temperature

$$t = t_s$$

where the temperatures t are prescribed on a boundary to a temperature t_s.

b) For convection to surrounding air

$$q = h(t - t_g)$$

where q is the rate of convective heat transfer from a unit area surface to across an air boundary layer. The air outside the boundary layer has a temperature t_g which is lower than the temperature t at the surface. The uniform surface conductance is denoted by h.

c) For an adiabatic surface or for a representation of a line of symmetry

$$\frac{\partial t}{\partial n} = 0$$

where n is the outward normal to the boundary surface.

From variational calculus, the governing differential equation with its boundary equations can be transformed into the variational form as explained by Berg (22). Considering the differential formulation in the form of Euler equation, the variation of the functional I is

$$\delta I = \iint \left(g \frac{d^2t}{dx^2} + g \frac{d^2t}{dy^2}\right) \delta t \, dx \, dy + \int h(t-t_g) \delta t \, ds = 0$$

where s designates the boundary surface of the beams.

Integration by parts yields

$$I = \iint \frac{1}{2} \{g \left(\frac{dt}{dx}\right)^2 + g\left(\frac{dt}{dy}\right)^2\} \, dx \, dy + \int h \left(\frac{1}{2} t^2 - t_g t\right) ds \qquad 3.2$$

The function $t(x,y)$, that makes the functional stationary $\delta I = 0$, is the solution to the differential heat conduction equation 3.1 Since the temperature function is unknown, it is therefore necessary to approximate a function for which the functional has a value approximately equal to its stationary value.

The approximate temperature field throughout the cross section of the beams can be constructed by an assembly of a finite number of discrete elements where over each element, a temperature function is assumed. These elements are interconnected at assigned points along their boundaries and these points are called nodes. The assumed temperature function within the elements is expressed in terms of the temperature at its nodes. These nodal temperatures act as generalized coordinates. The choice of the function must be such that the temperature field construction over the cross section of the beams has no discontinuities between adjacent elements. In that case, the elements are interconnected along the interface boundaries as well.

The unknown nodal temperatures can be evaluated when the functional, for the system of all the elements that constitute an analytical model of the cross section of the beams, is stationary. Over each of these elements, a functional can be written so that the entire functional may be expressed as a summation of the subfunctionals. The functional of the individual elements is related to its nodal temperatures by substituting

the assumed function into Equation 3.2. To minimize I of each element, the derivatives of the functional with respect to the nodal temperatures t_i in an element are set equal to zero. This minimization procedure yields a set of algebraic equations in which the nodal temperatures within the element are related to each other. These equations can be written in matrix form

$$\frac{dI}{dt_i} = [K_e]\{t\} = 0 \qquad 3.3$$

where K_e is the so-called element stiffness matrix in structural analysis and $\{t\}$ signifies the scalar temperature field expressed in terms of the nodal temperatures.

On assembling the elements into a representation of the cross section of the beams

$$\sum [K_e]\{t\} = 0$$

and applying the boundary conditions, the resulting set of simultaneous equations can be written in the form

$$[K]\{X\} = \{F\} \qquad 3.4$$

where K denotes the structure stiffness matrix

X signifies the unknown scalar temperature at the nodes

F contains the known temperatures to which the nodes of the structure are exposed

Equation 3.4 can be solved for the nodal temperatures.

The approximate solution will converge to an exact solution when the number of elements is increased. The rate of convergences of the solution largely depends on the selection of the temperature functions within the finite element. The sufficient conditions for the finite element to ensure monotonic convergence of the functional I to its exact value are that the temperatures and their gradients at the boundaries of adjoining elements be continuous.

The temperature field is unknown. It can be approximated by a piecewise function. Depending on the nature of the problem, the general behaviour of the desired solution is usually known and a function among the polynomials, the trigonometric functions, or any other functions can be selected to best represent the solution. The temperature variation in a differential element is described by Fourier Law of heat conduction. The temperature profile within a solid conducting element of uniform thermal conductivity can be taken as linear. Having a linear temperature distribution within the elements does not necessarily imply that the temperature variation throughout the structure is linear.

Both rectangular and triangular elements, having a linear temperature variation, were used in the finite element method to determine the temperature field in the composite beam and T-beam. The size of the elements is considered to remain unaffected by the temperature changes.

3.2 Derivation of Properties of the Linear Temperature Triangular Element

Coordinate Systems

The two coordinate systems used with the triangular element are shown in Figure 11. The properties of the element are first derived in the local coordinate system ζ-η and then transformed to the global coordinate system x-y where the assembled cross section of the beams is located.

The vertices, which are the nodal temperatures of the particular element, are numbered in a counter-clockwise order as shown in Figure 11. The local coordinate system for each element is located with the ζ-axis passed along the base of the triangle, that is, from vertex 1 to vertex 2. The η-axis is directed through the third vertex of the triangle.

The dimensions of the triangle are given as follows; the lengths

$$a = [(x_2 - x_3)(x_2 - x_1) + (y_2 - y_3)(y_2 - y_1)]/r$$

$$b = [(x_3 - x_1)(x_2 - x_1) + (y_3 - y_1)(y_2 - y_1)]/r$$

$$c = [(x_2 - x_1)(y_3 - y_1) - (x_3 - x_1)(y_2 - y_1)]/r$$

where

$$r = \sqrt{(x_2 - x_1)^2 \quad (y_2 - y_1)^2}$$

the rotation angle θ

$$\text{Cos}\ \theta = \frac{x_2-x_1}{r} \quad \text{and Sin}\ \theta = \frac{y_2-y_1}{r}$$

Temperature Function

For a linear temperature distribution within each element, the temperature function is represented by

$$t(\zeta,\eta) = a_1 + a_2\zeta + a_3\eta \qquad 3.5$$

or in matrix form

$$t(\zeta,\eta) = \begin{bmatrix}1 & \zeta & \eta\end{bmatrix}\begin{bmatrix}a_1\\a_2\\a_3\end{bmatrix}$$

$$= \{C\}^T\{A\} \qquad 3.6$$

Introduction of the nodal coordinates into Equation 3.5, yields, in matrix form, the nodal temperatures within the element in terms of the arbitrary parameters $\{A\}$.

$$\begin{bmatrix}t_1\\t_2\\t_3\end{bmatrix} = \begin{bmatrix}1 & -b & 0\\1 & a & 0\\1 & 0 & c\end{bmatrix}\begin{bmatrix}a_1\\a_2\\a_3\end{bmatrix}$$

or using matrix notation $\{t\} = [T]\ \{A\}$ 3.7

Provided that the determinant of $[T]$ is not zero, that is, $c(a+b) \neq 0$, the triangle having an area $\frac{1}{2}c(a+b)$ exists.

Thus,

$$\{A\} = [T^{-1}]\ \{t\} \qquad 3.8$$

The temperature, which is uniquely defined at any point in the element by its nodal temperatures, is given by

$$t(\zeta,\eta) = \{C\}^T[T^{-1}]\{t\}$$

The continuity of temperature along the common edges between adjacent elements is satisfied. The temperature distribution along the edges of the triangular elements is linear and uniquely defined in terms of the nodal temperatures along that particular edge. In the adjacent element, the linear temperature profile along the common edge is expressed in terms of the same nodal temperatures, thus ensuring temperature compatibility along the interfaces of adjoining elements.

The temperature gradients, which are the first derivatives of the temperature function with respect to the spatial coordinates, do not coincide at the interfaces between elements. They are constant within each element and vary from element to element. The reason for attaching such importance to the temperature gradient compatibility is due to its physical significance. The product of the gradient and the thermal conductivity of the material yields the rate of heat flow. The rate of heat leaving one element through the boundary surface must be equal to that entering the other element. This requirement of energy balance is not met in this analytical model made of a system of triangular elements. However, the inter-element temperature gradient compatibility does not ensure energy balance between elements. The adjacent elements can have different thermal conductivities.

Element Stiffness Matrix

The stiffness matrix of an element is obtained from the functional in Equation 3.2 but without considering its convective boundary term. The matrix, representing the contribution from the convective boundary term, is derived separately and then is combined with the stiffness matrix whenever the element edges are exposed to ambient air at a uniform and steady temperature t_g. The functional of a single element is given by

$$I = \frac{1}{2} \iint \{g \left(\frac{dt}{d\xi}\right)^2 + g \left(\frac{dt}{d\eta}\right)^2 \} \, d\xi \, d\eta \qquad 3.9$$

Substituting the assumed linear temperature function (3.5) into Equation 3.9 and performing the necessary integrations over the area of the element, the functional can be arranged in the form.

$$I = \frac{1}{2} \{A\}^T [k] \{A\}$$

$$\text{where } [k] = \begin{bmatrix} 0 & 0 & 0 \\ 0 & 1 & 0 \\ 0 & 0 & 1 \end{bmatrix} \frac{c(a+b)}{2} g$$

Using Equation 3.8

$$I = \frac{1}{2} \{t\}^T [T^{-1}]^T [k][T^{-1}] \{t\} \qquad 3.10$$

I is a quadratic function of the temperatures.

The differentiation of the functional with respect to the generalized nodal temperatures leads to

$$[K_e]\{t\} = 0 \qquad 3.11$$

where the element stiffness matrix can be evaluated as $[K_e] = [T^{-1}]^T[k][T^{-1}]$

The stiffness matrix becomes

$$[K_e] = g \begin{bmatrix} \frac{c^2+a^2}{2(a+b)c} & \frac{-c^2+ab}{2(a+b)c} & \frac{-a}{2c} \\ \frac{-c^2+ab}{2(a+b)c} & \frac{c^2+b^2}{2(a+b)c} & \frac{-b}{2c} \\ \frac{-a}{2c} & \frac{-b}{2c} & \frac{a+b}{2c} \end{bmatrix} \qquad 3.12$$

Convective boundary matrix

If the side of the element, in Figure 11, along the ζ-axis is exposed to an ambient air at temperature t_g, the temperature function between nodal points 1 and 2 is reduced to

$$t(\zeta) = a_1 + a_2 \zeta$$

By expressing the convective functional - $\int ht_g t ds + \frac{1}{2}\int ht^2 ds$ in terms of the two temperature nodes and differentiating, the resulting set of equations can be written in the following matrix form

$$- \begin{bmatrix} \frac{1}{2} \\ \frac{1}{2} \end{bmatrix} h\ell t_g + h\ell \begin{bmatrix} \frac{1}{3} & \frac{1}{6} \\ \frac{1}{6} & \frac{1}{3} \end{bmatrix} \begin{bmatrix} t_1 \\ t_2 \end{bmatrix} \qquad 3.13$$

or in the matrix notation

$$- \{F_e\} + [K_c] \{t\}$$

Here, ℓ is the distance along the exposed edge and h, which is the uniform surface conductance along that edge, can vary from one element to the next. The matrix K_c, in Equation 3.13, is called the consistent convective stiffness matrix.

An alternate matrix, known as the lumped convective stiffness, is given by

$$- \begin{bmatrix} \frac{1}{2} \\ \frac{1}{2} \end{bmatrix} h\ell t_g + h\ell \begin{bmatrix} \frac{1}{2} & 0 \\ 0 & \frac{1}{2} \end{bmatrix} \begin{bmatrix} t_1 \\ t_2 \end{bmatrix} \qquad 3.14$$

This matrix has been derived on the basis of the rate of convective heat transmitted to the surface. The steady rate of heat flow through the ambient air to the entire exposed surface of the element is given by $q = h\ell(t-t_g)$. This rate of heat transfer q is distributed in equal shares to the two nodes on the convective side of the element in order to yield the lumped convective stiffness 3.14.

The modifications, necessitated in the element stiffness matrix by incorporating the consistent convective matrix, have affected the terms in the main diagonal as well as the terms off the diagonal. Using the lumped convective stiffness matrix, the convective coefficients appear only on the main diagonal of the element stiffness matrix.

The concept in the derivation of the lumped convective matrix is not consistent with the assumption made in the problem for the temperature function. The convective matrix is derived over the edge surface of an element. The edge can be interpreted as a one-dimensional line element of length ℓ and having a node at each ends. In the consistent convective element, the temperature along the edge is distributed linearly. When this element is combined with either the linear temperature triangular or rectangular element, the temperatures along the common boundary are compatible. In the lumped convective element, the temperature contrarily to that assumed is constant along its length and, in the assembly, the temperature compatibility is not satisfied. The combination of lumped convective element and linear temperature element yields a different functional than that in Equation 3.2. As the number of element are increased in the model of the beam, the piecewise temperature field will not eventually become the true temperature field since a different functional was minimized. The solution to the differential heat equation 3.1 is the continuous temperature function that minimizes the functional I.

3.3 Derivation of Properties of the Linear Temperature Rectangular Element

Two rectangular elements were considered. One was derived in the same manner as the triangular element. The other element, which will be referred to as the modified rectangular element, is formed from an assembly of triangular elements.

Following closely the procedure outlined for the triangular element, the linear temperature function of x and y is assumed over each element

$$t\ (x,y) \ = \ a_1 + a_2x + a_3y + a_4xy \qquad 3.15$$

The origin of the local coordinate system is shown in Figure 12.

The assumed bi-linear function ensures continuity of temperature at the interfaces of adjacent elements. The temperature profile, along the line joining nodes 3 and 4, is described by $t(x) = xt_3 + (1-x)\ t_4$. In the adjacent element, the temperature, along that same edge, is defined as $t(x) = xt_2 + (1-x)t_1$. The nodal temperatures, which are the same for both elements, make the temperature variations along a common boundary compatible.

The stiffness matrix of the rectangular element is given by

$$[K_e] = \frac{g}{6ab} \begin{bmatrix} 2(a^2+b^2) & a^2-2b^2 & -a^2-b^2 & b^2-2a^2 \\ a^2-2b^2 & 2(a^2+b^2) & b^2-2a^2 & -a^2-b^2 \\ -a^2-b^2 & b^2-2a^2 & 2(a^2+b^2) & a^2-2b^2 \\ b^2-2a^2 & -a^2-b^2 & a^2-2b^2 & 2(a^2+b^2) \end{bmatrix} \qquad 3.16$$

The modified rectangular element is obtained by averaging the stiffness matrices resulting from two different arrangements of right-angled triangular elements which are combined to yield a rectangular element.

The possible arrangements are shown as follows

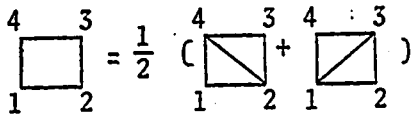

$$[K_e] = \frac{1}{2}\,(K_{\Delta 124} + K_{\Delta 423}) + \frac{1}{2}\,(K_{\Delta 134} + K_{\Delta 123})$$

where the indices specify the triangle under consideration

$$[K_e] = \frac{g}{2ab}\begin{bmatrix} a^2+b^2 & -b^2 & 0 & -a^2 \\ -b^2 & a^2+b^2 & -a^2 & 0 \\ 0 & -a^2 & a^2+b^2 & -b^2 \\ -a^2 & 0 & -b^2 & a^2+b^2 \end{bmatrix} \qquad 3.17$$

In this case, the averaging procedure of the stiffness matrices has no merit since both configurations of right-angled triangles lead to identical stiffness matrix. The reason for this is that the right-angled triangles have failed to relate the opposite nodal temperatures in the diagonal direction as it is indicated by the presence of zeros in the stiffness matrix of the modified rectangular element. In the triangular element stiffness matrix given in Equation 3.12 the coefficients, that relate the two nodal temperatures along the hypothenuse, become zero since either $a = 0$ or $b = 0$ or $c^2 = ab$.

In certain problems, this type of rectangular element has proven to be very effective as shown by Fujino and Ohsaka (23). In their analysis of the stationary temperature variation in a plate, the system of modified rectangular elements has yielded fairly

accurate results. The governing differential equation, describing the heat conducted through the plate and dissipated to the surroundings by convection, is different from that given in Equation 3.1.

3.4 Solution of the Temperature Problem

Assembly

The stiffnesses of all the individual elements, that represent the cross-sectional area of the beams, are combined in order to obtain the structure stiffness matrix K. This is easily accomplished by assigning the coefficients of each element stiffness matrix to a definite position in the structure stiffness matrix. These positions are specified by the numbering system of all the nodes in the cross-sectional area. The overlapping coefficients, which occur when elements meet at common nodes, are simply added. For each nodal temperature in the structure, an equation is written. The equation relates the particular nodal temperature to the nodal temperatures of its element as well as to those of the adjoining elements that are associated with the node under consideration. The structure stiffness matrix is symmetrically and sparsely populated.

The assembly of the elements into a representation of the cross-sectional area can be most conveniently accomplished within a computer subroutine. This program has been called the Subroutine Setup and is presented in Appendix D. The subroutine stores only the upper band portion of the symmetric and sparse stiffness matrix K.

Boundary Conditions

The structure stiffness matrix K, in the initial assembled form, is singular. The matrix is rendered nonsingular by the application of the temperature boundary conditions.

The convective boundary condition is conveniently taken into consideration during the assembly of elements. For the sides of the elements that are exposed to convection, either Equation 3.13 or 3.14 are incorporated into the element stiffness matrix. The assembly of all the elements may be presented in the following form

$$\sum ([K_e] + [K_c]) \{t\} - \{F_e\} = 0$$

The procedure results in a set of linear equations written in matrix Equation 3.4, which is

$$[K] \{X\} = \{F\}$$

For elements with specified temperature boundary conditions, the structure stiffness matrix is modified by equating the appropriate surface nodal temperatures to the known temperature t_s such that the final set of equations can be solved for the nodal temperatures. The modification can be done in various ways and are briefly described as follows.

In the structure stiffness matrix, the rows corresponding to the specified nodal temperatures are removed. The coefficients, in the corresponding columns, are multiplied by the temperature t_s and the results are transferred to the column matrix {F} which initially consisted of zeros only. The remaining rows and columns are rearranged to

to occupy the deleted rows and vacated columns. This results in a reduction of the matrix size and the system of linear equations has the form given in Equation 3.4.

Alternate approach results in maintaining the original size of the stiffness matrix K. The coefficients in the corresponding rows to the specified nodal temperature are set equal to zero with the exception of the main diagonal coefficients which take on a unit value. The corresponding coefficients in {F} are set equal to the temperature t_s. The products of the coefficients in the corresponding columns with the temperature t_s are transferred to {F} . These coefficients of the corresponding columns are replaced by zeroes. The resulting equations are written in the form given in Equation 3.4.

A simpler method in dealing with the specified temperature boundary conditions is to consider that surface as being exposed to convective boundary condition. The nodal surface temperatures are set equal to the specified temperature by assuming a high unit surface conductance h. A value of 900,000 BTU/hr-ft-in-^{o}F for h was used in the calculations.

Idealization of the Cross-Sectional Area

From symmetry, only half of the beams' cross section need be considered. The areas of the composite beam and the reinforced concrete T-beam are divided into rectangular elements which are further subdivided into two right-angled triangles as shown in Figures 10 and 10a.

As previously discussed, if the rectangles were subdivided by either one of the diagonals and using a linear temperature elements, the resulting temperatures, in the beam subjected to convection or to specified temperatures, would be identical.

In order to obtain the narrowest band width in the structure stiffness matrix, the nodes, in the finite element idealization of the composite section and the T-beam, are numbered in different ways. For the composite section, the numbering scheme is shown in Figure 10. The nodes in the concrete slab are numbered beginning at the edge from top to bottom and moving towards the center line. In the T-beam, the nodal numbering system follows a diagonal pattern as shown in Figure 10a.

The cross-sectional areas can be idealized by any system of elements varying in size. In the idealization of unequal element size, the accuracy of the results is reduced. This type of idealization is best used in problems in which the variation of the unknown function is more pronounced in certain regions. These regions of high variation of the function can be represented by a large concentration of smaller elements.

Solution of Nodal Temperatures

Taking advantage of symmetry and the sparseness of the structure stiffness matrix, the set of linear equations given in Equation 3.4 is solved for the nodal temperatures by means of Cholesky's square root method. Details of this method are presented in Appendix A. A computer program called Subroutine BSOLVE is given in Appendix D.

Two sets of results for the two sections were obtained. One was based on an idealization of rectangular elements and the other on a triangular element idealization as previously shown in Figures 10 and 10a.

Verification of Results

If the final temperatures are correct, the rate of heat gained by the surface of the beams is equal to the rate of heat transmitted out of the beams. The convective heat transferred to one of the element sides, as discussed previously, is given by

$$q = h\ell \left(\frac{1}{2} t_1 + \frac{1}{2} t_2 - t_g\right)$$

The total heat transfer rate accross the upper surface or lower surfaces of the half section of the beam is computed as the summation of q

$$Q = \sum q \qquad \text{BTU/hr-ft.} \qquad 3.18$$

For the beams with isothermal surfaces t_s, the quantity of heat entering or leaving can be determined by summing the heat flow by conduction of all the rectangular elements that are located along the isothermal surfaces. If, in the rectangular element in Figure 12, the side between nodal points 3 and 4 has a temperature t_s, the heat conducted through the element is in the amount of

$$q = g \frac{a}{b} \left(\frac{1}{2} t_1 + \frac{1}{2} t_2 - t_s\right) \quad \text{BTU/hr-ft.}$$

3.5 Comparison to the Finite Difference Method

The temperature, at the nodes given in Figures 10 and 10a, can be determined by means of the finite difference method. For the beams exposed the convection or subjected to specified surface temperature, the set of linear equations resulting from the finite difference formulation is identical to those obtained in the finite element method. That is, of course, when the right-angled triangular element and the lumped convective matrix 3.14 are used in the analysis. The reason that both methods, finite element and finite difference, yield identical solutions is due to the fact that its formulation was based on the assumption that the temperature varies linearly between nodes.

In the finite difference approximation, where ℓ is a typical distance between nodes, the second derivatives $\frac{d^2t}{dx^2}$ and $\frac{d^2t}{dy^2}$, having neglected all terms containing fourth or higher powers of ℓ, are accurate to $0(\ell^4)$ for uniform grid. For an unequal grid, the accuracy is reduced to $0(\ell^3)$. The difference equations can be modified for higher precision.

The main advantage of the finite element method over the finite difference method is in its capability to represent the structure under consideration by a system of elements of varying size. In addition curved boundaries, which presented considerable difficulties to other methods, can be most conveniently handled by using triangular elements.

3.6 Evaluation of Surface Conductance and Thermal Conductivity from Experimental Results

The evaluation of unit surface conductances, which depend on the temperature, physical properties, and velocity of the air in the conducting system, is extremely difficult. These results were approximated from the experimental results. Using the surface temperatures measured with thermocouples, the rate of heat transmitted to or from the upper surface can be calculated according to Equation 3.18. The uniform surface conductance can be estimated by equating the rate of heat transfer to that supplied by the heating elements in Equation 2.1. Its units used were BTU/hr-ft-in-^{o}F. They correspond to the units of the surface dimensions of the elements which are in inches.

The calculated value is a crude approximation. It was assumed that there was no loss of heat from the styrofoam chamber. In addition, the exact surface conductance varies over a nonisothermal surface. Of the temperature conditions imposed on the beams, the largest temperature difference resulting on the upper slab surface between the edge and center line was less than 6^{o}F. The error introduced by considering a uniform surface conductance is small.

With the estimated surface conductance, the conductivity of concrete can be obtained from a one-dimensional analysis of heat conduction at sections where the thermocouples register temperatures at sufficient distances from the center line. The conductivity was computed from

$$g = \frac{d_c h\ (t_s - t_g)}{\Delta t} \qquad \text{BTU/hr-ft-}^{o}\text{F} \qquad 3.19$$

where Δt designates the measured temperature difference between the upper and lower surface at a section of the concrete slab of thickness denoted by d_c.

The thermal conductivity of concrete in this experimental investigation has mainly a dependence on the moisture content. Its temperature dependency, within the relatively small temperature change of interest, is not severe and is neglected.

When the surfaces of the beams were subjected to melting ice temperature , the concrete was fully saturated. A series of concrete conductivities with its corresponding surface conductance h can be obtained according to Equation 3.19. The concrete conductivity can vary from 1.5 to 3.0 BTU/hr-ft-^{o}F with its corresponding surface conductance without producing any substantial effect on the results. The surface conductance is greater when the beams are treated to melting ice conditions than when heated because of the film condensation of air forming on the surfaces.

The surface conductance h_v for the vertical surface in the steel beam can be determined from the analytical solution of heat conduction in the web which is considered to be, in respect of the theory of heat transfer, a fin. The temperature variation across the very thin steel web can be neglected so that a one-dimensional analytical treatment as shown in Jakob's textbook (24) on page 211 may be applied to determine the temperatures in the steel web. The surface conductance h_v can be found by recording the temperatures at the top corner t_c of the web and the embedded flange in concrete, at mid-depth t_m and at the bottom of the steel beam t_e and then substituting these temperatures into equation

$$h_y = gw\left(\frac{2}{d}\right) \ln\left(\frac{t_c+t_e-2t_g}{2t_m-2t_g} + \sqrt{\left(\frac{t_c+t_e-2t_g}{2t_m-2t_g}\right)^2-1}\right)^2$$

Here the steel beam of depth d and web thickness w has a thermal conductivity g of 31 BTU/hr-ft-^{o}F.

CHAPTER 4

Analysis of Thermoelasticity Problem by Finite Elements

4.1 General

The calculation of stresses and deformations, produced in the unrestrained beam by the steady two-dimensional temperature distributions just determined, can now be carried out. The thermoelasticity problems of the unrestrained beams, which are subjected to the two-dimensional temperature distributions in their cross-sectional coordinates, can be reduced to two-dimensional problems in plane strain. The analysis by finite elements is separated into three stages.

1) Restrained Thermal Problem

A set of artificial restraints is applied at the ends of the beams such that the stresses produced by the temperatures and by the restraints are obtained as a plane strain solution. In addition, the resultant force and moment of these fictitious restraints acting at the ends of the beam in order to maintain the state of plane strain, are determined.

2) Force Restraint (Nonthermal) Problem

The stresses and deformations, produced solely by the fictitious resultant force applied at the ends in the previous problem, are computed

3) Flexural Restraint (Nonthermal) Problem

The stresses and deformations resulting from the resultant moment prescribed at the ends in the restrained thermal problem are calculated.

The three solutions are then superposed to yield a solution to the thermoelastic problem for the unrestrained beams. The formulation of the problems and the application of the principle of superposition to the problem are based on the following assumptions.

The beams are considered to be made of homogeneous, isotropic materials obeying Hooke's law. The concrete, however, is a much different material from that assumed. It is heterogeneous, anisotropic and does not follow Hooke's law very far. For compressive stresses up to half the cylinder strength, the concrete behaves nearly in a linear elastic manner, that is, stresses and strains are closely proportional. The above simplifying assumptions are introduced with little error in the analysis of the unrestrained beams subjected to small temperature changes that produce, in the concrete, compressive stresses within the elastic range of the stress-strain curve.

In the analysis, the concrete can sustain tensile forces that do not cause the concrete to crack. It is assumed that no tension cracks were formed since the tensile bending strength (modulus of rupture) has not been exceeded. According to the ACI 435-201 (in Reference 25), the modulus of rupture ranges from 7.5 to 12 times the square root of the compressive strength. For concretes of compressive strength of 4100 psi and 4300 psi, it is taken as 8 times, which is, 512 and 525 psi respectively. The slope of the stress-strain curve for tensile

stresses up to half the ultimate value is very nearly the same as that of the stress-strain curve for the same range of compressive stress.

The finite element technique, which discretizes the structure into a system of finite elements, can be modified to deal with the tension cracks in the concrete whenever they occur as shown by Ngo and Scordelis (26). The cracks are introduced in the elements when their principal stresses exceed the tensile strength. The tensile loads are removed from the elements that can no longer sustain any load and are redistributed in adjacent elements.

Since the experimental investigation is confined to small temperature changes and to small deformations, the products of the small displacements derivatives and with small temperature changes are negligible in comparison with the quantities themselves in the stress-strain relations and strain-displacement relations. For an isotropic homogeneous material that obeys the linear elasticity theory, the thermal stress-strain relations resulting from this assumption are expressed as follows:

$$\begin{aligned} \varepsilon_x - \alpha t &= \frac{1}{E}(\sigma_x - \nu(\sigma_y+\sigma_z)) \\ \varepsilon_y - \alpha t &= \frac{1}{E}(\sigma_y - \nu(\sigma_x+\sigma_z)) \\ \varepsilon_z - \alpha t &= \frac{1}{E}(\sigma_z - \nu(\sigma_x+\sigma_y)) \end{aligned} \qquad 4.1$$

where E is the elastic modulus

ν is the Poisson's ratio

α is the coefficient of thermal expansion

t is the temperature change from the unstressed state

The linearized strain-displacement relations, where u and v are the displacement components in the x and y directions respectively, are presented as

$$\varepsilon_x = \frac{\partial u}{\partial x}$$

$$\varepsilon_y = \frac{\partial v}{\partial y} \qquad 4.2$$

$$\gamma_{xy} = \frac{\partial u}{\partial y} + \frac{\partial v}{\partial x}$$

The effect of the small displacements on the geometry of the elements in the finite element idealization is negligible only when the displacements are small as compared to the element size. The sizes of the elements can be assumed constant under this action of thermal loading. Such consideration has no serious effect on the element stiffness matrix and on the element load vector which are derived on the basis of the area of the element.

Based on the assumption that the stiffnesses of the elements remain unaltered and that the beams act as a linear elastic structure, the principle of superposition can be readily used to combine the three separate solutions in order to yield a solution of the unrestrained beam. If the behaviour of the beam is not in accordance with the elastic theory, the problem can be treated in the step by step response of the beam due to incremented loading conditions and thus, reducing the problem to the solution of a series of linear problems.

The nonthermal solutions represent an approximate solutions. The formulation of the nonthermal problems takes no account of the detailed distribution of the end restraints but only of their resultant force and moment. According to Saint-Venant's principle, the approximate nonthermal solutions of the beam whose length is large compared with its cross-sectional dimensions can be considered satisfactory, except in regions at the ends of the beam. These end regions are extended at distances smaller than the maximum cross-sectional dimension. Near the ends, a large concentration of shear forces will occur, especially at the interface of steel and concrete in the composite steel-concrete member. The ends of the beams will not remain plane in cross section.

The temperature along the length of the composite steel-concrete beam is not uniform as assumed in the heat conduction analysis. There will be variations in temperature gradients occurring in the vicinity of shear connectors $1\frac{1}{2}$ u 1.17 spaced at $4\frac{1}{4}$ inches and of transverse reinforcing wires D4 spaced at $4\frac{1}{4}$ inches. This nonuniform temperature variation along the length of the beam will produce stresses. In the vicinity of the shear connectors, a concentration of shear stresses will occur and will increase in magnitude for shear connectors near the ends of the beam. This effect is not taken into account in the analysis. Complete interaction between the steel and concrete is assumed.

The physical properties of steel and concrete such as the coefficient of thermal expansion and the modulus of elasticity which are temperature dependent are considered to be constant within the small temperature range of $32^{\circ}F$ to $126^{\circ}F$. The influence of this temperature

change on the properties is negligible. For steel, according to AISC (in Reference 19), the coefficient of expansion between room temperature and 200°F is 6.5 X 10^{-6} in/in./°F. The modulus of elasticity is close to 30 X 10^{6} psi at room temperature. It decreases linearly to 25 X 10^{6} psi at 900°F. For the concrete of same mix proportion, Sarkar (13) has measured, at 84 days, the coefficient of expansion of dry and wet concrete between 32°F and 150°F to be 4.0 X 10^{-6} and 3.72 X 10^{-6} in./in./°F respectively. In addition, at 84 days the dynamic modulus of elasticity from 32°F to 150°F decreases from 4.4 X 10^{6} to 4.2 X 10^{6} psi for dry concrete and from 5.4 X 10^{6} to 5.2 X 10^{6} psi for wet concrete. In this calculation, to show the effect of variation in coefficient of expansion of the concrete on the results, values of 5.5 X 10^{-6} and 4.5 X 10^{-6} in./in./°F were used. Calculations were carried out with a modular ratio of 8.

4.2 Restrained Thermal Problem

The thermal stresses and the resultants of the fictitious restraints at the ends of the beams are obtained by means of the finite element method

4.2.1 Plane Strain Formulation

The problem is reduced to a plane strain problem where the displacement in the axial direction is prevented, that is, $\varepsilon_z = 0$ in Equation 4.1. The longitudinal normal stress becomes

$$\sigma_z = \nu(\sigma_x + \sigma_y) - \alpha E t \qquad 4.3$$

The stress components in the x and y directions are obtained from

$$\sigma_x = \frac{E(1-\nu)}{(1-2\nu)(1+\nu)} \left[\varepsilon_x + \frac{\nu}{1-\nu}\ \varepsilon_y\right] - \frac{E\alpha t}{1-2\nu}$$

$$\sigma_y = \frac{E(1-\nu)}{(1-2\nu)(1+\nu)} \left[\varepsilon_y + \frac{\nu}{1-\nu}\ \varepsilon_x\right] - \frac{E\alpha t}{1-2\nu} \qquad 4.4$$

Similar to the plane stress problem, the plane strain problem is solved for the normal stresses σ_x and σ_y. Once these stresses are obtained, the axial stress σ_z can be determined using Equation 4.3. The solution of the two-dimensional problem can be obtained by means of energy principles used in conjunction with the finite element technique

4.2.2 Minimum Potential Energy

This boundary-value problem can be expressed in a variational formulation where the functional is called the total potential energy Π. The total potential energy is the elastic-strain energy U stored in the

beam plus the potential energy V of the external loads acting on the beam.

$$\Pi = U - V \tag{4.5}$$

The strain energy, stored in the beams of a unit length, is given by

$$U = \frac{1}{2} D \iint \{[\varepsilon_x - (1+\nu)\alpha t]^2 + [\varepsilon_y - (1+\nu)\alpha t]^2 + \frac{2\nu}{1-\nu}[\varepsilon_x - (1+\nu)\alpha t][\varepsilon_y - (1+\nu)\alpha t] + \frac{1-2\nu}{2(1-\nu)}\gamma_{xy}^2\} dx dy$$

where $$D = \frac{E(1-\nu)}{(1+\nu)(1+2\nu)}$$

It is convenient to separate the strain energy expression into two parts such that

$$U = U_k + U_t$$

where $$U_k = \frac{1}{2} D \iint [\varepsilon_x^2 + \varepsilon_y^2 + \frac{2\nu}{1-\nu}(\varepsilon_x + \varepsilon_y)^2 + \frac{1-2\nu}{2(1-\nu)} \gamma_{xy}^2] \, dx \, dy \tag{4.6}$$

and $$U_t = \frac{1}{2} D \iint [-2(\frac{1+\nu}{1-\nu}) \alpha t \, (\varepsilon_x + \varepsilon_y) + 2 \frac{(1+\nu)^2}{(1-\nu)} (\alpha t)^2] \, dx \, dy \tag{4.7}$$

The principle of potential energy states that Π is stationary for the compatible displacements which satisfy the equilibrium conditions. That is, the first variation of the total potential energy is $\delta\Pi = \delta U = 0$ where the beam is free from external forces ($V = 0$). The minimization of Π can be expressed by summing the differentiations, with respect to the displacement components $\{{}^{u}_{v}\}$, of the total potential energies over the elements that form the structure and then setting the results equal to zero

$$\frac{\partial \Pi}{\partial \{{}^{u}_{v}\}} = [K]\{X\} - \{F\} = 0 \tag{4.8}$$

where K is designated as the stiffness matrix of the structure and is determined when U_k is differentiated

X represents the unknown displacement vector,

F signifies the thermal load obtained from the differentiation of U_k

4.2.3 Derivation of Linear Strain Triangular Element

The linear temperature variation in the element for the two-dimensional heat conduction yields a linear strain within the element.

Displacement Function

In the local coordinate system as shown in Figure 13, the displacements $\bar{u}$ and $\bar{v}$ in the directions of ζ and η respectively are approximated by a quadratic polynomial

$$\bar{u} = a_1 + a_2\zeta + a_3\eta + a_4\zeta^2 + a_5\zeta\eta + a_6\eta^2 \qquad 4.9$$

$$\bar{v} = a_7 + a_8\zeta + a_9\eta + a_{10}\zeta^2 + a_{11}\zeta\eta + a_2\eta^2$$

Taking the vertices and the mid-points displacements as generalized coordinates, the displacement vectors in the local coordinate system $\{\bar{\underline{u}}\}^T = [\bar{u}_1\ \bar{v}_1\ \bar{u}_2\ \bar{v}_2\ \ldots\ldots\bar{u}_6\ \bar{v}_6]$ can be related to the polynomial coefficients $\{A\}^T = [a_1\ a_2\ a_3\ldots.a_{12}]$ by

$$\{\bar{\underline{u}}\} = [T_1]\{A\} \qquad 4.10$$

The transformation matrix T_1 is non-singular as the determinant is only zero when the area of the triangle is nonexistant.

The displacements at any one point of the element in the local coordinate system can be related to any other coordinate system by means of well-known transformation formulas. The transformations related to displacements are established by the laws of vector transformation. The displacements u and v in the x and y directions respectively of the global coordinate system are related to the displacements $\bar{u}$ and $\bar{v}$ in the local system as follows:

$$u = \bar{u} \cos\theta - \bar{v} \sin\theta$$

$$v = \bar{u} \sin\theta + \bar{v} \cos\theta$$

In matrix form

$$\begin{Bmatrix} u \\ v \end{Bmatrix} = [R] \begin{Bmatrix} \bar{u} \\ \bar{v} \end{Bmatrix} \qquad 4.11$$

where R is referred to as the rotation matrix

The assumed displacement fields in the individual elements guarantee compatibility at the inter-element boundaries. The quadratic variation of displacements along the interface is uniquely defined by the three nodal displacements on that edge. Its first derivatives, which are the strains according to Equation 4.2, are not continuous from element to element.

Element Stiffness Matrix

The strain energy expression U_k will be used to derive the element stiffness matrix. The strain energy for an element of unit thickness can be expressed in terms of the displacements by means of Equation 4.2.

$$U_k = \frac{1}{2} D \iint \{\bar{u}_\zeta^2 + \bar{v}_\eta^2 + \frac{2\nu}{1-\nu} (\bar{u}_\zeta + \bar{v}_\eta)^2 + \frac{1-2\nu}{2(1-\nu)} (\bar{u}_\eta + \bar{v}_\zeta)^2\} \, d\zeta d\eta$$

where the subscripts denote the differentiation of local displacements with respect to the local coordinates.

Substituting the displacement function 4.9 and carrying out the integrations over the area of the element, the strain energy U_k can be written in matrix form

$$U_k = \frac{D}{2} \{A\}^T [k] \{A\} \qquad 4.12$$

Substitution of Equation 4.10 into Equation 4.12 gives the strain energy U_k in terms of the nodal displacements

$$U_k = \frac{D}{2} \{\bar{\bar{u}}\}^T [T_1^{-1}]^T [k] [T_1^{-1}] \{\bar{\bar{u}}\} \qquad 4.13$$

The differentiation of U_k with respect to the nodal displacements

$$\frac{\partial U_k}{\partial \{\bar{\bar{u}}\}} = [K_L] \{\bar{\bar{u}}\}$$

yields the stiffness matrix K_L of the element with respect to the local coordinate system

$$K_L = D [T_1^{-1}]^T [k] [T_1^{-1}] \qquad 4.14$$

To assemble the stiffness of each element, the stiffness matrix, based on the local coordinate system, is transformed by the use of Equation 4.11 to the global coordinate system. The stiffness matrix for the element in the global coordinate system is

$$[K_e] = [R]^T [K_L][R] \qquad 4.15$$

The manual computation of the matrix k becomes more complicated when higher degree of polynomials is used. The 12X12 matrix k can be evaluated automatically within the computer program as shown by Cowper, Lindberg, Kosko and Olson (10). Rewriting Equation 4.9 in summation notation

$$\bar{u} = \sum_{i=1}^{6} a_i \zeta^{m_i} \eta^{n_i}$$

$$\bar{v} = \sum_{i=7}^{12} a_i \zeta^{p_i} \eta^{q_i}$$

Differentiating

$$\bar{u}_\zeta = \sum_{i=1}^{6} a_i m_i \zeta^{m_i-1} \eta^{n_i}$$

and

$$\bar{u}_\zeta^{\,2} = \sum_{i=1}^{6} \sum_{j=1}^{6} a_i a_j m_i m_j \zeta^{m_i+m_j-2} \eta^{n_i+n_j}$$

such that the integration over the area of the triangular element is

$$\iint_A \bar{u}_\zeta^{\,2} \, d\zeta \, d\eta = \sum_{i=1}^{6} \sum_{j=1}^{6} a_i a_j m_i m_j \iint_A \zeta^{m_i+m_j-2} \eta^{n_i+n_j} d\zeta \, d\eta$$

The integration can be carried out by the use of the following integral formula, known as the modified Euler's beta function.

$$\iint_A \zeta^m \eta^n \, d\zeta \, d\eta = F(m,n)$$

$$= c^{n+1} \{a^{m+1} - (-b)^{m+1}\} \frac{m!\, n!}{(m+n+2)!}$$

where a,b,c are the given dimensions of the triangular element

The coefficients in matrix k are given by

$$k_{ij} = m_i m_j F(m_i+m_j-2, n_i+n_j) + q_i q_j F(p_i+p_j, q_i+q_j-2)$$

$$+ \frac{1-2\nu}{2(1-\nu)} [n_i n_j F(m_i+m_j, n_i+n_j-2) + p_i q_j F(p_i+p_j-2, q_i+q_j)]$$

$$+ [\frac{1-2\nu}{2(1-\nu)} n_j p_i + \frac{\nu}{1-\nu} m_j p_i] F(m_j+p_i-1, n_j+q_i-1) + [\frac{1-2\nu}{2(1-\nu)} n_i p_j + \frac{\nu}{1-\nu} m_i q_j] F(m_i+p_j-1, n_i+q_j-1)$$

Thermal Load Vector

The nodal force vector due to temperature is obtained from the thermal strain energy U_t given in Equation 4.7. After introducing the displacements into U_k by the linearized strain-displacement relations and discarding the products of the thermal strain since these quantities when differentiated with respect to the nodal displacements vanish, the thermal strain energy expression becomes

$$U_t = -\frac{D}{2} \iint 2 \left(\frac{1+\nu}{1-\nu}\right) \alpha t \, (\bar{u}_\zeta + \bar{v}_\eta) \, d\zeta \, d\eta \qquad 4.16$$

Following generally the same procedure as for the element stiffness, the thermal load vector of an element is given by

$$\{F_t\} = D\,[R]^T\,[T_1^{-1}]\,[k]\,[T^{-1}]\,\{t\} \qquad 4.17$$

Rewriting the linear temperature profile given in Equation 3.5 for the triangular element

$$t = \sum_{j=1}^{3} b_j\,\zeta^{r_j}\eta^{s_j}$$

such that

$$k_{ij} = \frac{1+\nu}{1-\nu}\,\alpha\left[m_i F(r_j+m_i-1, s_j+n_i) + q_i F(r_j+p_i, q_i+s_j-1)\right]$$

Stress-Strain Relationship

When the problem has been solved for the nodal displacements, the stresses within each element can be computed. From the obtained displacements, the strains can be determined by means of the strain-displacement relations and, from the strains, the stresses by means of Hooke's law for the prescribed temperature distribution.

The strain components, corresponding to the displacements assumed in Equation 4.9, are

$$\begin{bmatrix} \varepsilon_\zeta \\ \varepsilon_\eta \\ \gamma_{\zeta\eta} \end{bmatrix} = \begin{bmatrix} \bar{u}_\zeta \\ \bar{v}_\eta \\ \bar{u}_\eta + \bar{v}_\zeta \end{bmatrix} = \begin{bmatrix} 0 & 1 & 0 & 2\zeta & \eta & 0 & 0 & 0 & 0 & 0 & 0 & 0 \\ 0 & 0 & 0 & 0 & 0 & 0 & 0 & 0 & 1 & 0 & \zeta & 2\eta \\ 0 & 0 & 1 & 0 & \zeta & 2\eta & 0 & 1 & 0 & 2\zeta & \eta & 0 \end{bmatrix} \begin{bmatrix} a_1 \\ a_2 \\ \vdots \\ a_{12} \end{bmatrix}$$

----- 4.18

or

$$\{\bar{\varepsilon}\} = [T_d]\{A\}$$

These local strain components can be expressed in terms of the calculated nodal displacements and have the form

$$\{\bar{\varepsilon}\} = [T_d][T_1^{-1}][R]\begin{Bmatrix} u \\ v \end{Bmatrix} \qquad 4.19$$

The strain components with reference to the local system are referred to the global system as follows:

$$\begin{bmatrix} \varepsilon_x \\ \varepsilon_y \\ \gamma_{xy} \end{bmatrix} = \begin{bmatrix} \cos^2\theta & \sin^2\theta & -2\cos\theta\sin\theta \\ \sin^2\theta & \cos^2\theta & 2\cos\theta\sin\theta \\ \cos\theta\sin\theta & -\cos\theta\sin\theta & \cos^2\theta-\sin^2\theta \end{bmatrix} \begin{bmatrix} \varepsilon_\zeta \\ \varepsilon_\eta \\ \gamma_{\zeta\eta} \end{bmatrix} \qquad 4.20$$

It is evident from matrix T_d that the strains in the elements are a linear function of ζ and η. Only the strains at the vertices of each triangle are of interest while the mid-nodes strains are discarded.

The stresses, at the vertices of each triangle, are obtained from the constitutive relationship already given in Equation 4.4 for plane strain. Rewriting in matrix form

$$\begin{bmatrix} \sigma_x \\ \sigma_y \\ \tau_{xy} \end{bmatrix} = \frac{E(1-\nu)}{(1-2\nu)(1+\nu)} \begin{bmatrix} 1 & \frac{\nu}{1-\nu} & 0 \\ \frac{\nu}{1-\nu} & 1 & 0 \\ 0 & 0 & \frac{1-2\nu}{1-\nu} \end{bmatrix} \begin{bmatrix} \varepsilon_x \\ \varepsilon_y \\ \gamma_{xy} \end{bmatrix} - \frac{E\alpha t}{1-2\nu} \begin{bmatrix} 1 \\ 1 \\ 0 \end{bmatrix} \qquad 4.21$$

or $$\{\sigma\} = [D]\{\varepsilon\} + \{\varepsilon_t\}$$

Stress-strain Relationship

The stress components at any point in the element can be computed from

$$\begin{bmatrix} \sigma_x \\ \sigma_y \\ \gamma_{xy} \end{bmatrix} = [S] \begin{bmatrix} u_1 \\ v_1 \\ \vdots \\ u_4 \\ v_4 \end{bmatrix} - \frac{E\alpha t}{(1-2\nu)} \begin{bmatrix} 1 \\ 1 \\ 0 \end{bmatrix} \qquad 4.25$$

where

$$[S] = \frac{E_1}{1-\nu_1^2} \begin{bmatrix} \frac{y-b}{ab} & \frac{x-a}{ab}\nu_1 & \frac{b-y}{ab} & \frac{-x}{ab}\nu_1 & \frac{y}{ab} & \frac{x}{ab}\nu_1 & \frac{-y}{ab} & \frac{a-x}{ab}\nu_1 \\ \frac{y-b}{ab}\nu & \frac{x-a}{ab} & \frac{b-y}{ab}\nu_1 & \frac{-x}{ab} & \frac{y}{ab}\nu_1 & \frac{x}{ab} & \frac{-y}{ab}\nu_1 & \frac{a-x}{ab}\nu_1 \\ \frac{x-a}{ab}\lambda & \frac{y-b}{ab}\lambda & \frac{-x}{ab}\lambda & \frac{b-y}{ab}\lambda & \frac{x}{ab}\lambda & \frac{y}{ab}\lambda & \frac{a-x}{ab}\lambda & \frac{-y}{ab}\lambda \end{bmatrix}$$

$$\lambda = \frac{1}{2}(1-\nu_1)$$

and

$$\nu_1 = \frac{\nu}{1-\nu} \qquad E_1 = \frac{E}{1-\nu^2}$$

All three stress components at a common node of adjacent rectangles are incompatible. Each element yields a different stress value at a common node. In the analysis, the stresses were automatically averaged.

The stresses for each individual element can be interpreted from the nodal displacements in various ways. The stresses can be computed at the node points by means of Equation 4.21. These stresses at a common node of adjacent elements are incompatible. The stress components at a node can be evaluated as an arithmetic average of the stresses of the elements meeting at that node. An alternate solution is to compute the stresses at the centroid of the element. This method yields only a unique value of the stress components. The advantage is in a system of elements varying in size. For a uniform mesh, the procedure consisting in averaging the stresses may be more successful due to the fact that the stresses at a node can be as accurate as at the centroid. By taking an average the possibility of having a stress value extremely high or low is eliminated.

Another possible approach in determining the stress components is by applying finite difference operators. The strains at the nodes can be obtained from the approximate expressions for derivatives in terms of differences rather than from the assumed displacement function. The finite difference approach may be the most accurate since the difference expressions can be modified for higher precisions. The drawback of this approach is that it is not as flexible as the finite element technique when nonuniform mesh is encountered.

4.2.4 Linear Strain Rectangular Element

The derivation of the rectangular element properties follows the same general procedure as that used for the triangular element.

Displacement Function

To obtain a linear strain variation within the rectangular element shown in Figure 12. The displacements are taken to be bilinear in the x and y directions.

$$u = a_1 + a_2 x + a_3 y + a_4 xy \qquad 4.22$$

$$v = a_5 + a_6 x + a_7 y + a_8 xy$$

where the eight arbitrary coefficients can be found from the displacements of the four corners of the rectangle.

The displacement functions ensure the compatibility of displacements along a common boundary between adjacent elements. The first derivatives of the displacements are discontinuous across the common boundaries of adjacent elements.

Stiffness Matrix

The element stiffness matrix is readily given by

$$[K] = \frac{D}{12}\begin{bmatrix} K_1 & & & & & & & \\ K_2 & K_3 & & & & & & \\ K_4 & K_5 & K_1 & & \text{symmetric} & & & \\ -K_5 & K_6 & -K_2 & K_3 & & & & \\ K_7 & -K_2 & K_8 & K_5 & K_1 & & & \\ -K_2 & K_9 & -K_5 & K_{10} & K_2 & K_3 & & \\ K_8 & -K_5 & K_7 & K_2 & K_4 & K_5 & K_1 & \\ K_5 & K_{10} & K_2 & K_9 & -K_5 & K_6 & -K_2 & K_3 \end{bmatrix} \qquad 4.23$$

where

$$K_1 = 4b/a + \frac{2(1-2\nu)a}{(1-\nu)b} \qquad K_4 = -4b/a + \frac{(1-2\nu)a}{(1-\nu)b} \qquad K_7 = -2b/a - \frac{a(1-2\nu)}{b(1-\nu)}$$

$$K_2 = \frac{1.5}{1-\nu} \qquad K_5 = \frac{1.5(1-4\nu)}{(1-\nu)} \qquad K_8 = 2b/a - \frac{2a(1-2\nu)}{b(1-\nu)}$$

$$K_3 = 4a/b + \frac{2b(1-2\nu)}{a(1-\nu)} \qquad K_6 = 2a/b - \frac{2b(1-2\nu)}{a(1-\nu)} \qquad K_9 = 2a/b - \frac{b(1-2\nu)}{a(1-\nu)}$$

$$K_{10} = -4a/b + \frac{b(1-2\nu)}{a(1-\nu)}$$

Thermal Load Vector

The thermal load vector for a linear temperature variation within the element is given by

$$\{F_t\} = \frac{D(1+\nu)\alpha}{12(1-\nu)} \begin{bmatrix} -2b & -2b & -b & -b \\ -2a & -a & -a & -2a \\ 2b & 2b & b & b \\ -a & -2a & -2a & -a \\ b & b & 2b & 2b \\ a & 2a & a & 2a \\ -b & -b & -2b & -2b \\ 2a & a & a & 2a \end{bmatrix} \begin{bmatrix} t_1 \\ t_2 \\ t_3 \\ t_4 \end{bmatrix} \qquad 4.24$$

The thermal load vector F_t given in Equation 4.24 is restricted to a linear temperature variation which includes a uniform temperature change throughout the element.

4.2.5 Determination of Nodal Displacements

The thermoelastic problem of the beams is a continuation of the heat conduction problem. The same idealization of the cross-sectional area of the composite steel-concrete beam and of the T-beam was employed. The problem was analyzed by using the linear strain rectangular element. The numbering systems for these two sections remain unchanged. The problem can be reanalyzed by means of the linear strain triangular element which results from the division of rectangles.

The assembly of the elements follows generally the same process as discussed in the heat transfer problem. The relation between the thermal load vector and the nodal displacement vector are given by matrix equation 4.8 which is

$$\{F\} = [k]\{X\}$$

Since the resulting structure stiffness matrix is symmetrically and sparsely populated, it is sufficient to store, in the computer program, the upper sparse portion of the matrix. Once the boundary conditions have been incorporated in the set of Equations 4.8, these equations are solved for the nodal displacement vectors by Cholesky's square root method.

Boundary Conditions

In the assembled form, the structure stiffness matrix which represents half of the cross-sectional area of the beams, is singular. This implies that the idealized two-dimensional structure is not restrained against rigid-body motion (two translations and one rotation).

It is, therefore, necessary to apply constraints to the displacement nodes in order to eliminate these rigid body modes. The matrix then becomes non-singular.

If the beam, considered with its full cross-sectional area, were to expand or contract, the horizontal displacements of the particles would result in the direction away from the plane of symmetry, which is, where the y-axis passes through. Along the y-axis, the horizontal displacements are zero. In addition, the vertical expansion or contraction of the section requires a relative or fixed position from where the displacements would proceed. The fixed position, is chosen at the origin of the x,y coordinate system in Figures 10 and 10a and the vertical displacement at that node is zero.

These boundary displacement conditions can be incorporated in the resulting system of Equations 4.8 in two different ways. In the stiffness matrix K, the rows and columns corresponding to the zero displacement components are omitted. The corresponding coefficients in the load vector F are discarded as well. As a result, the dimensions of the stiffness matrix are reduced by the number of displacement components to be eliminated.

The other possible approach consists of setting the corresponding rows and columns equal to zero and then assigning a unit value in the main diagonal. The corresponding coefficients in the load vector are also set equal to zero. When the problem is solved for the nodal displacements, the zero displacements, prescribed at the nodes, appear as zero. This approach was used in the analysis

since it is the most convenient from a programming viewpoint. The first approach is advantageous when a large number of equations are to be deleted. With the reduction of the size of the stiffness matrix, a smaller memory core in the computer is required.

4.2.6 Calculation of Axial Stresses and Artificial Restraints

The axial thermal stresses, at any node in the idealized beams with its ends completely restrained against axial deformation, are given in Equation 4.3 which is

$$\sigma_z = \nu(\sigma_x + \sigma_y) - \alpha E t$$

The restraints, produced at the ends due to the restriction of axial temperature displacements, are determined as the resultant force and moment. The resultant force is the sum of the stress volume of each individual elements

$$P = \int_A \sigma_z \, dx \, dy \qquad 4.26$$

The resultant moment is given by summing the moments of the elements about the centroid of the idealized cross-sectional area of the beam

$$M = \int_A \sigma_z (y_b + y_c) \, dx \, dy \qquad 4.27$$

where y_b is the distance from the centroid of the section to the base of the rectangular element and the centroid of the rectangular stress volume, in which σ_1, σ_2, σ_3, σ_4 are the nodal stresses, is given by

$$y_c = \frac{b(\sigma_1 + \sigma_2 + 2\sigma_3 + 2\sigma_4)}{3(\sigma_1 + \sigma_2 + \sigma_3 + \sigma_4)}$$

For the right-angled triangle, the distance from the base (which is, from nodes 1 to 2) to the centroid of the stress volume is given by

$$y_c = \frac{c(\sigma_1+\sigma_2+2\sigma_3)}{4(\sigma_1+\sigma_2+\sigma_3)}$$

4.3 Force Restraint Problem

To find the stresses and strains produced by the force restraints in the thermal problem, a set of forces is applied on the end surfaces of the beams. The resultant of these forces is equal and opposite to that calculated in Equation 4.26. The solution gives the stresses at a sufficient distance from the ends. The results are superposed on the thermal solution.

4.3.1 Plane Strain Formulation

The axial resultant force applied on the end surfaces of the beam is considered to produce a uniform longitudinal strain throughout the depth according to the assumption that the plane cross section remains plane after deformation. This deformation and the accompanying stresses are determined in the plane strain formulation.

In the formulation of the problem, the beams are undergoing an assumed uniform longitudinal strain ε_A. The resultant force, required at the ends of the beams to prevent this strain ε_A to proceed, can be determined with the stresses and strains in the plane strain solution. From this nonthermal solution, the stresses and strains due to the resultant force applied on the ends of the beams in the restrained thermal problem can be obtained.

Writing the stress-strain relationship in terms of the uniform axial strain ε_A

$$\begin{aligned} \varepsilon_x &= \frac{1}{E}\left(\sigma_x - \nu(\sigma_y + \sigma_z')\right) \\ \varepsilon_y &= \frac{1}{E}\left(\sigma_y - \nu(\sigma_x + \sigma_z')\right) \\ \varepsilon_z - \varepsilon_A &= \frac{1}{E}\left(\sigma_z' - \nu(\sigma_x + \sigma_y)\right) \end{aligned} \qquad 4.28$$

The third equation of 4.28 is similar to the thermal stress-strain Equations 4.1 with the exception that ε_A replaces αt. The analysis can now be carried out as a plane strain problem where $\varepsilon_z = 0$ and the axial normal stress is given by

$$\sigma'_z = \nu(\sigma_x + \sigma_y) - E\varepsilon_A \qquad 4.29$$

The strains become

$$\varepsilon_x - \nu\varepsilon_A = \frac{1-\nu^2}{E}\left(\sigma_y - \frac{\nu}{1-\nu}\sigma_x\right)$$

$$\varepsilon_y - \nu\varepsilon_A = \frac{1-\nu^2}{E}\left(\sigma_x - \frac{\nu}{1-\nu}\sigma_y\right)$$

4.3.2 Energy Expression

The formulation of this problem follows the general procedure outlined in the thermal problem. The strain energy stored in an element can be expressed by

$$U = \frac{D}{2}\iint\left[(\varepsilon_x-\nu\varepsilon_A)^2+(\varepsilon_y-\nu\varepsilon_A)^2+\frac{2\nu}{1-\nu}(\varepsilon_x-\nu\varepsilon_A)(\varepsilon_y-\nu\varepsilon_A)+\frac{1-2\nu}{2(1-\nu)}\gamma_{xy}^2\right]dx\,dy$$

Considering the strain energy expression in two parts by writing it as

$$U = U_k + U_A$$

where U_k is given in Equation 4.6

and

$$U_A = \frac{1}{2}D\iint\left[\frac{-2\nu}{1-\nu}\varepsilon_A(\varepsilon_x+\varepsilon_y)+\frac{2\nu^2}{1-\nu}\varepsilon_A^2\right]dx\,dy \qquad 4.30$$

After minimizing and assembling the elements, the displacements can be obtained from

$$[K]\{X\} - \{F\} = 0$$

The assumption that plane transverse sections remain plane is retained. The axial strains throughout the section are equal to ε_A.

4.3.2 Lateral Contractions Load

The load vector of an element is established from the strain energy expression U_A. Taking into account only the quantities that contribute to the load vector, the strain energy expression reduces to

$$U_A = \frac{D}{2} \iint \frac{-2\nu}{1-\nu} \varepsilon_A(\varepsilon_x + \varepsilon_y)\, dx\, dy$$

The load vector of a rectangular element is readily given in matrix form

$$\{F_A\} = \frac{D}{12} \frac{6\nu\varepsilon_A}{1-\nu} \begin{bmatrix} -b \\ -a \\ b \\ -a \\ b \\ a \\ -b \\ a \end{bmatrix} \qquad 4.31$$

For triangular element

$$\{F_A\} = D[R]^T [T_1^{-1}]^T [k] \qquad 4.32$$

where $$k_i = \frac{\nu}{1-\nu} \varepsilon_A [m_i F(m_i-1, n_i) + q_i F(p_i, q_i-1)]$$

4.3.3 Stresses

$$\begin{bmatrix}\sigma_x\\ \sigma_y\\ \tau_{xy}\end{bmatrix} = \frac{E(1-\nu)}{(1+\nu)(1-2\nu)}\begin{bmatrix}1 & \frac{\nu}{1-\nu} & 0\\ \frac{\nu}{1-\nu} & 1 & 0\\ 0 & 0 & \frac{1-2\nu}{1-\nu}\end{bmatrix}\begin{bmatrix}\varepsilon_x\\ \varepsilon_y\\ \gamma_{xy}\end{bmatrix} - \frac{E\nu\,\varepsilon_A}{(1+\nu)(1-2\nu)}\begin{bmatrix}1\\ 1\\ 0\end{bmatrix}$$

--- 4.33

When the Poisson's ratio is constant throughout the section, the strains ε_x and ε_y are equal to $\nu\varepsilon_A$. The stresses σ_x and σ_y are then reduced to zero and the axial normal stresses given in Equation 4.29 become

$$\sigma_z' = -E\varepsilon_A$$

Interaction effect between the different materials occur when the beams are made of materials of different Poisson's Ratios. This gives rise to stresses σ_x and σ_y. These stresses are concentrated in the vicinity of the two different materials.

The normal axial stresses are expressed in terms of ε_A. The uniform axial strain ε_A, produced in the thermal problem if only uniform longitudinal deformation is permitted, can be determined by equating the axial resultant force of the nonthermal problem $P_A = \int \sigma_z' \, dx\, dy$ to that computed in Equation 4.26. The substitutions of the calculated uniform axial strain ε_A into the stress expressions give a solution for the stresses in the beams due to the artificial resultant force prescribed at the ends in the thermal problem.

4.4 Flexural Restraint Problem

This analysis is carried out in a similar manner as the force restraint problem. It is required to compute the longitudinal stresses and strains solely due to the resultant bending moment applied at the ends of the beam in the thermal problem.

4.4.1 Plane Strain Formulation

Complete restraint against bending is provided in the beams. These bending restraints at the ends prevent the transverse sections of the beam to rotate about the x-axis. This rotation is defined by the bending strain ε_B times Y where Y is the distance from the centroid of the section to the point at which the strain is considered. The stress-strain relations in terms of the linear longitudinal strain is

$$\varepsilon_x = \frac{1}{E}(\sigma_x - \nu(\sigma_y + \sigma_z''))$$

$$\varepsilon_y = \frac{1}{E}(\sigma_y - \nu(\sigma_x + \sigma_z'')) \qquad 4.34$$

$$\varepsilon_z - \varepsilon_B Y = \frac{1}{E}(\sigma_z'' - \nu(\sigma_x + \sigma_y))$$

Treating the problem as one of plane strain where $\varepsilon_z = 0$, the longitudinal bending stresses become

$$\sigma_z'' = \nu(\sigma_x + \sigma_y) - E\varepsilon_B Y \qquad 4.35$$

The strains are

$$\varepsilon_x - \nu\varepsilon_B Y = \frac{1-\nu^2}{E}\left(\sigma_x - \frac{\nu}{1-\nu}\sigma_y\right)$$

$$\varepsilon_y - \nu\varepsilon_B Y = \frac{1-\nu^2}{E}\left(\sigma_y - \frac{\nu}{1-\nu}\sigma_x\right)$$

The strain energy expression becomes

$$U = \frac{D}{2}\iint[(\varepsilon_x - \nu\varepsilon_B Y)^2 + (\varepsilon_y - \nu\varepsilon_B Y)^2 + \frac{2\nu}{1-\nu}(\varepsilon_x - \nu\varepsilon_B Y)(\varepsilon_y - \nu\varepsilon_B Y) + \frac{1-2\nu}{2(1-\nu)}\gamma_{xy}^2]\, dx\, dy$$

Separating the strain energy into two parts by rewriting it as

$$U = U_k + U_B$$

where U_k is given in Equation 4.6

and

$$U_B = \frac{D}{2}\iint[\frac{-2\nu}{1-\nu}\varepsilon_B Y(\varepsilon_x + \varepsilon_y) + \frac{2\nu^2}{1-\nu}\varepsilon_B{}^2 Y^2]\, dx\, dy \qquad 4.36$$

The minimization of the strain energy U for an assumed displacement function yields a system of solvable linear equations written in the following form

$$[K]\{X\} - \{F\} = 0$$

4.4.2 Lateral Contractions Load

The load vector of an element is obtained from the following terms in Equation 4.36. Rewriting, the equation becomes

$$U_B = \frac{D}{2}\iint \frac{-2\nu}{1-\nu}\varepsilon_B Y(\varepsilon_x + \varepsilon_y)\, dx\, dy$$

For rectangular element, the load vector in matrix form is

$$\{F_B\} = \frac{D\ \nu\varepsilon_B}{12\ (1-\nu)} \begin{bmatrix} -2b^2 \\ -3ab \\ -2b^2 \\ -3ab \\ 4b^2 \\ 3ab \\ -4b^2 \\ 3ab \end{bmatrix} + y_b\{F_A\} \qquad 4.37$$

and for the triangular element

$$\{F_B\} = D\,[R]^T\,[T_1^{-1}]^T\,[k] + y_b\{F_A\} \qquad 4.38$$

where

$$k_i = \frac{\nu\varepsilon_B}{1-\nu}\ m_i F(m_i-1, n_i+1) + q_i F(p_i, q_i)$$

4.4.3 Stresses

The stresses at any nodal points are given by

$$\begin{bmatrix} \sigma_x \\ \sigma_y \\ \tau_{xy} \end{bmatrix} = \frac{E(1-\nu)}{(1+\nu)(1-2\nu)} \begin{bmatrix} 1 & \frac{\nu}{1-\nu} & 0 \\ \frac{\nu}{1-\nu} & 1 & 0 \\ 0 & 0 & \frac{1-2\nu}{1-\nu} \end{bmatrix} \begin{bmatrix} \varepsilon_x \\ \varepsilon_y \\ \gamma_{xy} \end{bmatrix} - \frac{\nu E\ \varepsilon_B Y}{(1+\nu)(1-2\nu)} \begin{bmatrix} 1 \\ 1 \\ 0 \end{bmatrix}$$

---- 4.39

The stresses are expressed in terms of ε_B and the resultant moment applied at the end surfaces of the beam is given by the summation about the x-axis of moments produced by the restraining stresses σ_z'' in each element

$$M_B = \int_A \sigma_z''\ (y_b + y_c)\ dx\,dy \qquad 4.40$$

The strain ε_B, produced in the thermal problem if the ends are free from bending restraints only, are determined by equating the resultants in Equations 4.40 and 4.27. The value of ε_B is substituted into the stress expressions in order to give the restraining stresses due to the bending restraints applied at the ends of the beam in the thermal problem.

4.5 Solution for the Unrestrained Thermoelastic Beam

The solution of the thermoelastic problem for the beams having their ends free of external restraints is obtained by superposing on the solution of the restrained thermal problem the nonthermal solutions of the beam subjected to the resultants of the end restraints. According to Saint-Venant's principle, this is the solution at distances from the end smaller than the maximum cross-sectional dimension.

The axial normal stresses in the unrestrained beams are

$$\sigma_z = -\nu(\sigma_x + \sigma_y) - \alpha E t \quad -\sigma_z' \quad - \sigma_z'' \tag{4.41}$$

and the axial strains are

$$\varepsilon_z = \varepsilon_A + \varepsilon_B Y \tag{4.42}$$

The final thermal stresses in the beams with free ends were verified. The thermal stress systems are self-equilibrating.

CHAPTER 5

DISCUSSION OF RESULTS

5.1 Temperature

The temperatures recorded by the thermocouples, when the four distinct temperature conditions were imposed on the composite steel-concrete beam, are presented with the temperatures obtained using the linear temperature triangular element in Tables 1 to 3. Similarly, tables 4 to 6 exhibit the resulting temperatures that are pertaining to the reinforced concrete T-beam. From the finite element temperatures, a temperature field for each of the four different conditions has been plotted in Figures 14 to 21.

The finite element method provides a means to determine within the beams the temperature field which is required to compute the temperature stresses and strains. The finite element results can be comparable with those of experiment only when the surface conductance for the upper and lower surfaces of the reinforced concrete slab and the vertical surface conductance of the reinforced rectangular concrete beam are known to an accuracy of ±0.002 BTU/hr-ft-in-^{o}F. These values as well as the conductivity of concrete were calculated from the experimental temperatures. However, these properties fail to yield the desired accuracy. The finite element temperatures were determined by adjusting the approximate values of the surface conductance until the temperatures along the surfaces of the sections coincide with those in the experiment.

The systems of 1652 and 1097 equations resulting from the finite element idealization of the composite and T-beam respectively were solved using Cholesky's square root method in double precision.

The correction method was not required as the equations were solved to an accuracy of $\pm 0.00001^{\circ}F$. These systems of equations are ideal for solving by Cholesky's method. The main diagonal coefficients are the largest coefficients in its respective equations and only the sum of the off diagonal coefficients is equal in magnitude to its main diagonal coefficient.

As shown in Figures 14 to 17, the temperature variation at section 1-1 is one-dimensional and experiences no effect of the two-dimensional temperature variation produced in the vicinity of the center line by the steel beam which behaves, according to the theory of heat conduction, as a fin. The fin, as mentioned previously, increases the heat exchange between the surface of the slab and the ambient air. In other words, the variable surface temperature of the slab will become, as approaching the steel beam, increasingly closer to the ambient air temperature to which the lower surface of the slab is exposed. This effect is illustrated by the isotherms in Figures 14, 15 and 17. The increasing number of isotherms in the vicinity of the center line of the concrete slab indicates an increase in heat flow through the thickness. This implies that the temperature differential between the two surfaces of the slab is larger at the center line than at the edge (section 1-1). The temperature variation through the thickness of the slab is linear except for the sections where the reinforcing bars are embedded as indicated by the noticeable sharp variations in the isotherms. It can be seen in the temperature variation across the width of the slab that half of the slab would bend about the center line if the adjacent half did not prevent it.

The material of high conductivity has a lower temperature gradient as shown in the temperature profile at the center line. The stresses, produced in the composite beam which has a different temperature differentials

in the steel beam and slab, are not as large as would be if the materials had identical coefficients of expansion. The curvature of the concrete slab having a greater temperature differential and a lower coefficient of expansion can be equivalent to the curvature of the steel beam having a smaller temperature differential and a higher coefficient of expansion. This type of construction is ideal for this nonuniform temperature distribution as the thermal stresses, induced by the unmatched curvatures whose difference is not as large, are lowered. Stresses are produced by the nonlinear temperature in the steel beam as well.

A two-dimensional temperature variation, as shown in the composite beam, does not reoccur in the identical reinforced slab of the T-beam. The isotherms in Figures 18 to 21 are very near horizontal straight lines. It can be concluded that the rate of heat flow through the depth at any sections from section 1-1 to the section at the center line is identical for the steady temperature field in Figures 18, 19 and 21. That is, the rectangular concrete beam of a low thermal conductivity does neither increase or decrease the heat flow. The temperature distribution in the T-beam can be analyzed as a one-dimensional heat conduction problem. Figure 20 presents the case where the rectangular concrete beam decreases the heat transfer in the slab.

The uniform temperature across the width of the T-beam does not tend to bend the half section about the center line. Stresses will be induced mostly from the different temperature differentials of the reinforced concrete slab and of the reinforced concrete beam which, in addition, has a nonlinear temperature variation. Examining the temperature profile at the center line, no sharp temperature variations occur in the area where the reinforcing

wires D15 are embedded. In that region, the temperature profile is smooth and the stresses will be caused by the difference in the coefficients of expansion. A series of thermocouples, placed at $10\frac{1}{2}$ and $23\frac{1}{2}$ inches from the ends of the beams has ensured that the temperature is uniform along the length of the beams except near the ends.

The tests, conducted on the composite beam subjected to forced convection CS-7 and CS-9, were not successful as expected. The purpose of the investigation was to apply a symmetric temperature variation about the center line. Having the upper surface cooled by a cross flow of air has produced a unsymmetric temperature distribution. A temperature difference of $4^{o}F$ was recorded on the upper surface at 10 3/8 inches from the center line. Such discrepancy was caused by the velocity drop of the blown air across the width of the slab and by the obstruction of air flow in the vicinity of the strain gauges.

Location of Embedded Thermocouples

Only the surface temperatures as well as the ambient air temperatures registered by the thermocouples are given in Tables 1 to 6. Temperature readings within the beam are not presented since the exact locations of these thermocouples are unknown. It is extremely difficult to assure that the embedded thermocouples at a specific location were not displaced during the placing of concrete. These locations of the thermocouples could have been measured accurately by simply cutting with a diamond saw the concrete beam at the plane of thermocouple layout after the experimental investigation has been completed.

Comparison of Results Using Lumped and Consistent Convective Matrix

The difference, in using the lumped or consistent convective matrix on the results obtained from the fine mesh size given in Figures 10 and 10a, is $0.005^{o}F$. Because of such a fine mesh, both matrices yield answers that are very close to the exact solution. The difference between the two convective boundary representations may be seen in a coarser mesh where the solutions are not as close to the exact one.

Comparison of Triangular and Rectangular Element Solution

The rectangular and triangular element idealizations yield a difference of $0.005^{o}F$ in the resulting temperatures. Again, an assessment of the elements, based on such idealization, cannot be made. The superiority of an element over the others is assessed in many ways. The choice of using a particular element depends mainly on the nature of the problem. In addition, it is desired to have an element that has a high rate of convergence and, at the same time, yields a small number of equations such that the computer storage is not exceeded.

Alternate Approach in Dealing with Surface Conductance

The procedure, in evaluating the vertical surface conductance of the steel web in the steel beam 10 X 4 B15, is adequate as no adjustment of the value was done. As for other surface conductances, these properties are not needed as an alternate procedure can be used. The surface temperatures measured with thermocouples can be plotted. From the plotted curves, the temperature for each surface node in the finite element idealization can be specified to the nodal points to determine the temperature field.

5.2 Thermoelasticity Solution

General

The corresponding experimental and finite element strains to the temperature conditions imposed on the composite steel-concrete beam are presented in Table 7. The strains in the reinforced concrete T-beam are given in Table 8. The analytical strains were obtained using the linear strain rectangular elements.

The reference temperature TR given in these tables is a uniform temperature of the beams prior to being subjected to the four different temperature conditions. This is the temperature at which the beam is considered to be in the state of free thermal stress and strain. Thermal deformations were measured and calculated in the beams that were subjected to any change in temperature from the reference temperature TR. In reality the reference temperature is the temperature at which the concrete has hardened.

When the composite steel-concrete beam is subjected to the temperature conditions CS-14 and CS-15 and the reinforced concrete T-beam to the temperature conditions T-8 and T-9, the temperatures in the beams are below the true reference temperature. The steel and concrete elements, which are assumed to be isotropic, will deform in different amount. Examining the contractions of the elements in the xy plane, the embedded steel, in the concrete such as the reinforcing wires and the top flange of the steel beam, will contract more than the surrounding concrete which has a lower coefficient of expansion. In this respect, no forces in the x and y directions are

developed between the dissimilar materials and the σ_x and the σ_y, in Equation 4.3, due to the interaction of the different materials, are zero at the interface of steel and concrete elements. However, these stresses σ_x and σ_y can still be induced in the concrete and in the steel by nonlinear temperature distributions. Complete intereaction between the reinforcing rods and the concrete in the z-direction does not exist as slippage occurs. Slippage may even occur between the top steel flange and the concrete despite the interconnection by the shear connectors. The finite element technique fails to take into account this separation of steel and concrete and treats the cooled beam problem in the similar manner as a heated beam problem in which the displacements at the boundaries of concrete and steel elements are compatible. This neglected effect in the finite element analysis of the cooled beam problem deviates the results from the exact solution.

Effects of Heat on Strain Gauges

The calculations of the contraction or expansion of the 10 inch aluminium rods have introduced errors in the measured surface deformations. The aluminium rods, exposed to ambient air temperature, are not undergoing a uniform temperature along its length as considered. These rods are fixed at one end to the beam surfaces by an aluminium mounting of very high thermal conductivity 117 BTU/hr-ft-^{o}F. Heat is transmitted through the mounting to the aluminium rod which has a nonuniform temperature distribution along its length. The interpretation of a uniform temperature distribution in the aluminium rods of high coefficient of expansion approximately 12.8 in/in/^{o}F will introduce error in the experimental measurements. The measurements, recorded by the gauges that were covered with melting ice, are considered

to be more accurate since the aluminium rods are subjected to a uniform temperature. In this investigation, it is desirable to have the rods made of Invar and the mountings of low thermal conductivity material.

On Finite Element Method

The assembly of linear strain rectangular elements into a representation of the composite section as shown in Figure 10 yields a total of 3304 equations with a half band width of 26 columns. These equations require a computer storage space of 410,000 bytes in single precision. In the rectangular idealization of the T-beam as shown in Figure 10a, the resulting structure stiffness matrix K, which is a 2194 by 44 matrix, requires a single precision storage capacity of 460,000 bytes in the computer. In solving the system of equations using of Cholesky's square root method, the coefficients of these equations were stored in single precision and the arithmetic operations were performed in double precision. The correction method, which is presented in Appendix A, was repeated five times.

The numerous repetitions of the correction method gives an indication of the accuracy of the results before the correction method has been applied. This correction method causes the results to converge to a certain degree of accuracy and then the results oscillate with no improvement in accuracy as the correction method is repeated. However, the results are sufficiently accurate to show the stress variation due to the various temperature conditions imposed on the beams. The results of the composite beam problem are more accurate than those of the T-beam problem. In a matrix of smaller band width, there are fewer arithmetic operations that produce roundoff errors.

There is a fallacy in the finite element idealization of the composite section in Figure 10. At the node situated in the lower corner of the top steel flange, the nodal vertical displacement v of the steel element and that of the concrete element should be separated. When the beam is subjected to a change in temperature, the particles on the surface edges of steel flange and those adjacent in the concrete displace independently of each other. To rectify this idealization, these nodal displacements can be detached from their adjacent elements by simply assigning the displacements to two nodes, one in the steel element and the other in the concrete element. The horizontal displacements u along that boundary remain compatible. The error, introduced by disregarding such effect, is negligible for such a fine mesh.

The solution, using linear strain triangular element in the idealizations shown in Figures 10 and 10a, was not obtained due to the limited storage capacity of 512,000 bytes in the computer. The number of equations resulting from the triangular idealizations is close to twice the number of equations in the rectangular idealizations. Even if the computer could accomodate such a large number of equations in single precision, the solution, obtained using Cholesky's square root method, will be meaningless due to the numerous roundoff errors.

Stresses and Strains due to Temperature Differentials

The experimental longitudinal stresses were not determined since the calculation of these stresses from the measured surface deformations are not wholly correct for these beams. These experimental longitudinal stresses would be related to only the applied temperature distribution throughout the depth and the measured longitudinal strains. Thus, the

stresses σ_x and σ_y are neglected. It is for this reason that only the experimental strains with those of the finite element method were presented.

Tables 9a to 12b present the longitudinal stresses as well as the strains obtained using linear strain rectangular element. These stresses and strains were computed for beams subjected to temperature differentials only and not to the temperature changes from the reference temperature of the beams prior to the tests. These temperature differentials were based on the lowest nodal temperature in the cross section of the beams and the temperature is denoted in the tables by TL or TU, which it may be either at the lower or upper surface of the beams. In addition, the stresses and strains due to a constant temperature change of 10^{o}F in the beams are presented such that the stresses or strains produced from a temperature change can be readily obtained by combining the stresses or strains due to the temperature differentials with those given for uniform temperature change.

To show the effect of the stresses σ_x and σ_y on the longitudinal stresses, only the stresses, in the composite steel-concrete beam subjected to a uniform temperature change of 10^{o}F and having its ends completely restrained against longitudinal expansion, will be discussed. At the edges of the reinforced concrete slab, the σ_x and σ_y are equal to zero and the longitudinal stresses σ_z in Equation 4.3 are reduced to $-\alpha_c E_c t$ which is - 206.25 psi. In the vicinity of the reinforcing steel, the wires, having its expansion in the x and y directions partially restrained by the surrounding concrete, experience compressive stresses σ_x and σ_y. The compressive stresses σ_z, in the steel, are increased while those in the surrounding concrete are slightly relieved. Similar effect occurs in the vicinity of the embedded steel flange. If the σ_x and σ_y are neglected, the longitudinal

stresses, in the steel flange, are -1950 psi. These compressive stresses σ_z along the interface are increased due to the compressive σ_x. At the centerline, the stress σ_z on the upper surface of the steel flange is -2011 psi where Poisson's ratio of concrete is 0.15. In the adjacent concrete, the tensile σ_x diminishes σ_z to - 195.9 psi and on the upper surface of the reinforced concrete slab the compressive σ_x increases σ_z to -211.7 psi.

The stresses σ_x and σ_y, which were discussed, are produced solely due to the difference in coefficients of expansion of the steel and concrete. These stresses can become more significant when the beams are undergoing a nonuniform temperature distribution through its depth.

In the nonthermal problems, the stresses σ_x and σ_y that result from the difference of Poisson's ratio of steel and concrete, are small as compared to those in the restrained thermal problem. The difference in Poisson's ratios has a similar effect as the difference in the coefficient of expansion. The Poisson's ratio of concrete, which is smaller than the steel, partially restrains the lateral deformation of steel when the beams are subjected to external load. When the Equations 4.3, 4.29 and 4.35 are combined, the final stresses σ_x and σ_y are slightly reduced from those in the restrained thermal problem.

Effect of Different Poisson's Ratio for Concrete

As the Poisson's ratio for concrete becomes closer to that of steel, the interference of lateral deformations in the two materials is decreased. If the Poisson's ratio of concrete is 0.18 in the composite steel-concrete beam which has its ends completely restrained and is subjected to a uniform temperature change of $10^{\circ}F$, the longitudinal stresses at the center line are -208.3 psi on the upper concrete surface and -196.8 psi

in the concrete at the interface of steel and concrete. The stress σ_z, given for concrete having Poisson's ratio 0.15 are -211.7 and -195.9 psi. As the Poisson's ratio is increased, the stresses σ_z become closer to -206.25 psi which is the stress computed as $\alpha_c E_c T$. This stress variation gives an indication of the accuracy of the equation solver with the correction method. It is the author's opinion that the system of equations is solved to an accuracy of ±1 psi for the stresses given in concrete.

The streses, given in Tables 10a, b and c for the composite beam which is subjected to different temperature differentials, follow a general pattern as the Poisson's ratio for concrete is varied. For temperature differentials having negative gradients, the stresses at the upper surface of the slab increase in tension while at the lower surface of the slab the stresses increase in compression. The stress pattern is reversed for positive temperature gradients. No conclusion is drawn from the stress variations for different Poisson's ratios of concrete in the T-beam since the results may be influenced by the round-off errors committed when solving the system of finite element equations.

It is difficult to reach a conclusion on the variation of the resultant restraints acting on the beams of different Poisson's ratio. The variation of Poisson's ratio affects the magnitude of σ_x and σ_y. The longitudinal strains and the resultants forces are computed from the σ_z which is a function of the transverse stresses. The resultants do vary with different Poisson's ratio. The variation of the resultants and the strains (as shown in Tables 7, 8, 9 and 11) is too small to arrive at a conclusion that can be mislead by the round-off errors in the results.

For the composite beam having the Poisson's ratio of concrete as 0.12, 0.15, and 0.18, the resultant axial force, which prevent a longitudinal

strain ε_A, is given as 1976, 1977, and 1977 $abE_c\varepsilon_A$ respectively. The resultant bending restraints are computed as 22444, 22462, and 22480 $abE_c\varepsilon_B$ respectively. The area and moment of inertia of the equivalent section is 1976ab and 22462ab. For the T-beam, the restraining resultant force is 1156, 1156, and 1155 $abE_c\varepsilon_A$ respectively and the restraining resultant moment is 19807, 19788, and 19778 $abE_c\varepsilon_A$ respectively. The section has an equivalent area of 1155ab and moment of inertia of 19761ab.

When the boundary conditions were imposed on the half section, the concrete slab was permitted to take on a anticlastic curvature resulting from transverse strains as it occurs in a narrow beam. In bending, a thin wide plate retains a straight surface in cross section except at the edge regions where the plate curves slightly. Because of the straight surface across the width, the stiffness of a slab in bending is greater than that of a narrow beam. The stiffness increases with an increase of Poisson's ratio for the slab.

Effect of Temperature Distribution on Stresses

The contours for the unrestrained longitudinal stresses which are produced by the temperature differentials whose isotherms have been previously presented, are given in Figures 22 to 31. These stress contours follow very closely the patterns outlined by the isotherms.

In Figures 22 and 25, the stresses, as predicted by the beam theory, are distributed linearly through the depth of the steel beam that undergoes uniform temperature change . For nonlinear temperature distributions, the steel beam is stressed nonlinearly.

The temperature distributions, as shown, tend to produce a greater flexural effect in the concrete slab than in the steel beam. With a lower coefficient of expansion for concrete, the bending of the slab is reduced

and the stresses as well, as indicated in Tables 9a to 10c. However, this may not always be the case for bridges exposed to seasonal temperatures. The steel beam, reacting to the sudden change in temperature more quickly than the concrete, will undergo a larger temperature change and due to the larger difference of the two coefficients of expansion, the stresses will increase.

Closure

The agreement between the experimental and analytical strains are generally good considering the fact that comparatively short beams were built for this investigation (i.e. 62 inches in length to a width of 35.4 inches in the concrete slab). The results obtained in this analysis are for sections at approximately 4 times the maximum cross-sectional dimension.

CHAPTER 6

Conclusions

The work represents an attempt to predict with a reasonable degree of certainty how model concrete and composite bridges behave under various steady temperature conditions. For given temperature boundary conditions, an accurate two-dimensional temperature distribution over the cross section of a complex bridge can be determined using linear finite elements. In addition, it can be seen from the results that the finite element method can be used to accurately determine the stress distribution in concrete and composite beams when subjected to various temperature conditions.

From the stress distributions produced by the various temperature distributions, the nonuniform temperatures and mainly the nonlinear temperatures are most severe on the beams. Results indicate that the stresses are not large enough to overstress the concrete in compression but they certainly can produce tension cracks in concrete. The critical regions in the concrete of the composite beam are shown to be in the vicinity of the embedded steel flange, which are, at the interface of steel and concrete and at the upper surface of the slab. Steel reinforcement should be provided within these regions in order to prevent complete separation of the concrete when cracked. It is the steel beam that exerts such force on the concrete slab that can be stressed to a greater extent in cases where larger steel beams or girders are used.

In the reinforced concrete T-beam, high stress concentrations, as shown, are localized at the center line such as, on the upper surface, at approximately mid-depth of the section and in the vicinity of the reinforcing wires D15 at the bottom.

The stress pictures are magnified in prototypes. In the cases of thicker concrete slabs and beams, greater temperature differentials usually exist and larger stresses as well.

The thermal effect can be detrimental when coupled with other forces that were not considered in this investigation such as, creep under stress, shrinkage, dead loads, and live loads. The thermal stresses can be additive numerically to dead and live loads stresses only for those problems that are based on the assumption of linear elasticity.

Recommendations for Further Study

Solutions to larger systems of equations will enable the sections of the beams to be idealized into systems of smaller elements. As the elements become smaller, the accuracy of the results can be established. With this large equation solver, a solution, for the idealization, presented in this investigation, of a system of linear strain triangular elements, can be obtained. The results of the triangular and rectangular element can be compared.

With the available storage capacity at the present time, the composite section and the T-beam can be reanalyzed using constant strain triangular element. From the obtained nodal displacements, the stresses can be computed by difference operators as previously mentioned. In the idealization of the T-beam, the number of equations would be half of the number as that in the rectangular idealization due to the numbering system of the nodes.

In the case of the anticlastic curvature in the concrete slab as previously discussed, the curvature can be restrained easily. Instead of having the x-axis passing through the bottom of the beams, it can be directed along the upper surface of the reinforced concrete slab. The vertical displace-

ments along this axis are set equal to zero except near the edge of the slab.

This investigation of thermal effect can be extended to simple span as well as continuous span bridges made of either composite beams or T-beams placed side by side to form a roadway.

Further research is required in order to predict transient temperatures which is the most realistic temperature conditions to which the bridges are exposed. Once these temperatures are determined, the deformations and stresses can be computed by the method presented in this investigation only if the effect of coupling between the displacements and temperatures is disregarded.

References

1. Timoskenko, S. P. and Goodier, J. N., "Theory of Elasticity", McGraw-Hill, New York, 2nd ed., 1959.

2. Gatewood, B. E., "Thermal Stresses", McGraw-Hill, New York, 1957.

3. Boley, B. A. and Weiner, J. H., "Theory of Thermal Stresses", John Wiley and Sons, New York, 1960.

4. Zuk, W., "Thermal and Shrinkage Stresses in Composite Beams"' J. of American Concrete Institute, Proc. v. 58, No. 3, September 1961.

5. Zuk, W., "Thermal Behaviour of Composite Bridges - Insulated and Unisulated", Highway Research Record, No. 76, 1965, pp. 231-253.

6. Berwanger, C., "A Continuous Steel-Concrete Bridge Prestressed by deformations at the Interior Supports", Second International Symposium on Concrete Bridge Design, SP26-33, ACI, Detroit, 1971.

7. Turner, M. L., Clough, R. W., Martin, H. C., Topp, L. J., "Stiffness and Deflection Analysis of Complex Structures", J. of Aeronautical Sciences, Vol. 23, No. 9 September 1956, pp. 805-823.

8. Gallagher, R. H., Padlog, J., Bijlaard, P. P., "Stress Analysis of Heated Complex Shapes", American Rocket Society Journal, May 1962, pp. 700-707.

9. Weber, J. P., "Plates in Plane Stress by the Finite Element Displacement Method", J. of Strain Analysis, v. 2, No. 1, 1967.

10. Cowper, G. R., Kosko, E., Lindberg, G. M., and Olson, M.D., "A High Precision Triangular Plate-Bending Element", NRC, NAE Aero. Report LR-514, National Research Council of Canada, December 1968.

11. Zienkiewez, O. C. and Cheung, Y. K, "The Finite Element Method in Structural and Continuum Mechanics", McGraw-Hill, New York, 1967.

12. Wilson, E. L. and Nickell, R. E., "Application of the Finite Element Method to Heat Conduction", Nuclear Engineering and Design, v.4, October 1966.

13. Sarkar, A. F., "

    M.A.Sc. Thesis, 1972, University of Ottawa.

14. Berwanger, C., "The Modulus of Concrete and the Coefficient of Expansion and Reinforced Concrete at Below Normal Temperatures", J. of American Concrete Institute, January 1972.

15. Lenzt, A. E., and Monfore, G. E., "Thermal Conductivity of Concrete at Very Low Temperatures", J. of Portland Cement Association Research and Development La-oratories, v.7, No. 2, May 1965.

16. Campbell-Allen, D. and Thorne, C. P., "The Thermal Conductivity of Concrete", Magazine of Concrete Research, v. 15, No. 43, March 1963.

17. Thompson, N. E., "A Note on the Difficulties of Measuring the Thermal Conductivity of Concrete", Magazine of Concrete Research", v. 20, No. 62, March 1968.

18. Brewer, H. W., "General Relation of Heat Flow Factors to the Unit Weight of Concrete", J. of Portland Cement Association Research and Development Laboratories, v. 9, No. 1, January 1967.

19. AISC Standards, "Manual of Steel Construction", American Institute of Steel Construction, New York, 6th ed. 1966.

20. ASTM Standards, "Structural and Boiler Steel; etc.", Part 4, American Society for Testing and Materials, Philadelphia, Pa., 1968.

21. ASTM Standards, "Concrete and Mineral Aggregates", Part 10, American Society for Testing and Materials, Philadelphia, Pa., 1968.

22. Berg, P. N., "Calculus of Variation", in 'Handbook of Engineering Mechanics', Chap. 16, ed. W. Flügge, McGraw-Hill, 1962.

23. Fujino, T. and Ohsaka, K., "The Heat Conduction and the Thermal Stress Analysis by the Finite Element Method", presented at the 2nd Conference on Matrix Methods Analysis, WPAFB, Ohio, October 1968.

24. Jakob, M., "Heat Transfer", Vol. 1, John Wiley and Sons, New York, 1949.

25. ACI Manual of Concrete Practice Part 2, "Structural Design, Structural Specifications, Structural Analysis", American Concrete Institute, 1968.

26. Ngo, D. and Scordelis, A. C., "Finite Element Analysis of Reinforced Concrete Beams", J. of American Concrete Institute, v. 69, No. 3, May 1967.

27. Faddeeva, V. N., "Computational Methods of Linear Algebra", Dover Publications, Inc., New York, 1959.

28. Salvador, M. C. and Baron, M. L., "Numerical Methods in Engineerings", Prentice-Hall, Inc., Englewood Cliffs, N.J., 1962.

29. Ramstad, H., "Convergence and Numerical Accuracy with Special Reference to Plate Bending", in 'Finite Element Methods in Stress Analysis', Tapir, Trondheim, Norway, 1969.

APPENDIX A

Solution to Symmetric Band Matrix by Cholesky's Square Root Method

The procedure for solving a system of N linear equations by Cholesky's square root method is carried out in detail as given in numerical textbooks (27 and 28). The set of linear equations is represented in matrix form

$$[K]\{X\} = \{F\} \qquad A.1$$

where the symmetric and sparse coefficient matrix K has a half band width of NUBW. It is only necessary to store the upper portion of the matrix in the computer program.

The matrix K can be transformed into the product of two matrices such that

$$[K] = [L]^T[L] \qquad A.2$$

where $[L]$ is the upper triangular band matrix and $[L]^T$ is its transpose.

Details of this development, which is referred to as triangularization, are given as follows

$$L_{1,1} = \sqrt{K_{1,1}}$$

$$L_{1,j} = \frac{K_{1,j}}{L_{1,j}} \qquad 1<j\leq NUBW$$

$$L_{i,1} = \sqrt{K_{i,1} - \sum_{n=1}^{i-1} L_{i-n,n+1}^2} \qquad n<NUBW$$

A negative or zero value will occur within the square root function when the matrix K is said to be ill-conditioned. This implies that the structure is unstable.

$$L_{i,j} = \frac{K_{i,j} - \sum_{n=1}^{i-1} L_{i-n,n+1} L_{i-n,j+n}}{L_{i,1}} \qquad \begin{matrix} 1<j\leq NUBW \\ n<NUBW \end{matrix}$$

Combining Equations A.1 and A.2, the system of equations to be solved can be written as

$$[L]^T[L]\{X\}=\{F\} \qquad A.3$$

Letting $[L]\{X\}=\{X^*\}$ A.4

such that Equation A.3 can be written as

$$[L]^T\{X^*\}=\{F\} \qquad A.5$$

The unknown vector X^* can be obtained by forward substitutions. The vector X can now be solved in the system of Equations A.4 by backward substitutions.

Details of both substitutions are outlined. The forward substitution procedure is described as follows

$$X_1^*=\frac{F_1}{L_{1,1}}$$

$$X_i^*=\frac{F_i-\sum_{n=1}^{i-1} L_{i-n,n+1}\,X_{i-n}^*}{L_{i,1}} \qquad \begin{matrix}1<i\\ n<NUBW\end{matrix}$$

The vector {X} is generated by the backward substitution

$$X_N=\frac{X_N^*}{L_{N,1}}$$

and

$$X_{N-i\ 1}=\frac{X_{N-i+1}^*-\sum_{n=1}^{i-1} L_{N-i+1,n\ 1}\,X_{N-i+n+1}}{L_{N-i+1,1}} \qquad \begin{matrix}1<i\\ n<NUBW\end{matrix}$$

In general, Cholesky's method leads to an efficient and very fast computer program for the solution of a large number of equations. Unfortunately, for a large system of equations with a large band width, the arithmetic operations become numerous and the round-off error may accumulate in such a manner as to produce considerable error in the solution. Ramstad(29) has discussed the rounding errors introduced in the triangularization. It is in that stage that the major part of the rounding errors is produced.

Improvement of Accuracy

The results, denoted by X^1, can be easily verified by the multiplication of K by X^1 where, as given by Equation A.1, the product is equal to F. Due to rounding errors committed when solving the system of equations, the differences between the results of the multiplication and F are evaluated as

$$\{\Delta F^1\} = \{F\} - [K]\{X^1\}$$

The solution of the system of linear equations can be improved. The error, produced in each coefficient of the column matrix X^1 to cause $\{\Delta F^1\}$, is obtained as the solution of the system of equations.

$$[K]\{\Delta X^1\} = \{\Delta F^1\}$$

The calculated incremental vector $\{\Delta X^1\}$ is then added to the previous solution such that the corrected answers are

$$\{X^2\} = \{X^1\} + \{\Delta X^1\}$$

The accuracy of X^2 can be verified in a similar manner as given for X^1. If the solution is not sufficiently accurate, the correction method can be repeated until the desired accuracy has been achieved.

The accumulated round-off errors can be reduced when the system of linear equations is solved in double precision with the computer. The computer storage for a double precision program is nearly twice the size as that for a single precision program. The number of equations involved in the problem and the desired degree of accuracy of the solution is controlled by the available computer storage. In problems where the computer cannot store the required number of equations in double precision but only in single precision, these equations can be solved with only the arithmetic operations executed in double precision. This solution is not as accurate as the double precision solution. Thus, the correction method is required to be repeated more frequently.

APPENDIX B - FIGURES

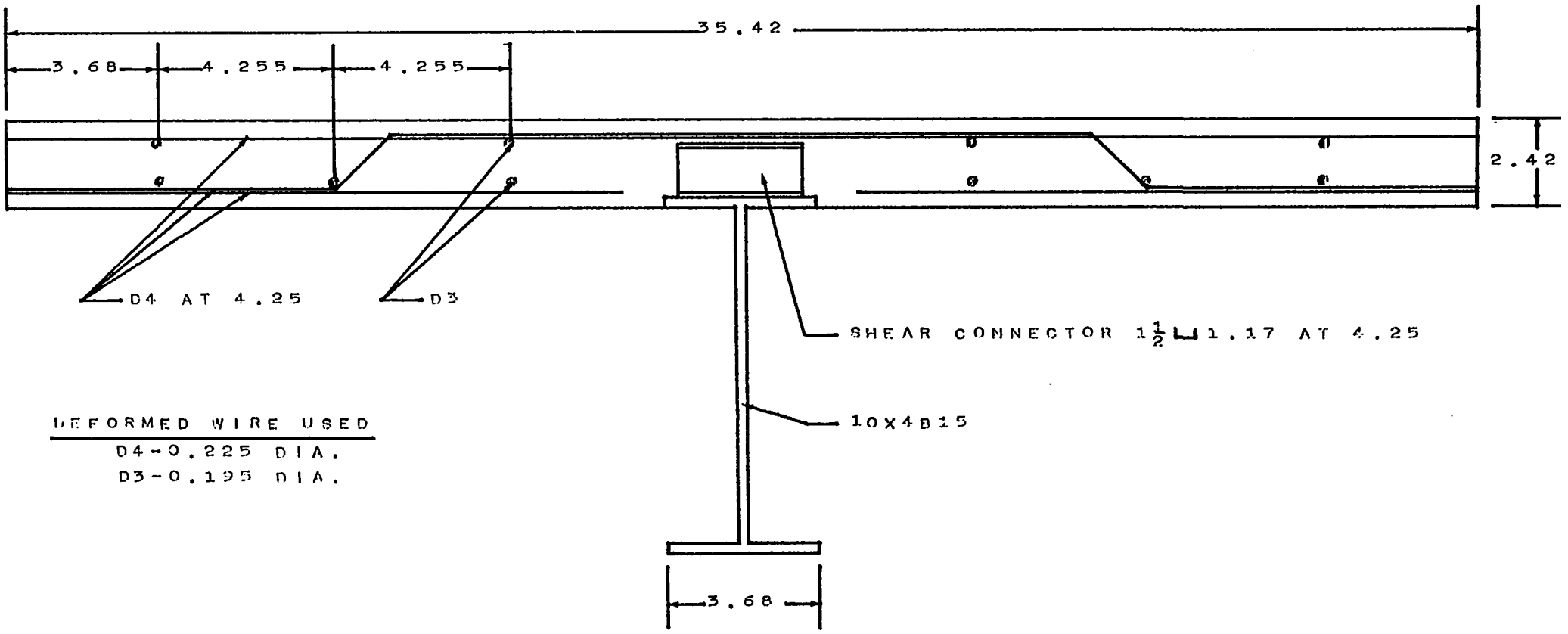

DEFORMED WIRE USED
D4-0.225 DIA.
D3-0.195 DIA.

SCALE 1=3.5

FIG.1 -COMPOSITE SECTION

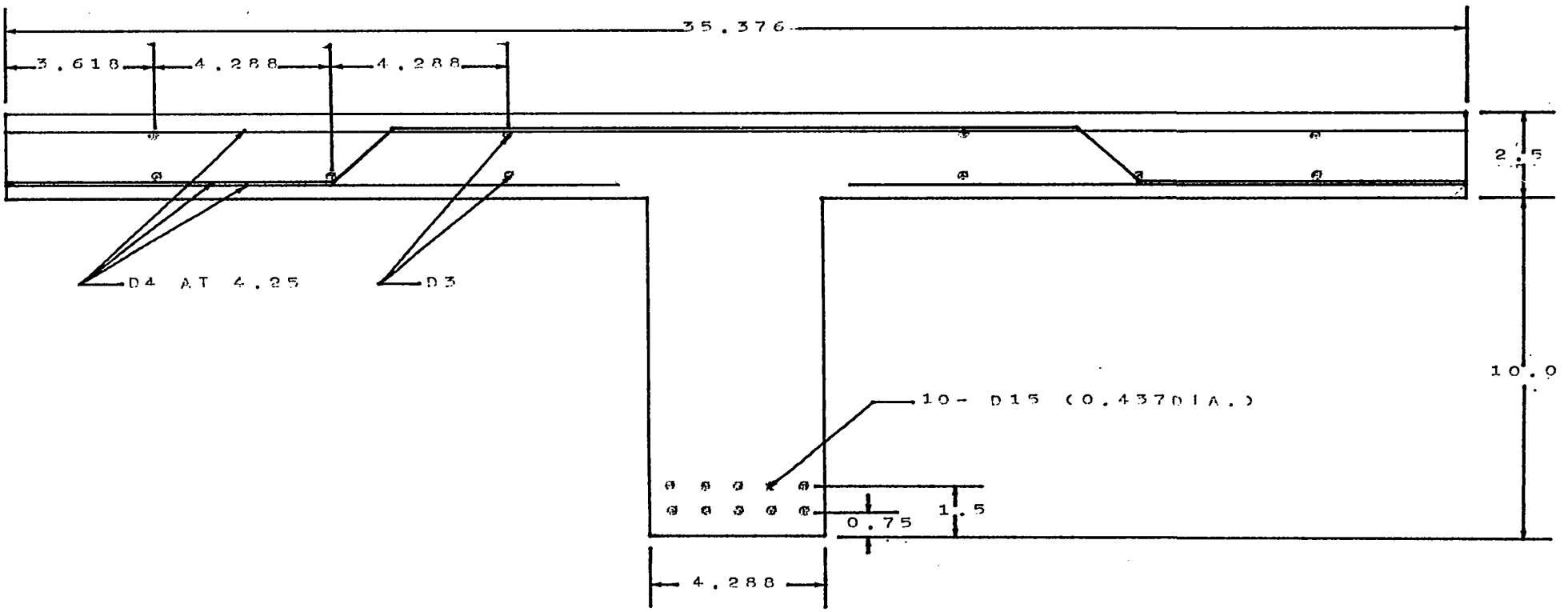

FIG.1A -REINFORCED CONCRETE T-BEAM

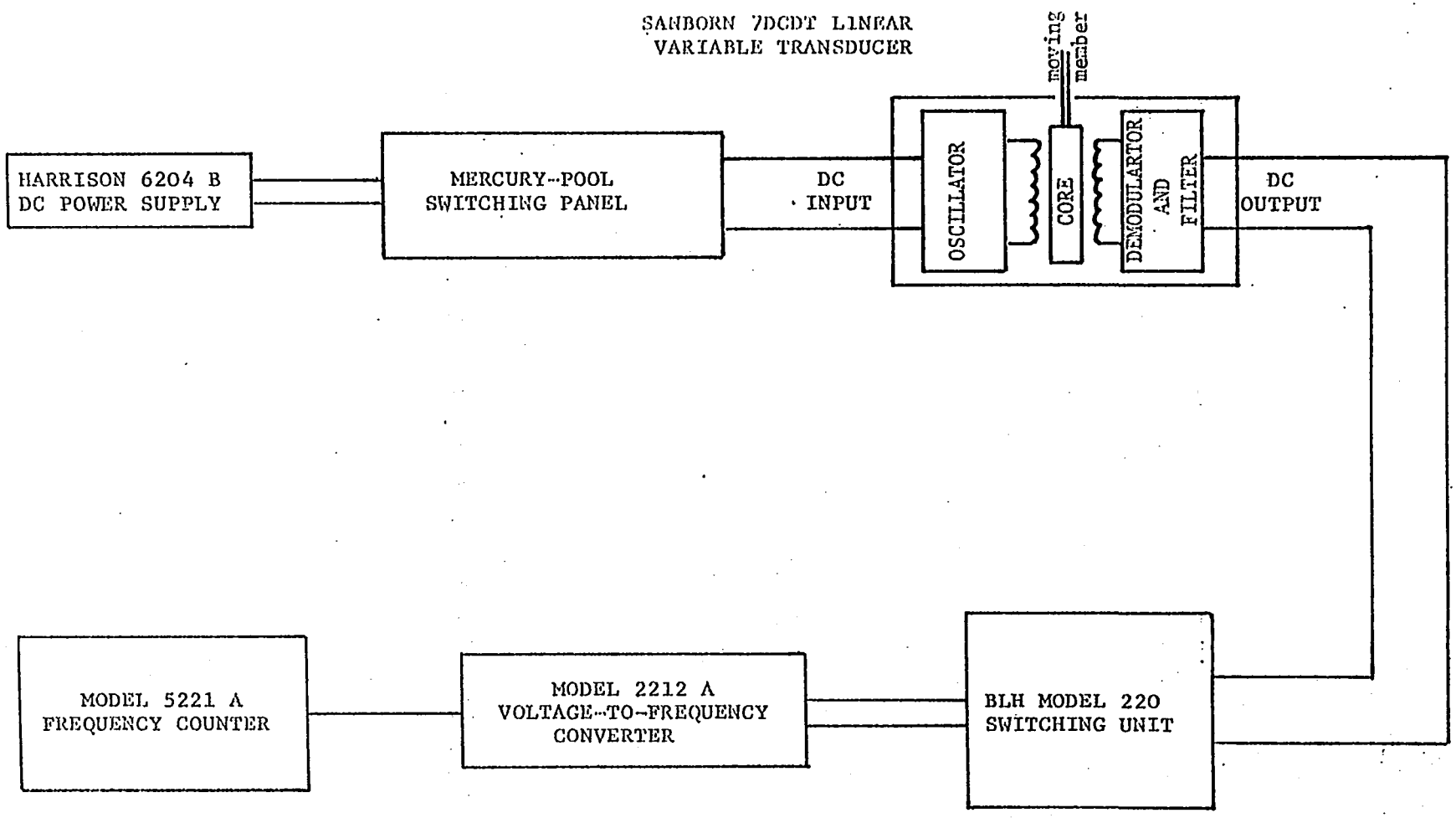

FIG. 2 SCHEMATIC LAYOUT OF MEASURING DEVICES

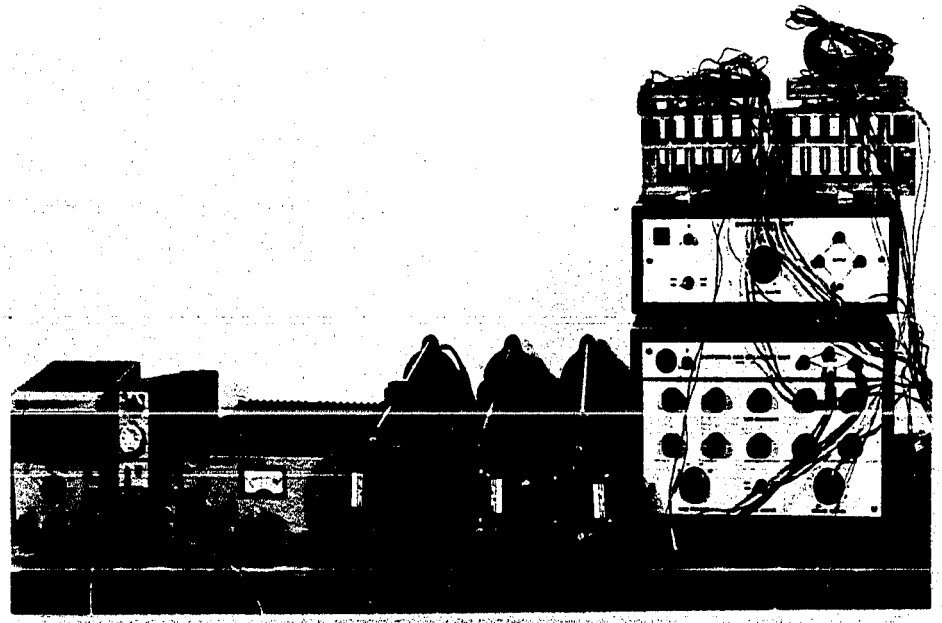

FIG. 3 MEASURING DEVICES

From left to right: frequency counter, voltage-to-frequency converter, DC power supply, three rheostats, mercury-pool switching panel on two switching units.

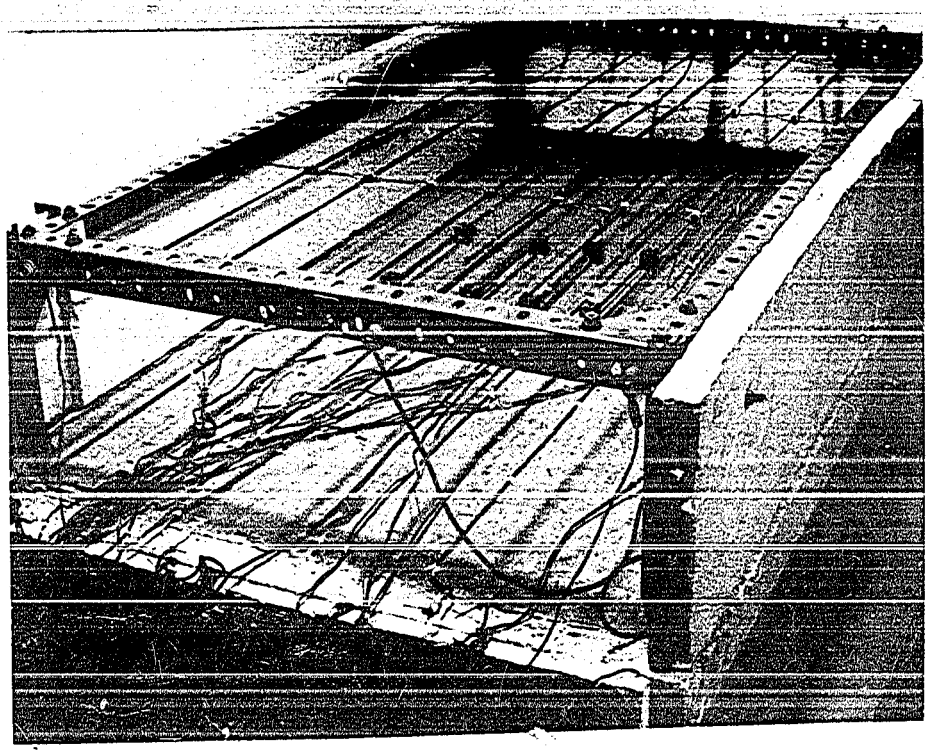

FIG. 4 ELECTRIC HEATER MOUNTED ON CONCRETE SURFACE

On top: nichrome strips on dexion frame which is enclosed by 2" styrofoam.

Bottom: strain guages and thermocouples on beam surface at mid-span.

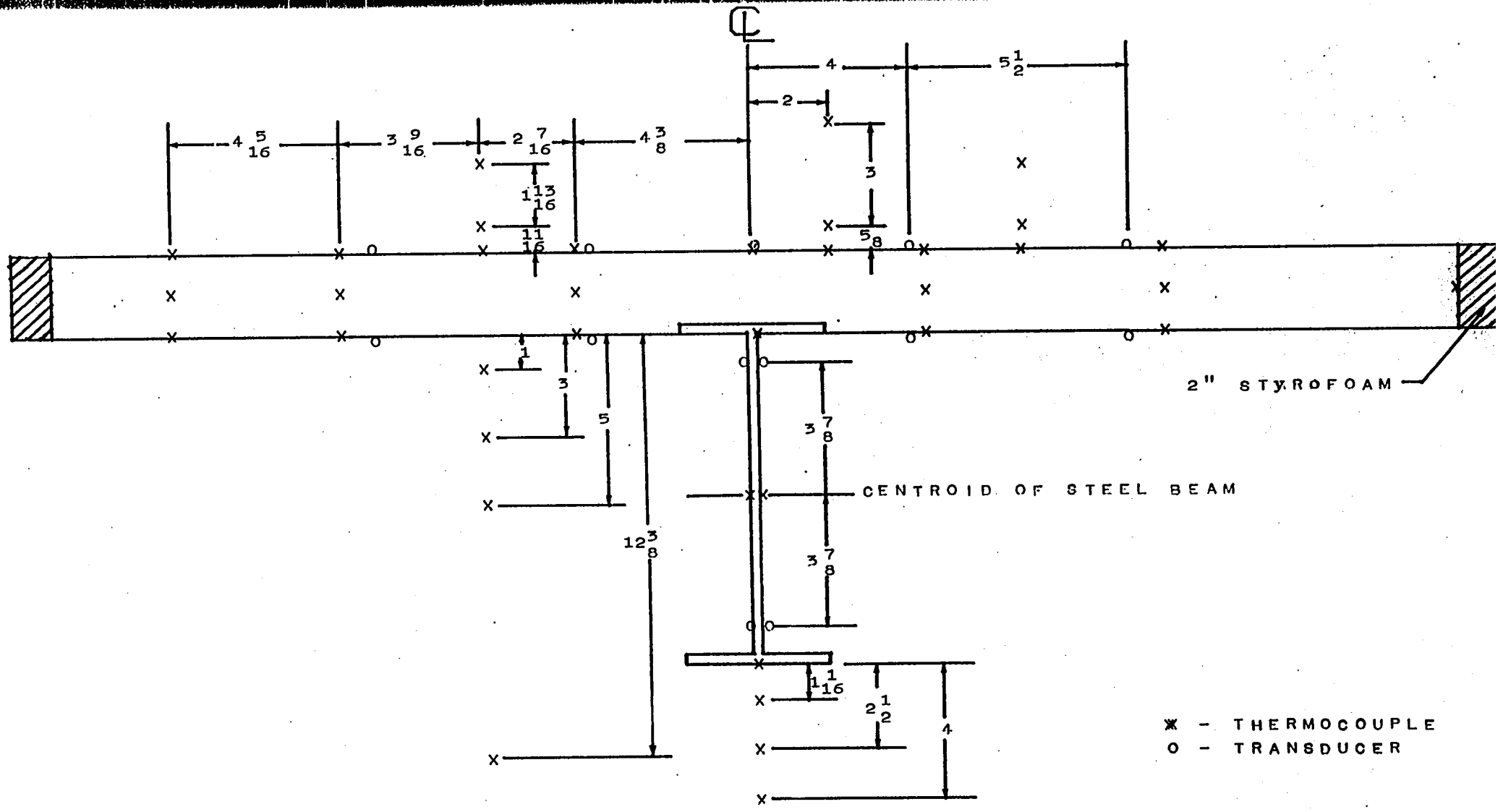

FIG.5 -ARRANGEMENT OF THERMOCOUPLES AND TRANSDUCERS

COMPOSITE SECTION

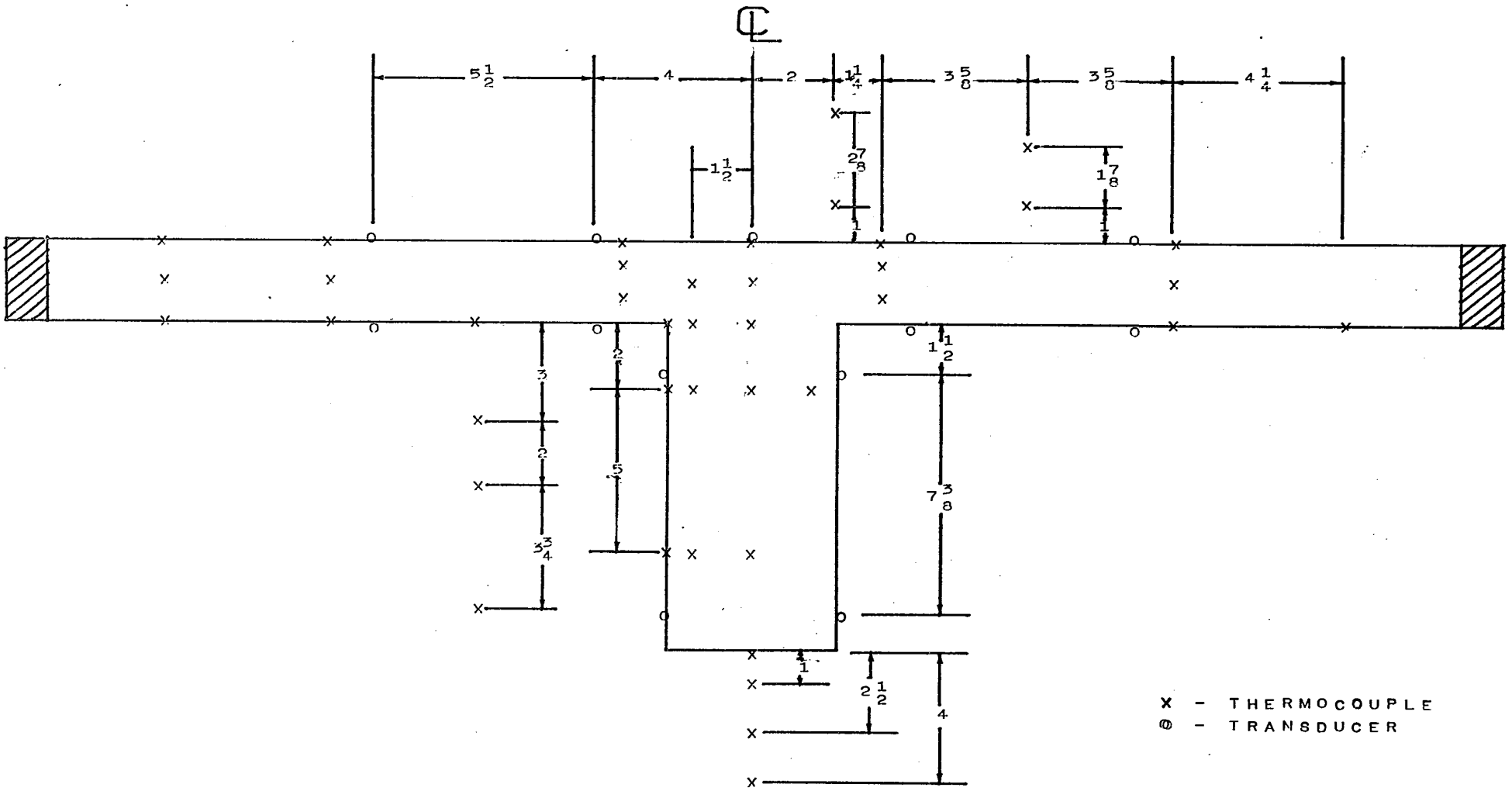

FIG.5A -ARRANGEMENT OF THERMOCOUPLES AND TRANSDUCERS T-BEAM

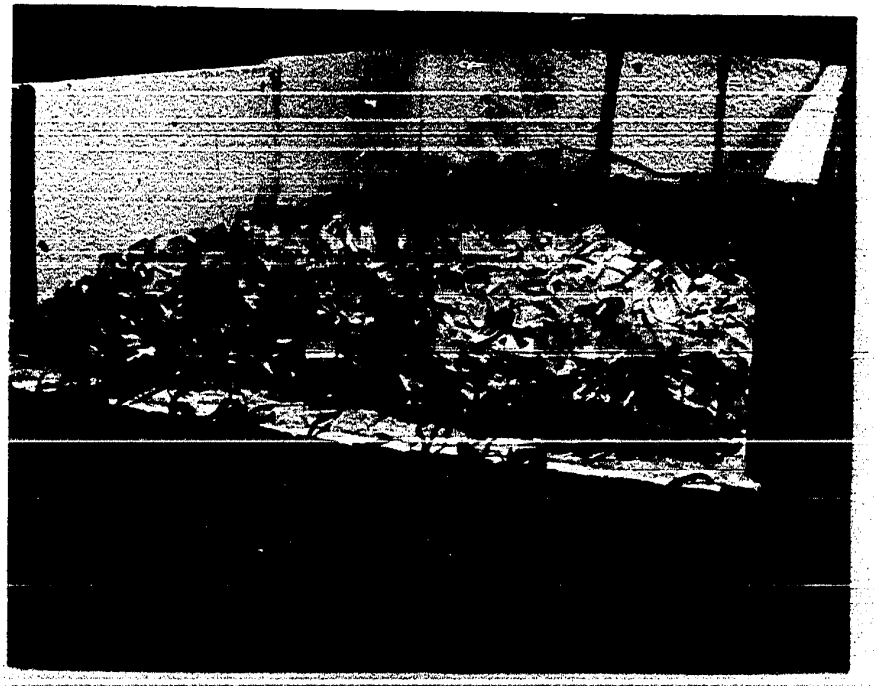

FIG. 6 UPPER SURFACE AT MELTING ICE TEMPERATURE

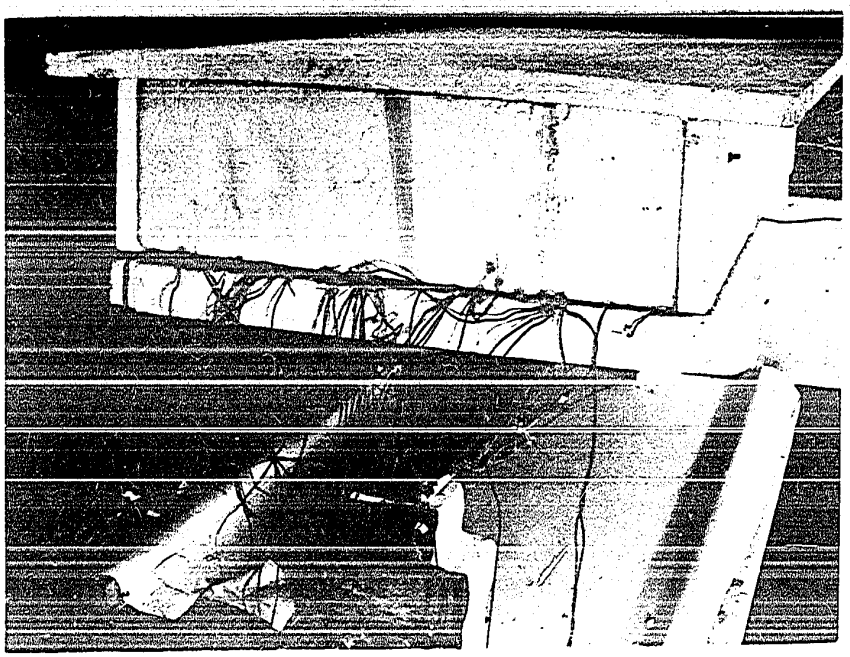

FIG. 7 UPPER SURFACE HEATED ELECTRICALLY

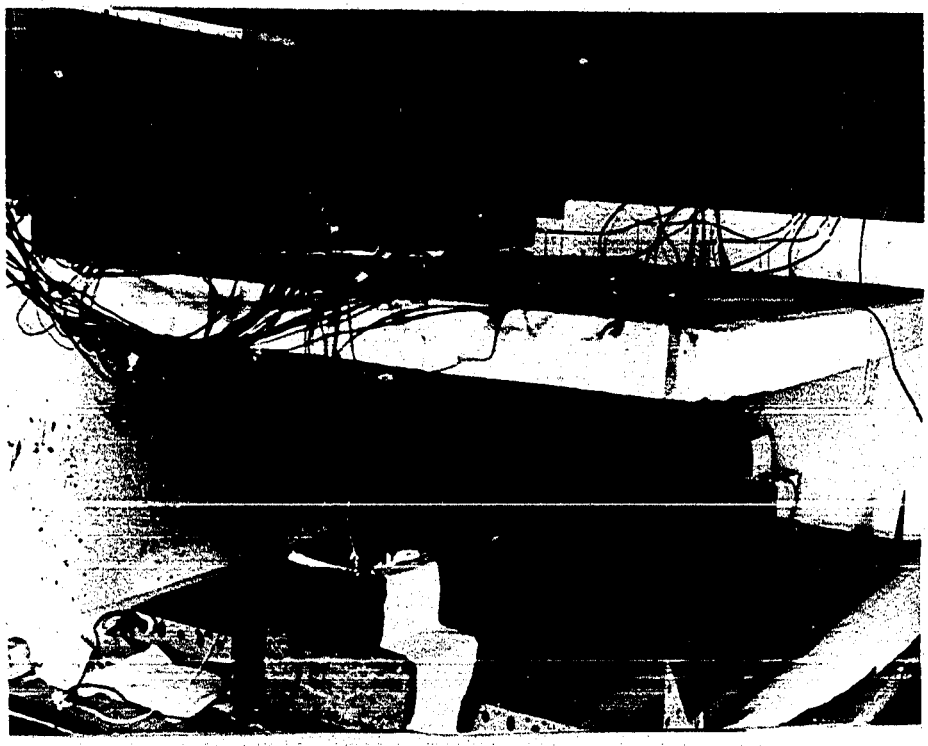

FIG. 8 LOWER SURFACES HEATED ELECTRICALLY

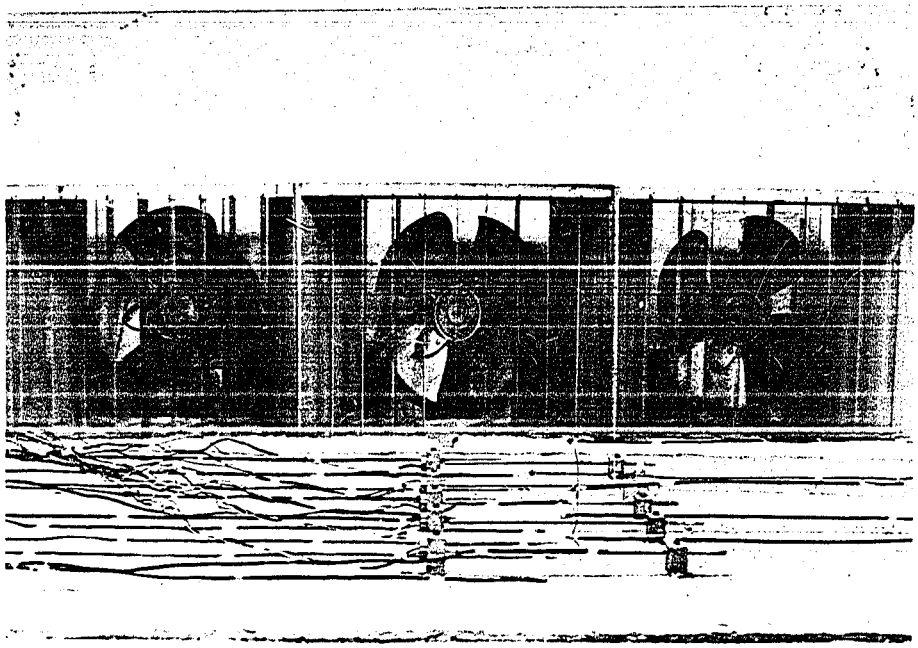

FIG. 9 UPPER SURFACE COOLED BY FORCED CONVECTION

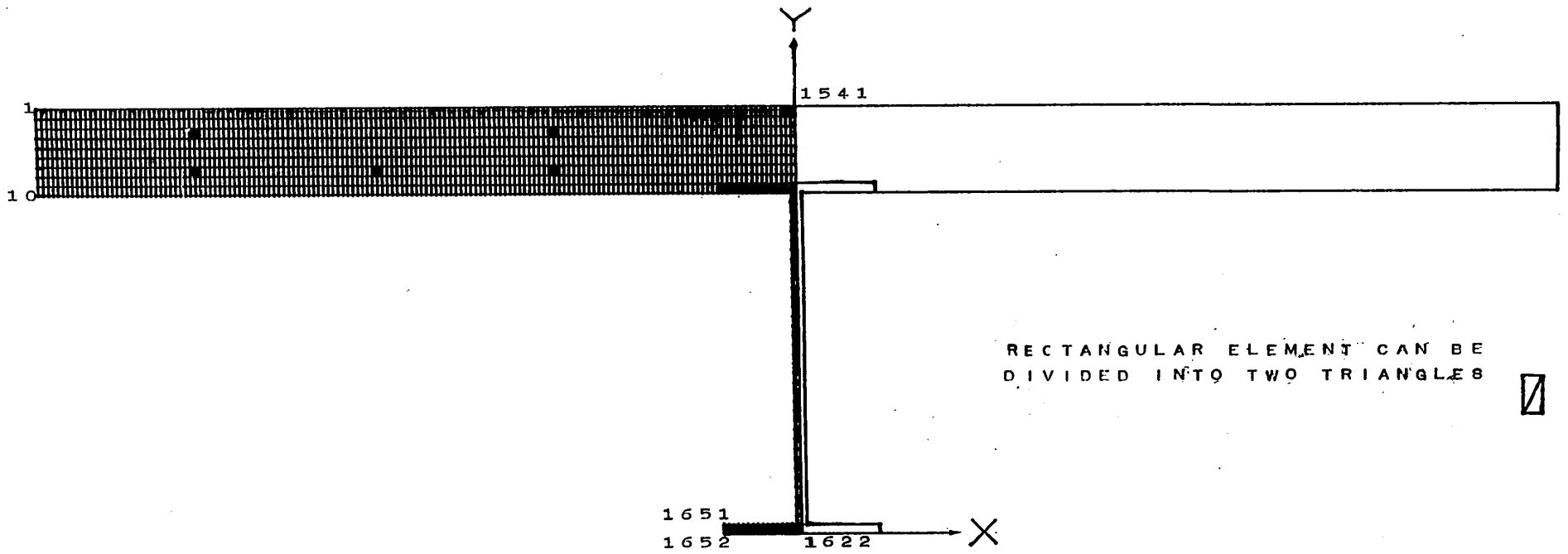

RECTANGULAR ELEMENT CAN BE DIVIDED INTO TWO TRIANGLES

DIVISION

HALF WIDTH OF SLAB IS DIVIDED INTO 154 EQUAL PARTS AND THE DEPTH OF SECTION INTO 45 EQUAL PARTS

SIZE OF RECTANGULAR ELEMENT 0.115X0.269

FIG. 10 -THE RECTANGULAR FINITE ELEMENT IDEALIZATION COMPOSITE SECTION

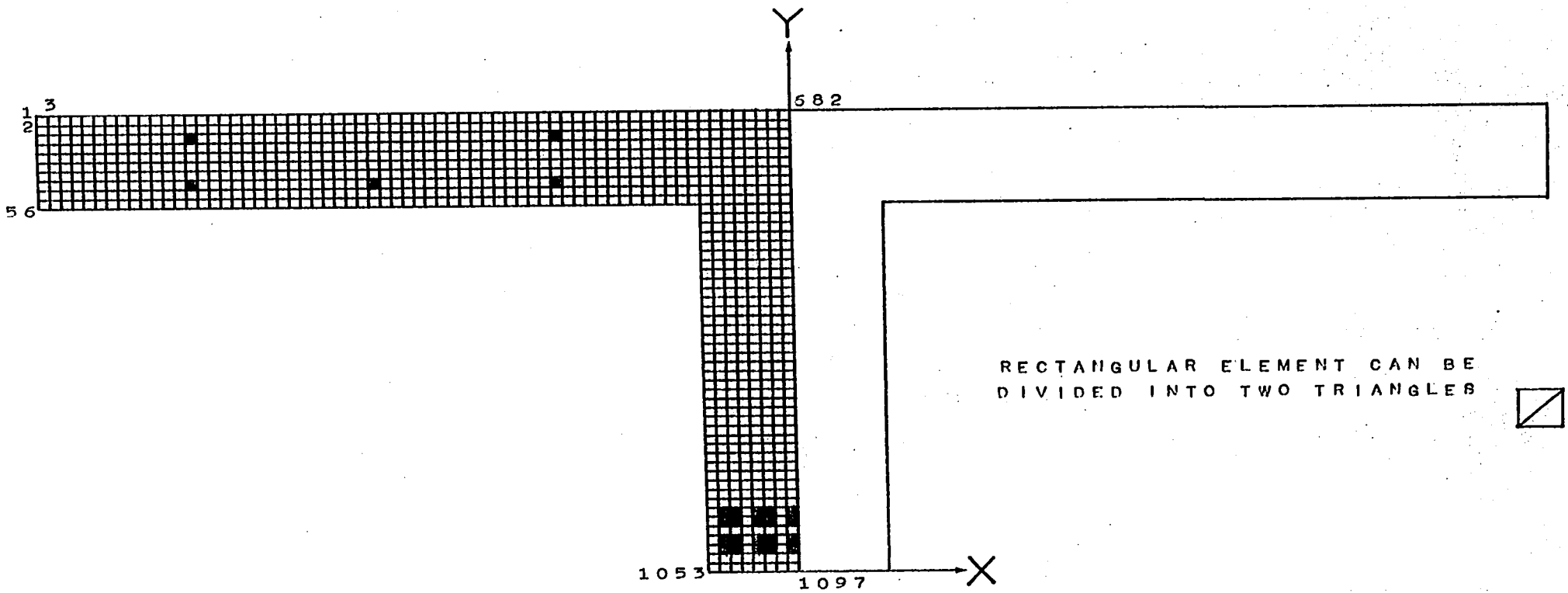

RECTANGULAR ELEMENT CAN BE DIVIDED INTO TWO TRIANGLES

DIVISION

HALF WIDTH OF SLAB IS DIVIDED INTO 66 EQUAL PARTS AND THE DEPTH OF SECTION INTO 50 EQUAL PARTS

SIZE OF RECTANGULAR ELEMENT 0.268X0.25

FIG.10A-THE RECTANGULAR FINITE ELEMENT IDEALIZATION T-BEAM

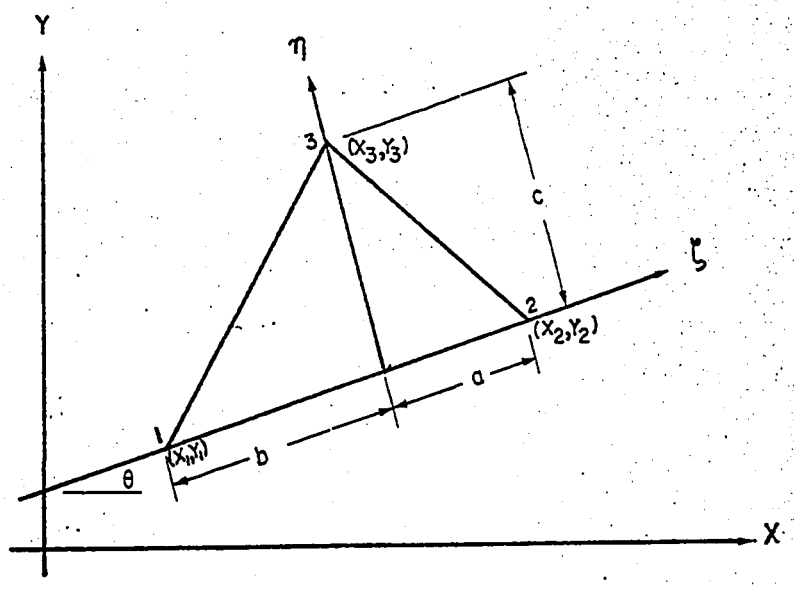

FIG. 11 TRIANGULAR ELEMENT WITH THREE NODES

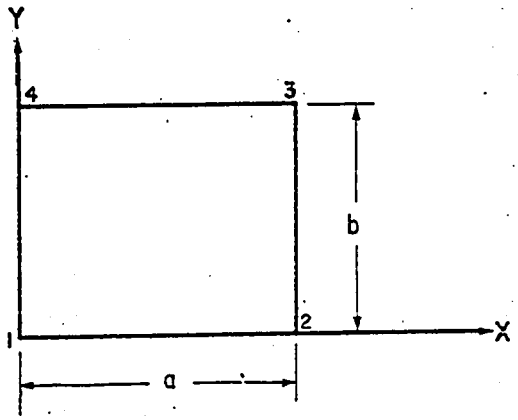

FIG. 12 RECTANGULAR ELEMENT

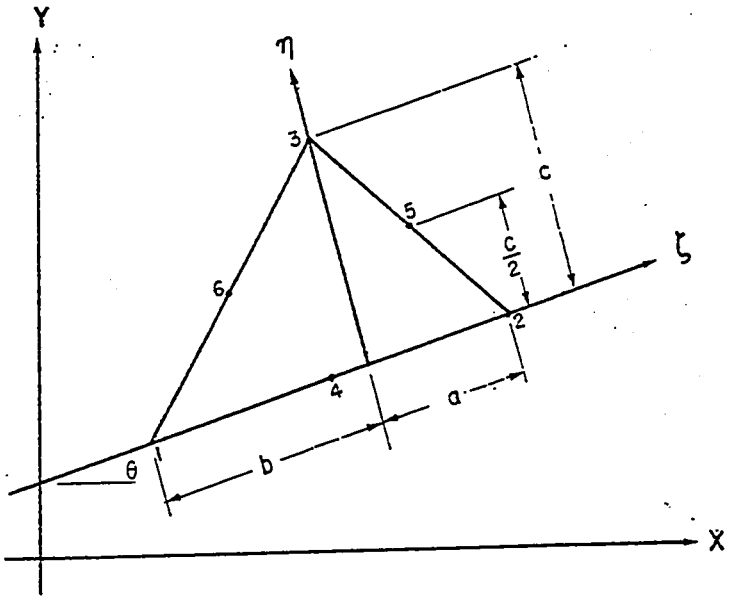

FIG. 13 TRIANGULAR ELEMENT WITH SIX NODES

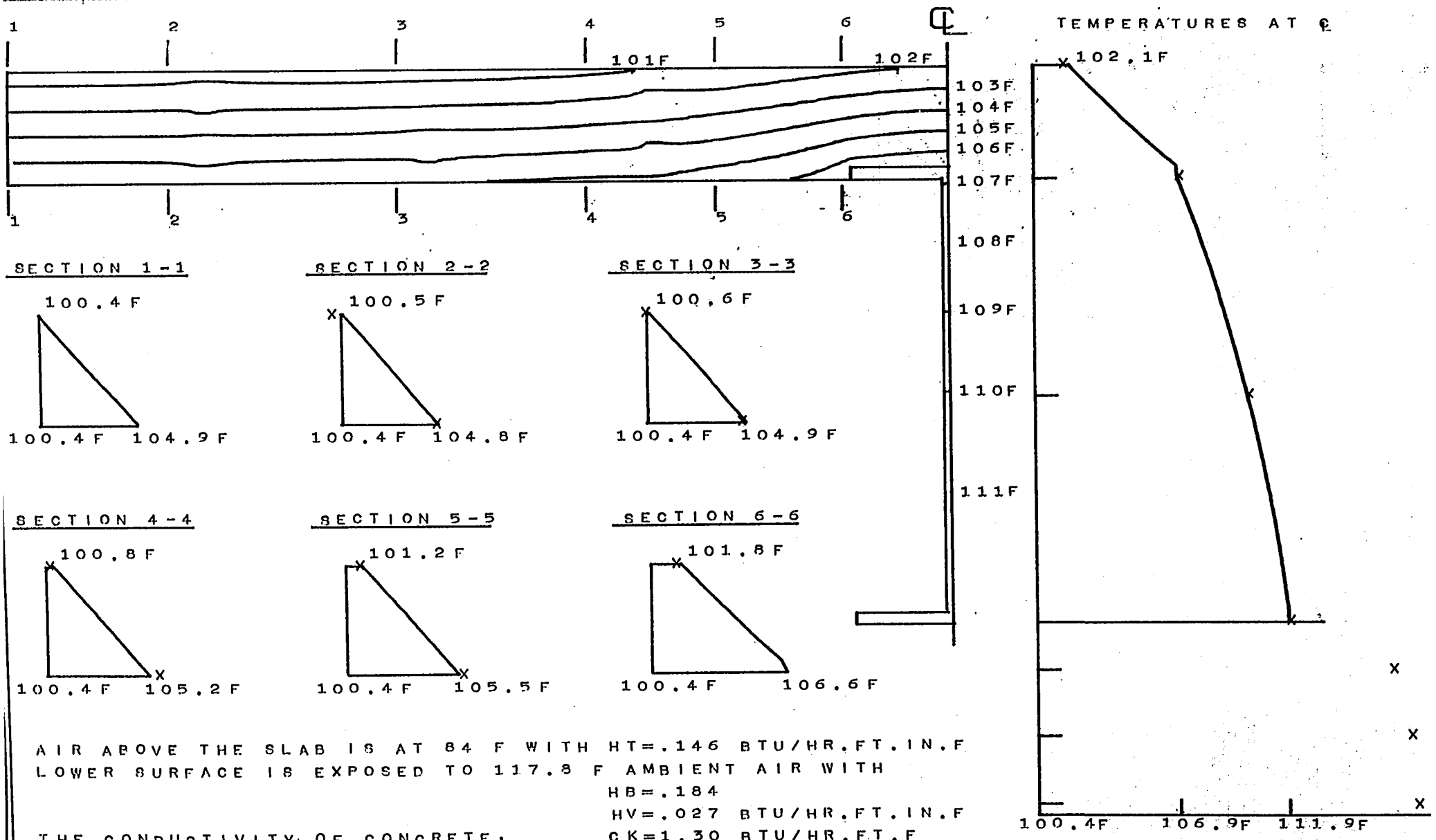

FIG. 14 TEMPERATURE FIELD IN COMPOSITE SECTION CS-2

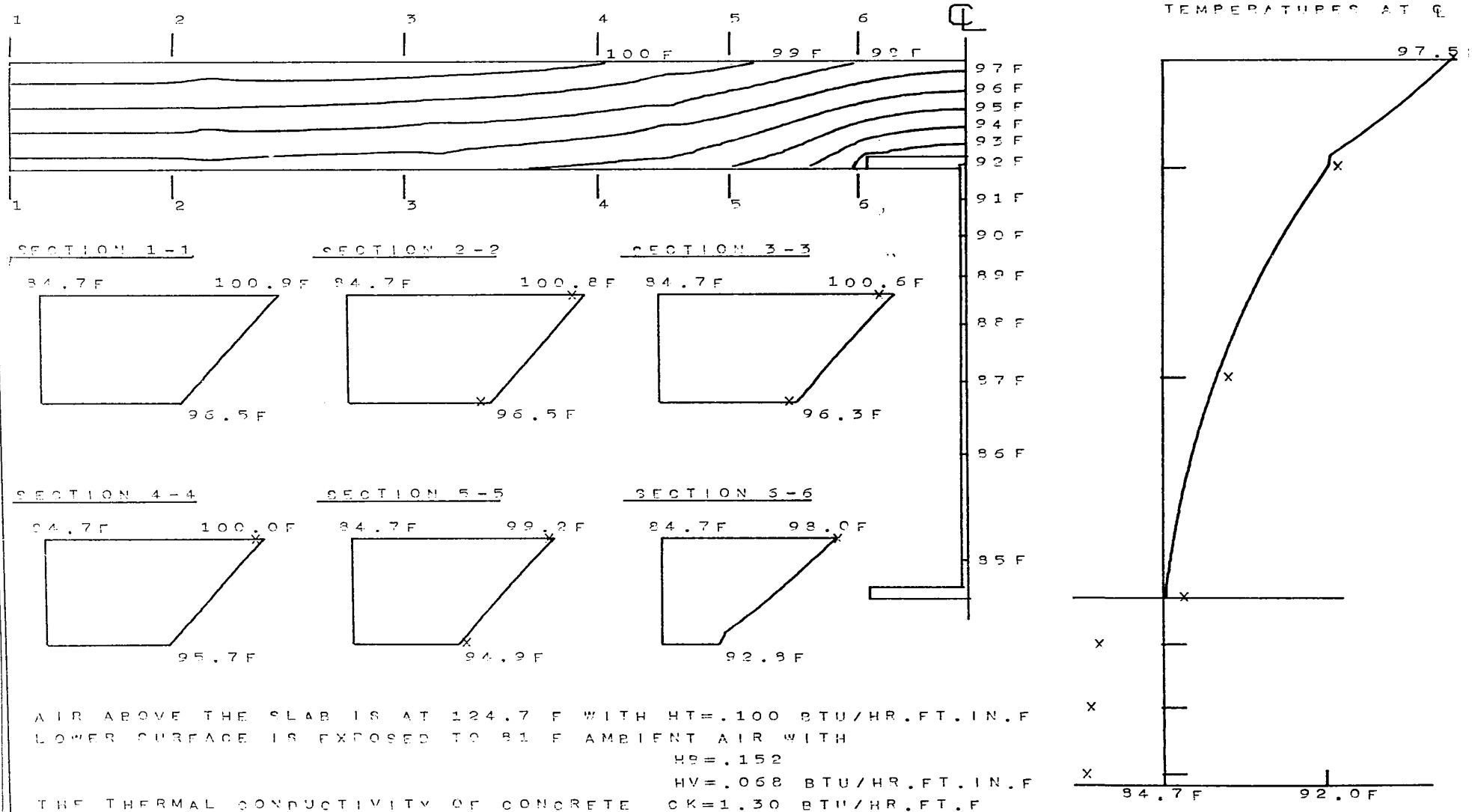

FIG. 15 TEMPERATURE FIELD IN COMPOSITE SECTION CS-11

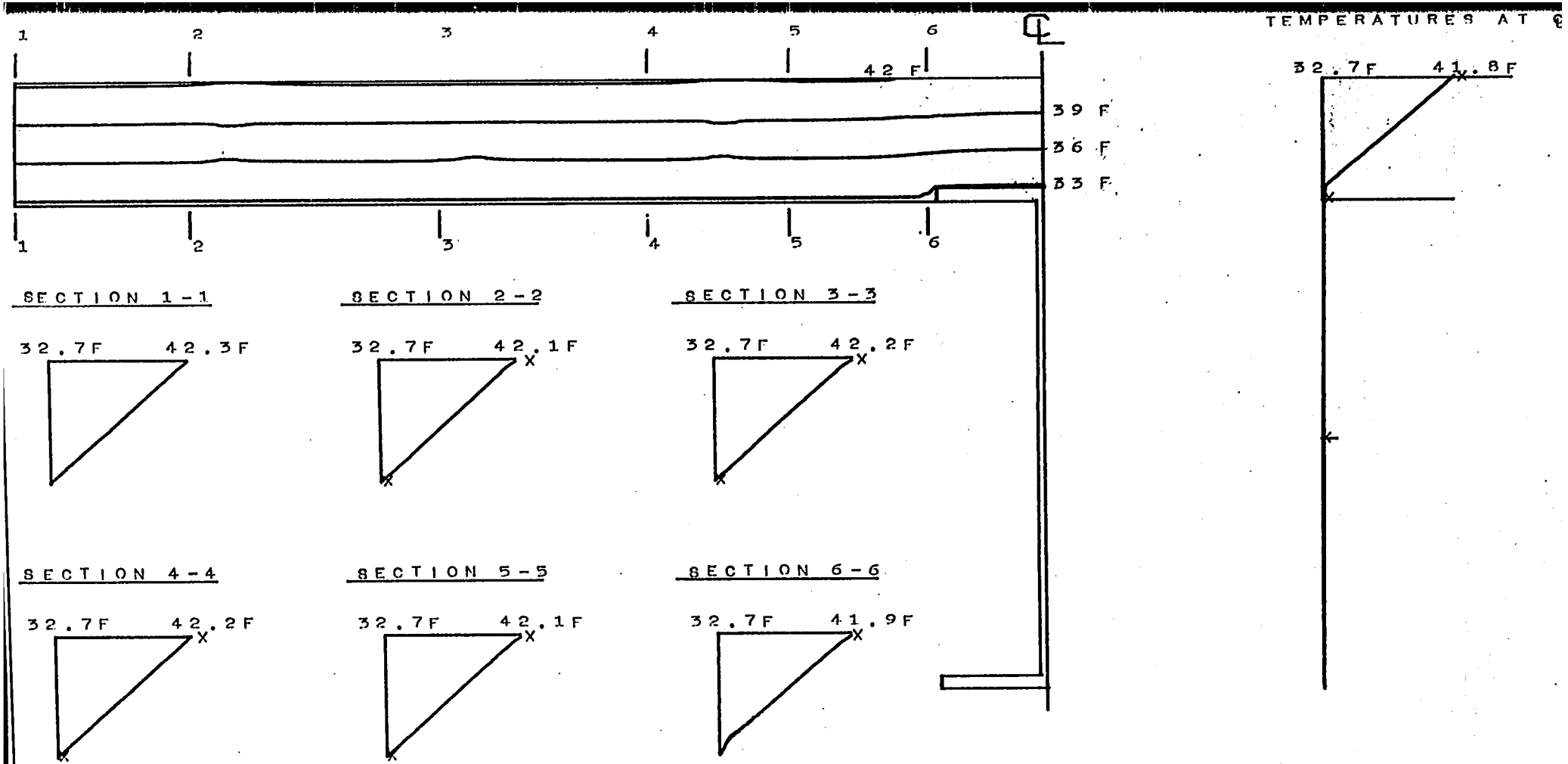

TEMPERATURE ABOVE THE SLAB IS AT 77.6 F WITH HT=.312 BTU/HR.FT.IN.F
THE BOTTOM SURFACE OF THE SLAB IS AT ICE TEMPERATURE 32.7 F
THE THERMAL CONDUCTIVITY OF SATURATED CONCRETE IS 2.75 BTU/HR.FT.F

FIG. 16 TEMPERATURE FIELD IN COMPOSITE SECTION CS-14

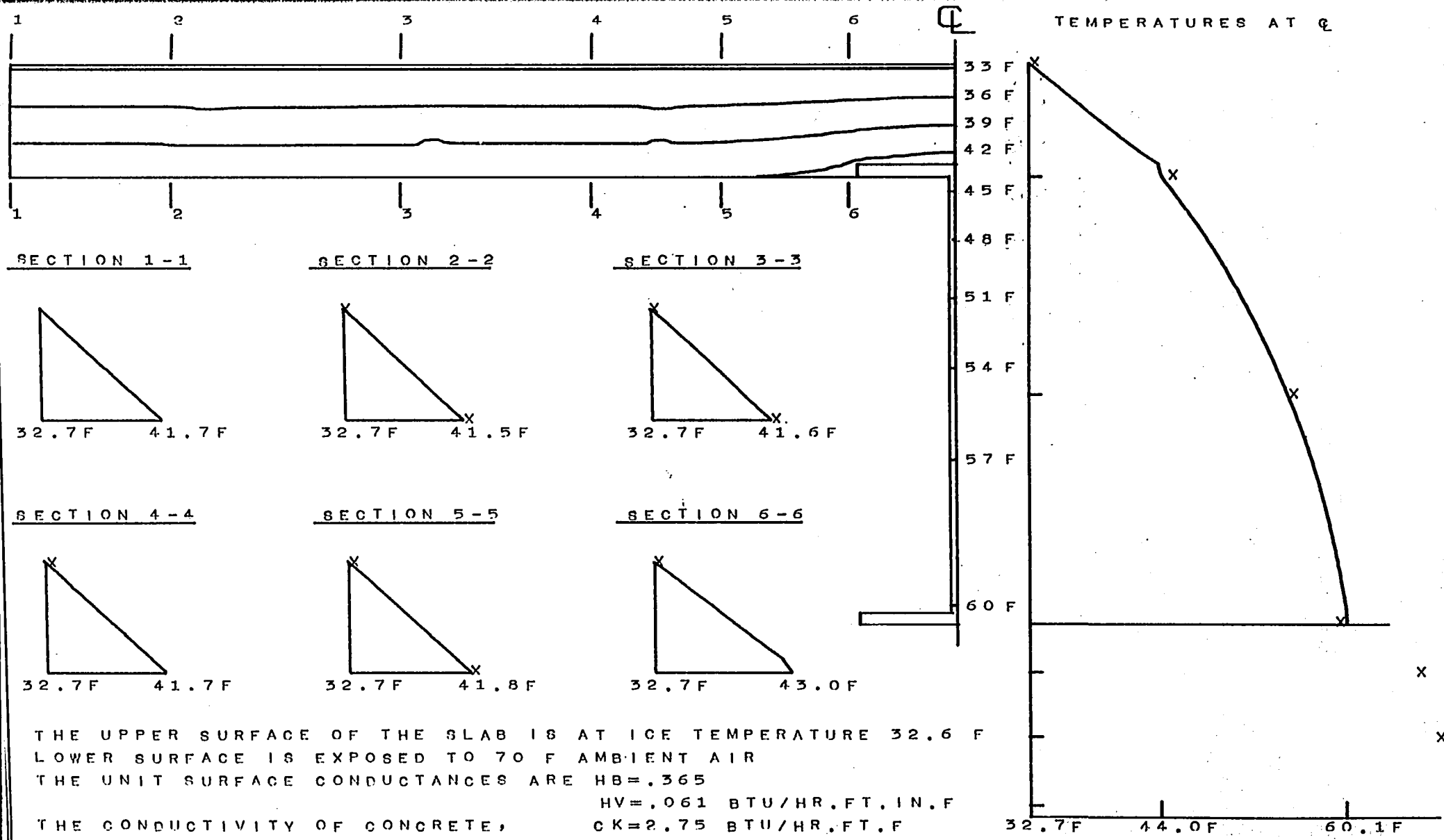

THE UPPER SURFACE OF THE SLAB IS AT ICE TEMPERATURE 32.6 F
LOWER SURFACE IS EXPOSED TO 70 F AMBIENT AIR
THE UNIT SURFACE CONDUCTANCES ARE HB=.365
HV=.061 BTU/HR.FT.IN.F
THE CONDUCTIVITY OF CONCRETE, CK=2.75 BTU/HR.FT.F

FIG. 17 TEMPERATURE FIELD IN COMPOSITE SECTION CS-15

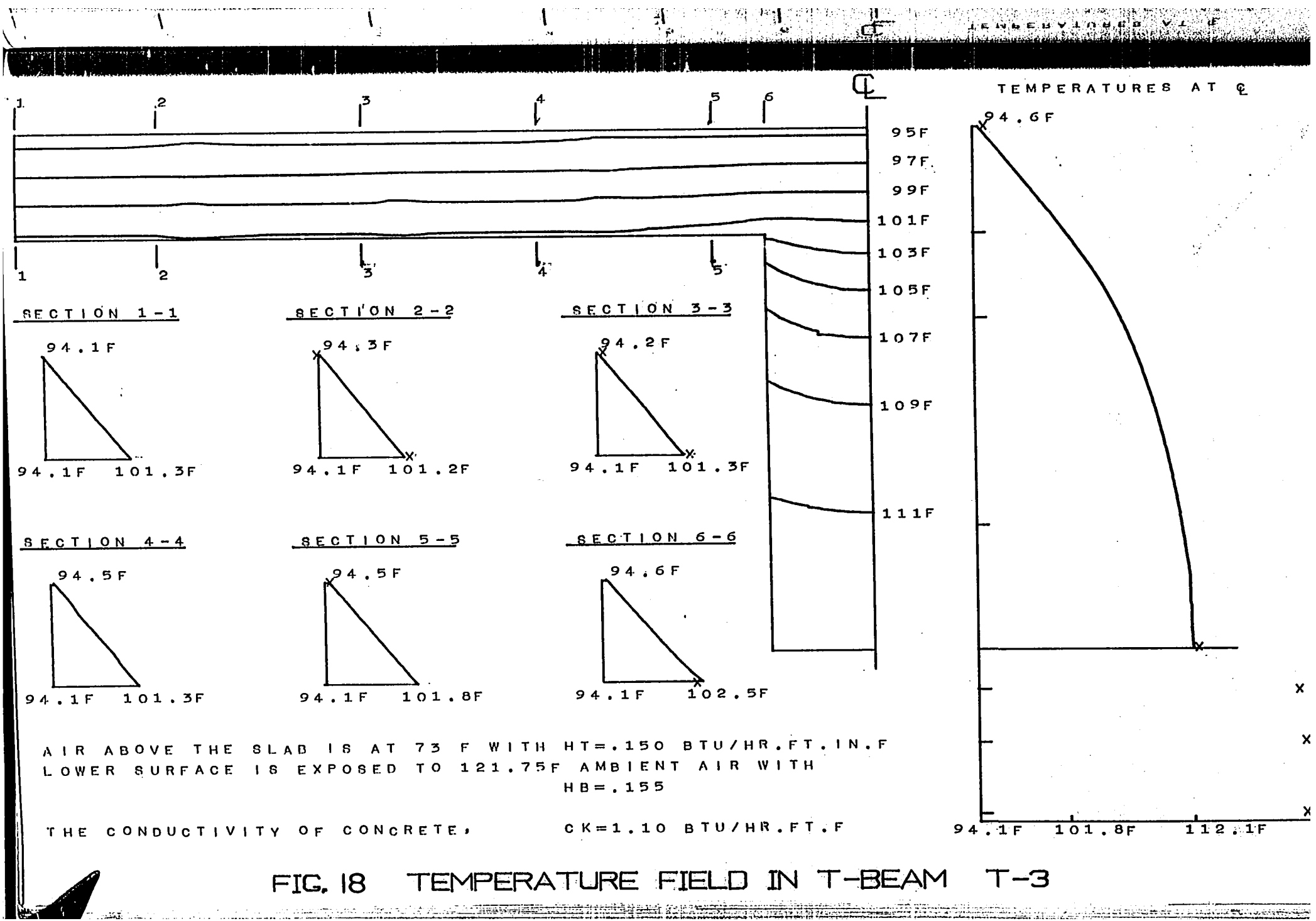

FIG. 18 TEMPERATURE FIELD IN T-BEAM T-3

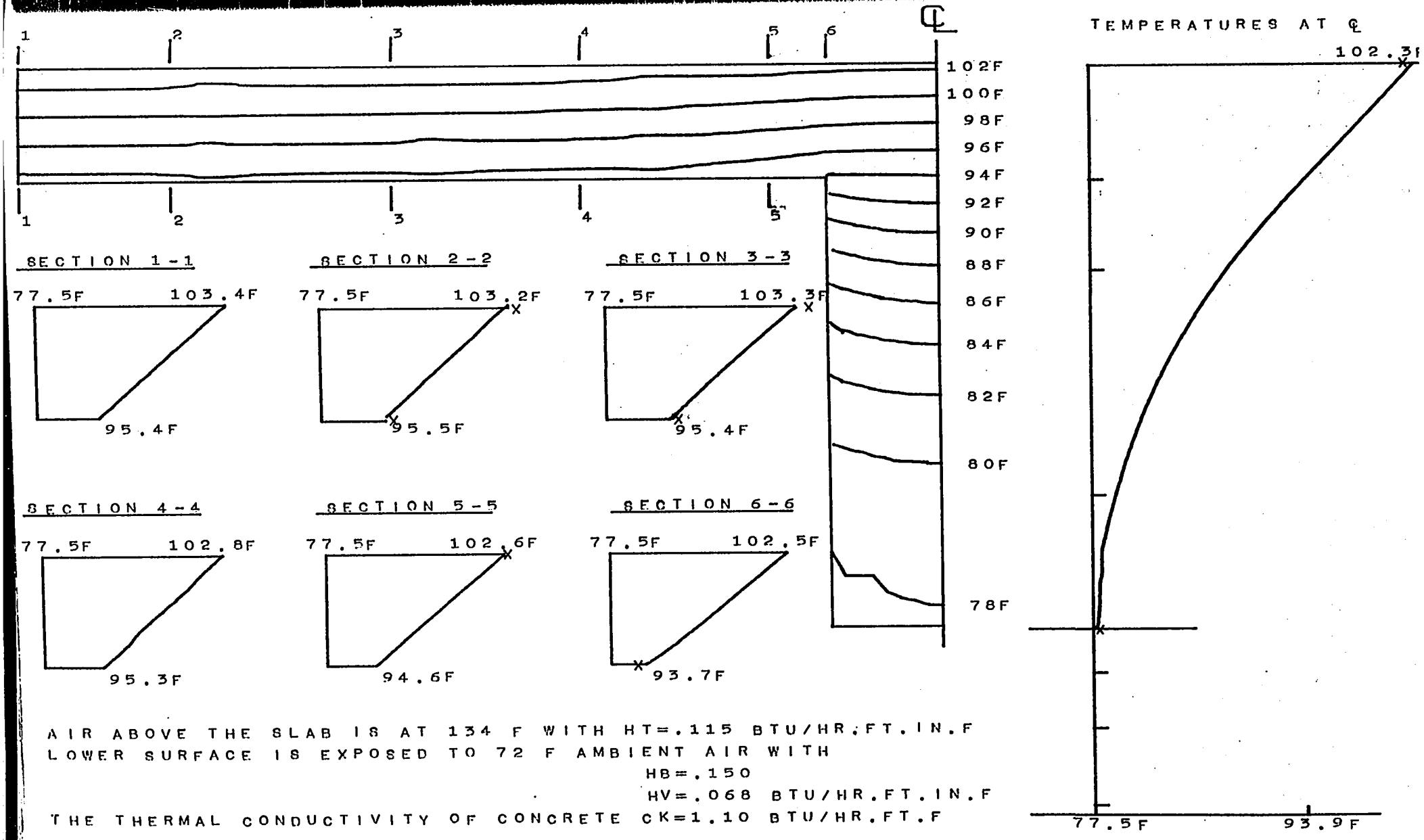

AIR ABOVE THE SLAB IS AT 134 F WITH HT=.115 BTU/HR.FT.IN.F
LOWER SURFACE IS EXPOSED TO 72 F AMBIENT AIR WITH
HB=.150
HV=.068 BTU/HR.FT.IN.F
THE THERMAL CONDUCTIVITY OF CONCRETE CK=1.10 BTU/HR.FT.F

FIG. 19 TEMPERATURE FIELD IN T-BEAM T-7

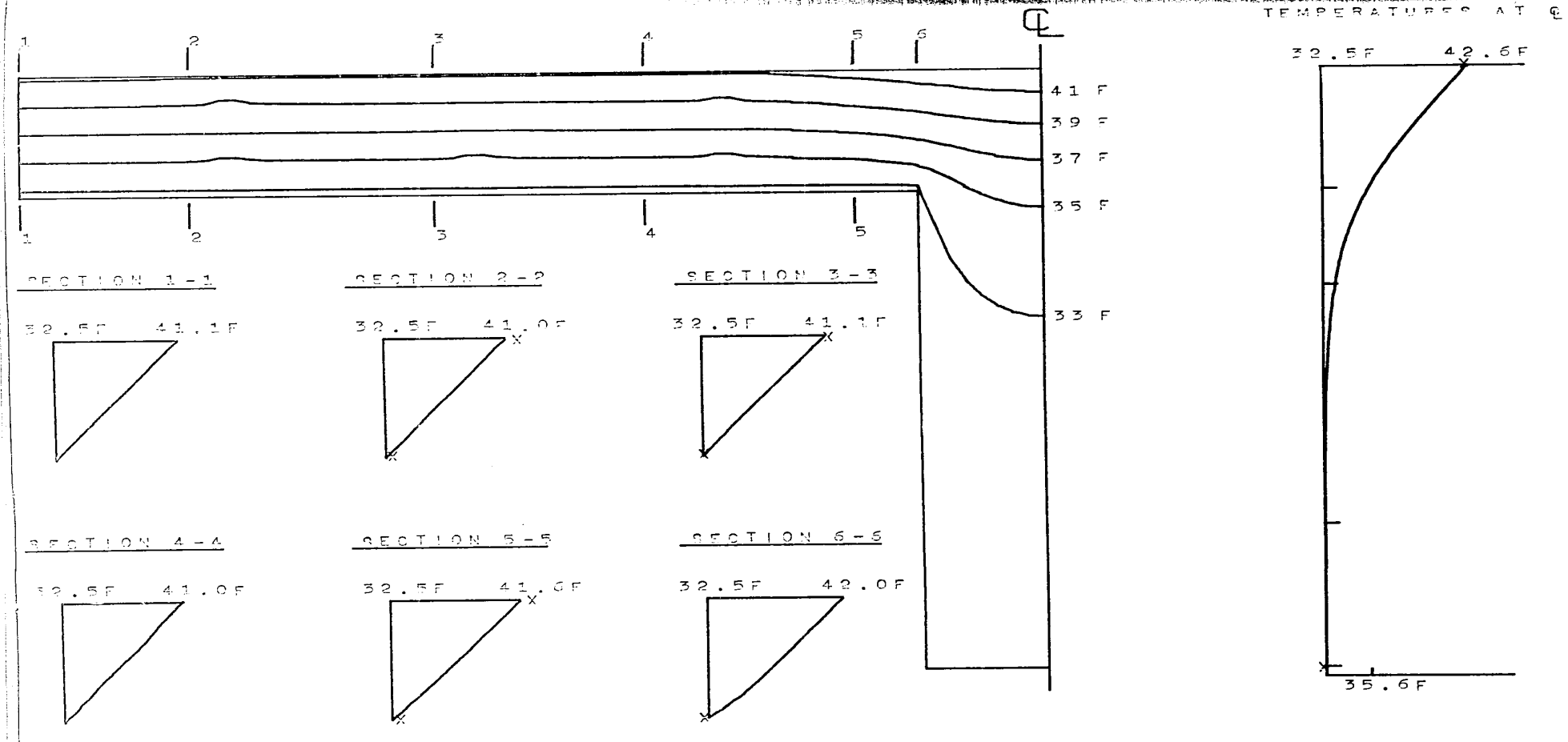

TEMPERATURE ABOVE THE SLAB IS AT 72 F WITH HT=.310 BTU/HR.FT.IN.F
THE BOTTOM SURFACE OF THE SLAB IS AT ICE TEMPERATURE 32.5 F
THE THERMAL CONDUCTIVITY OF SATURATED CONCRETE IS 2.75 BTU/HR.FT.F

FIG. 20 TEMPERATURE FIELD IN T-BEAM T-8

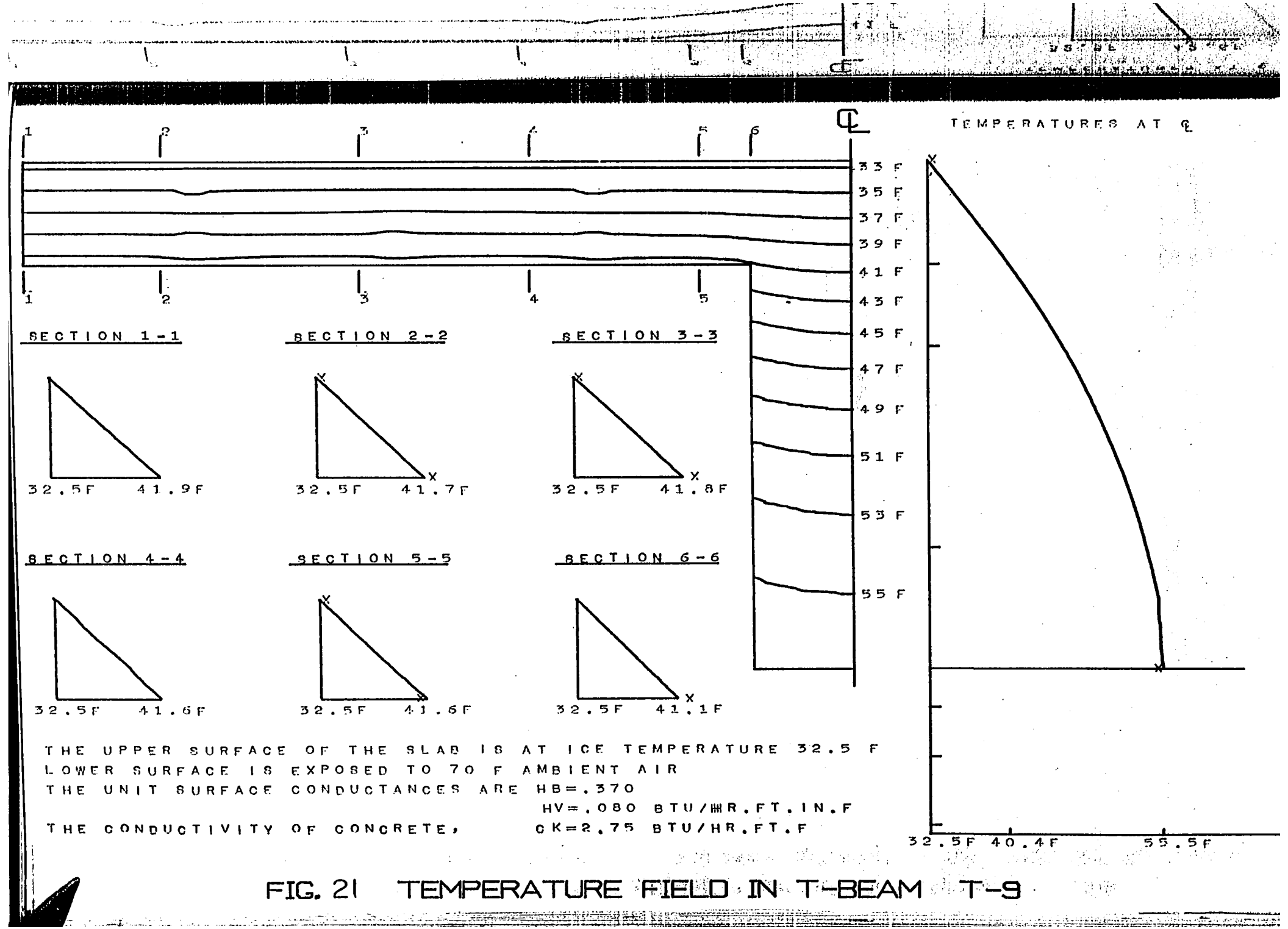

FIG. 21 TEMPERATURE FIELD IN T-BEAM T-9

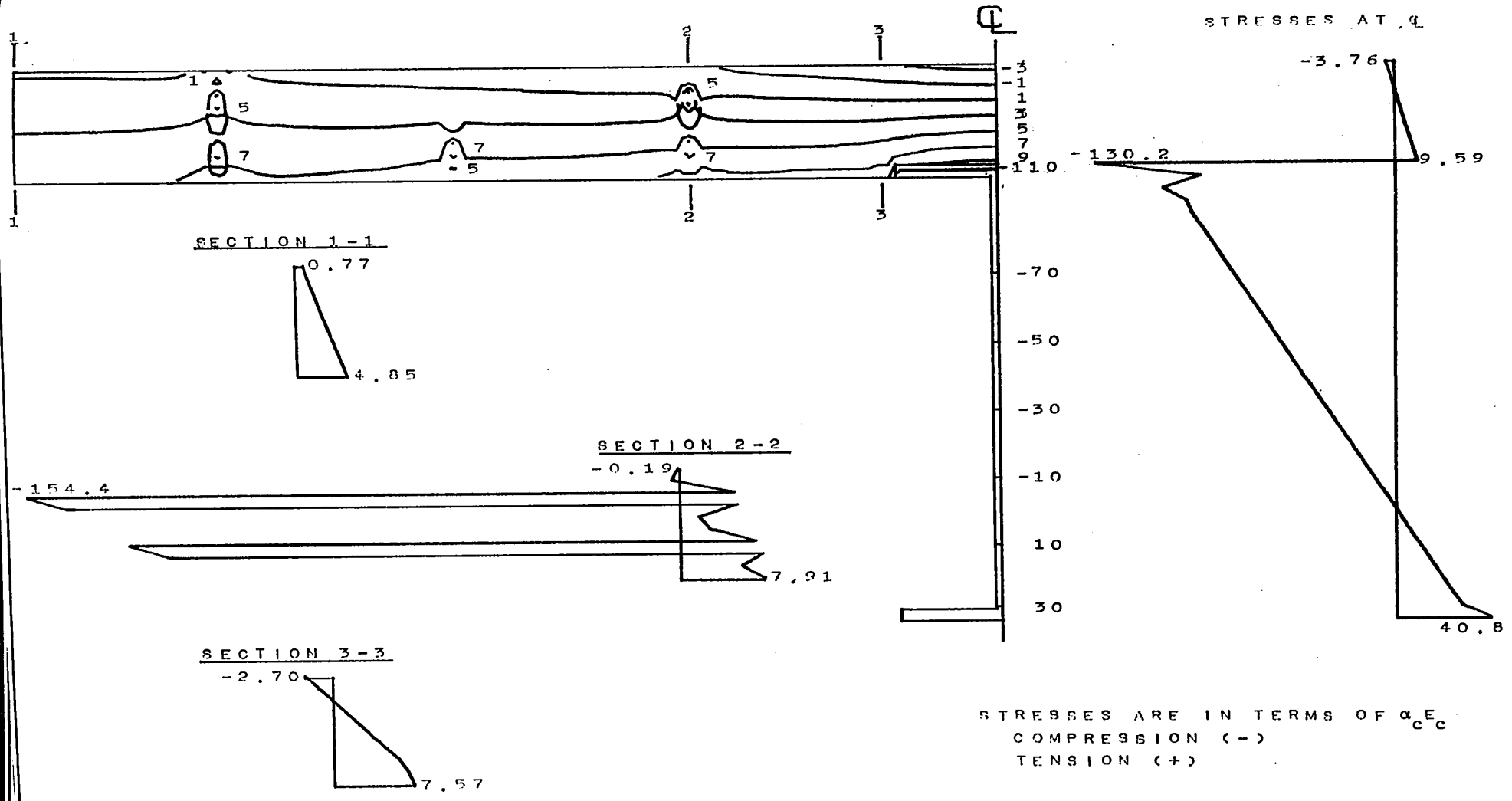

FIG. 22 STRESS DISTRIBUTION DUE TO UNIFORM TEMPERATURE CHANGE OF 100 F
COMPOSITE SECTION WITH POISSON RATIO OF CONCRETE 0.12

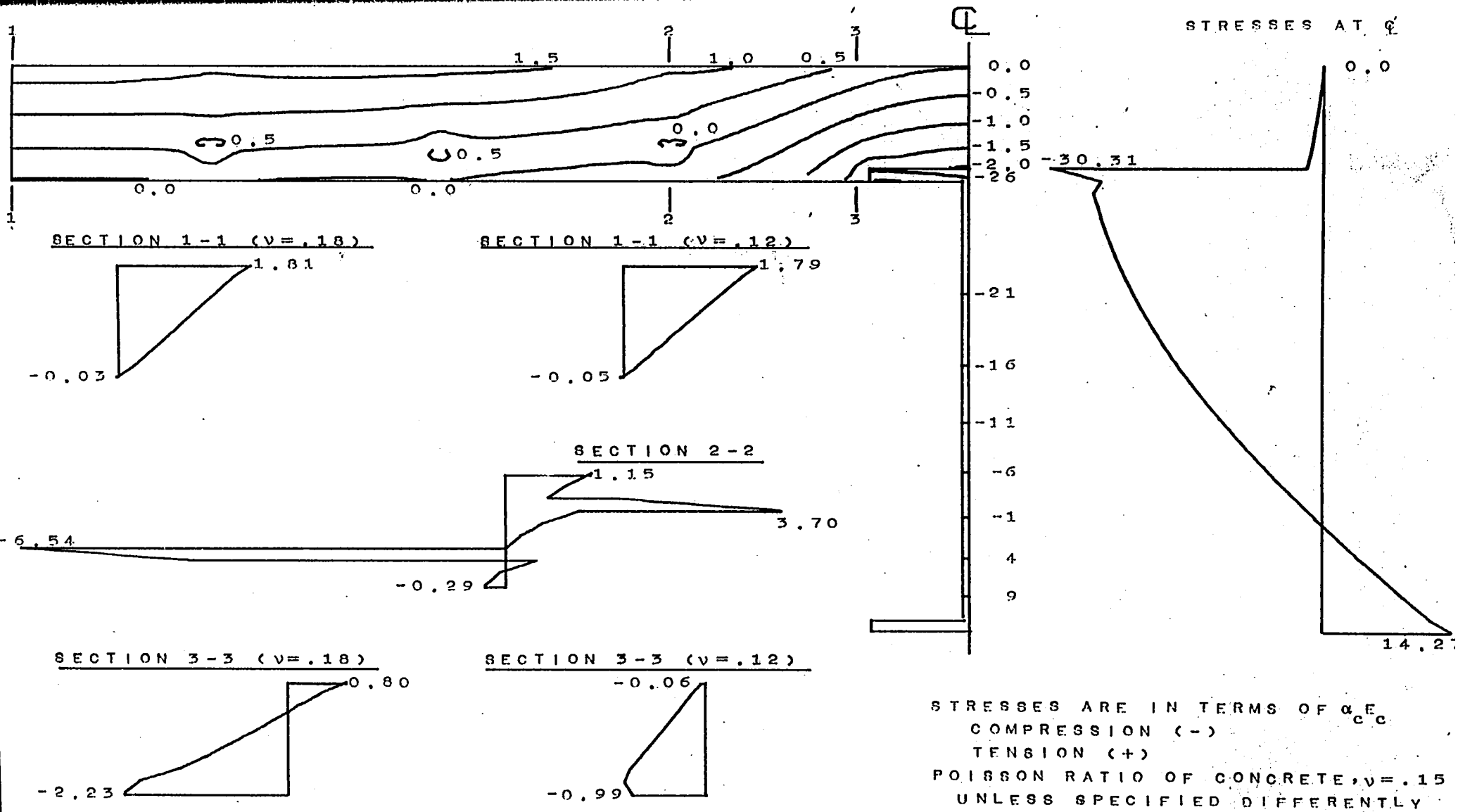

FIG. 23 STRESS DISTRIBUTION DUE TO TEMPERATURE VARIATION CS-2
COMPOSITE SECTION

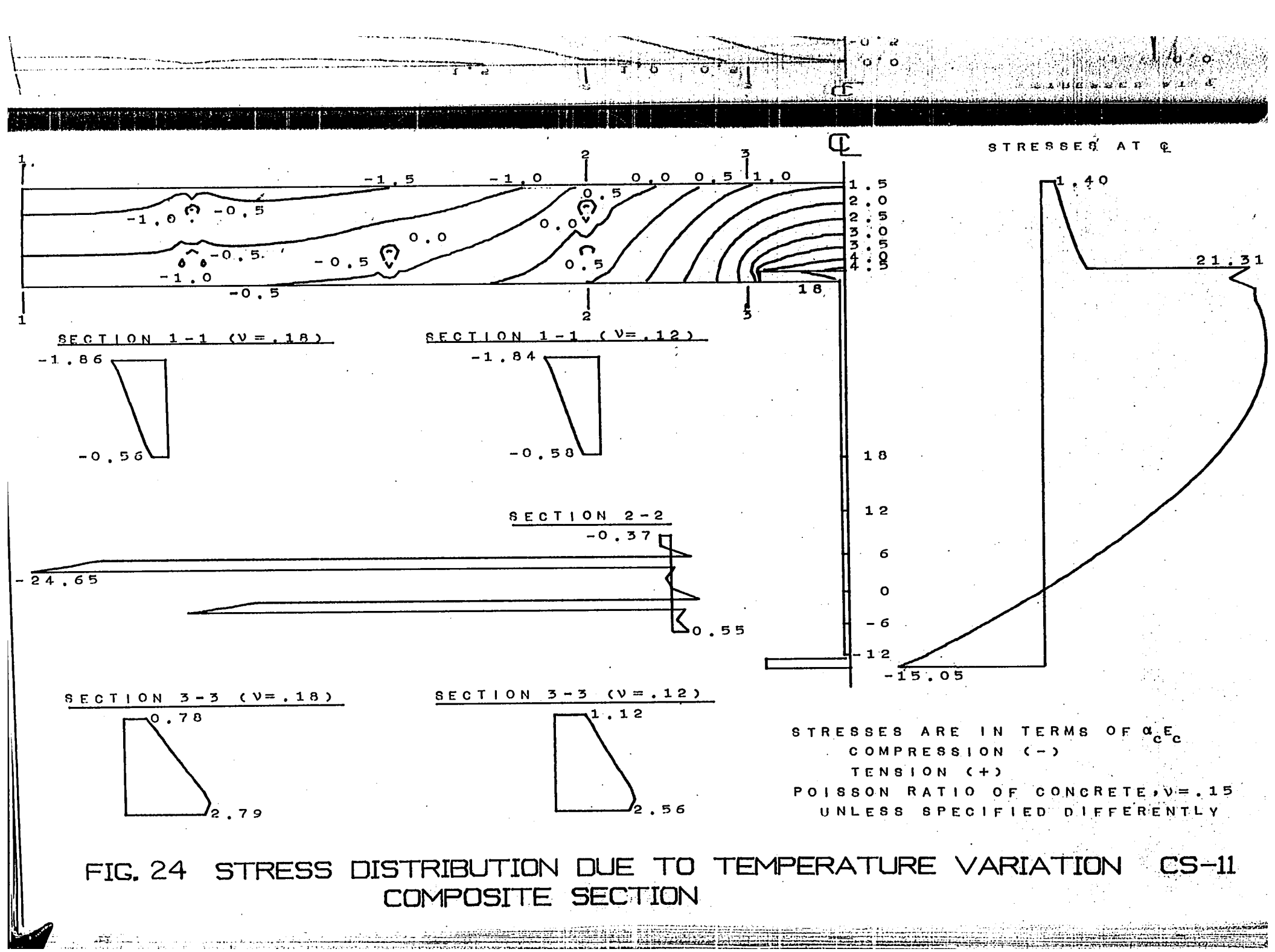

FIG. 24 STRESS DISTRIBUTION DUE TO TEMPERATURE VARIATION CS-11
COMPOSITE SECTION

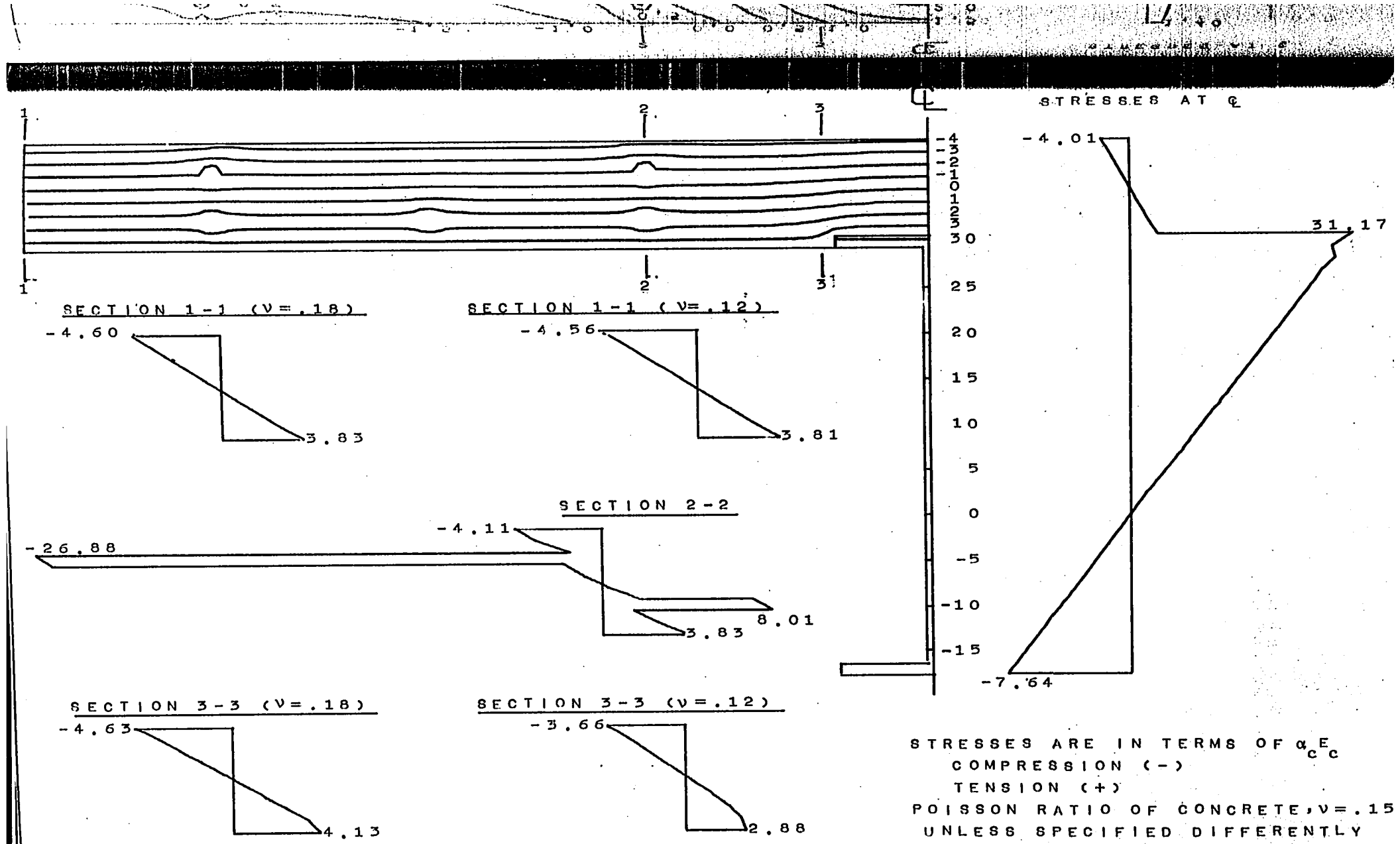

FIG. 25 STRESS DISTRIBUTION DUE TO TEMPERATURE VARIATION CS-14
COMPOSITE SECTION

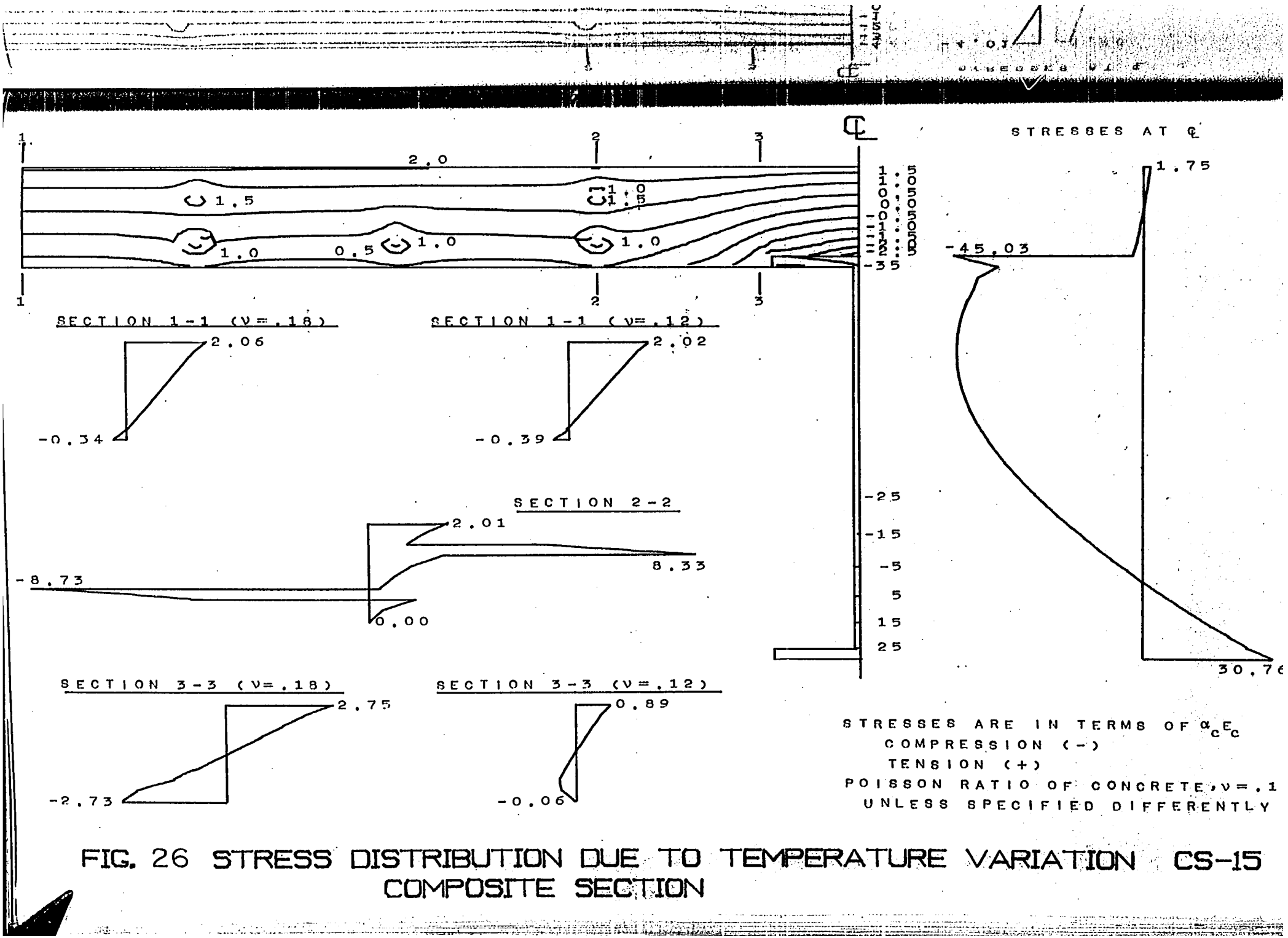

FIG. 26 STRESS DISTRIBUTION DUE TO TEMPERATURE VARIATION CS-15
COMPOSITE SECTION

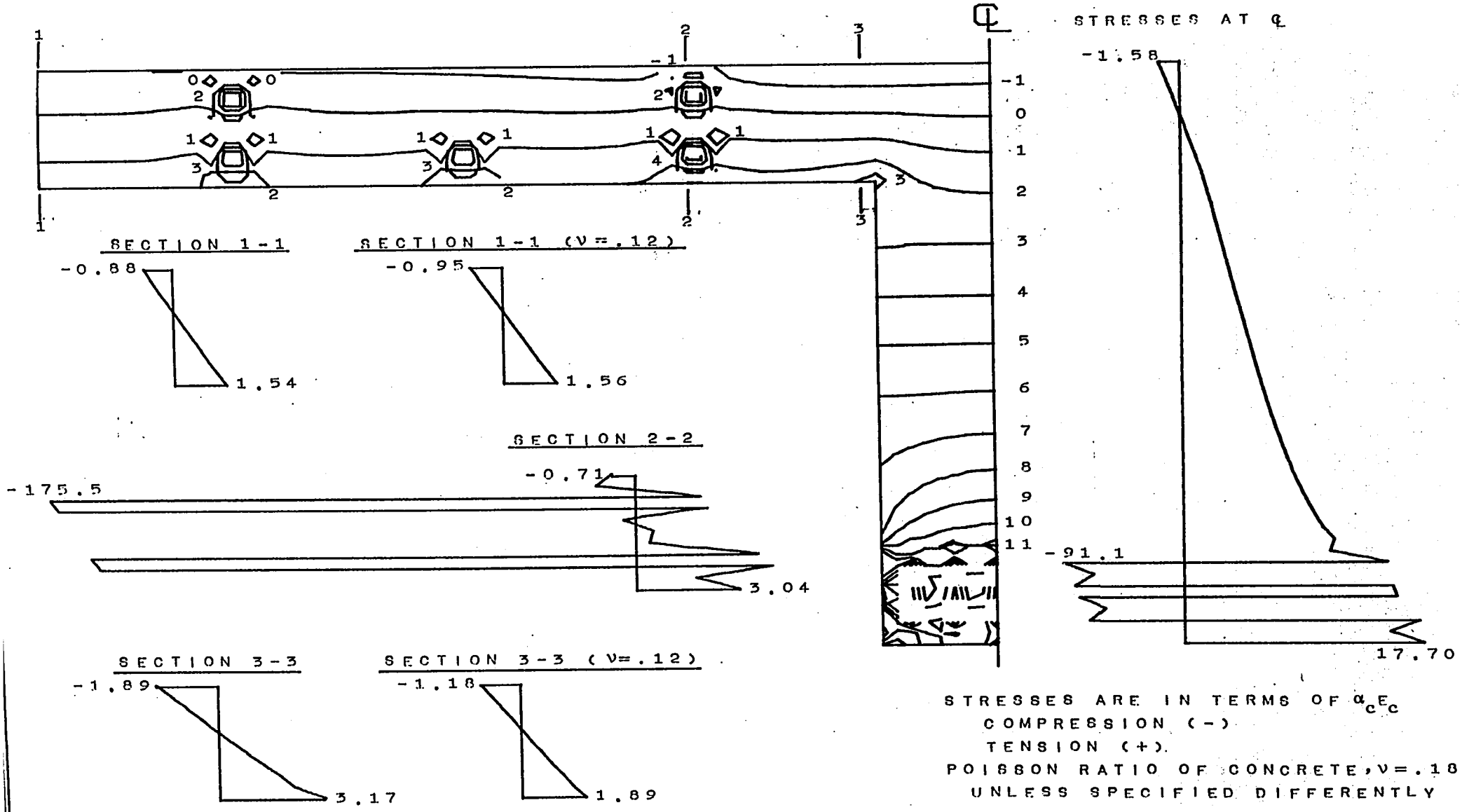

FIG.27 STRESS DISTRIBUTION DUE TO CONSTANT TEMPERATURE CHANGE OF 100 F
T-BEAM

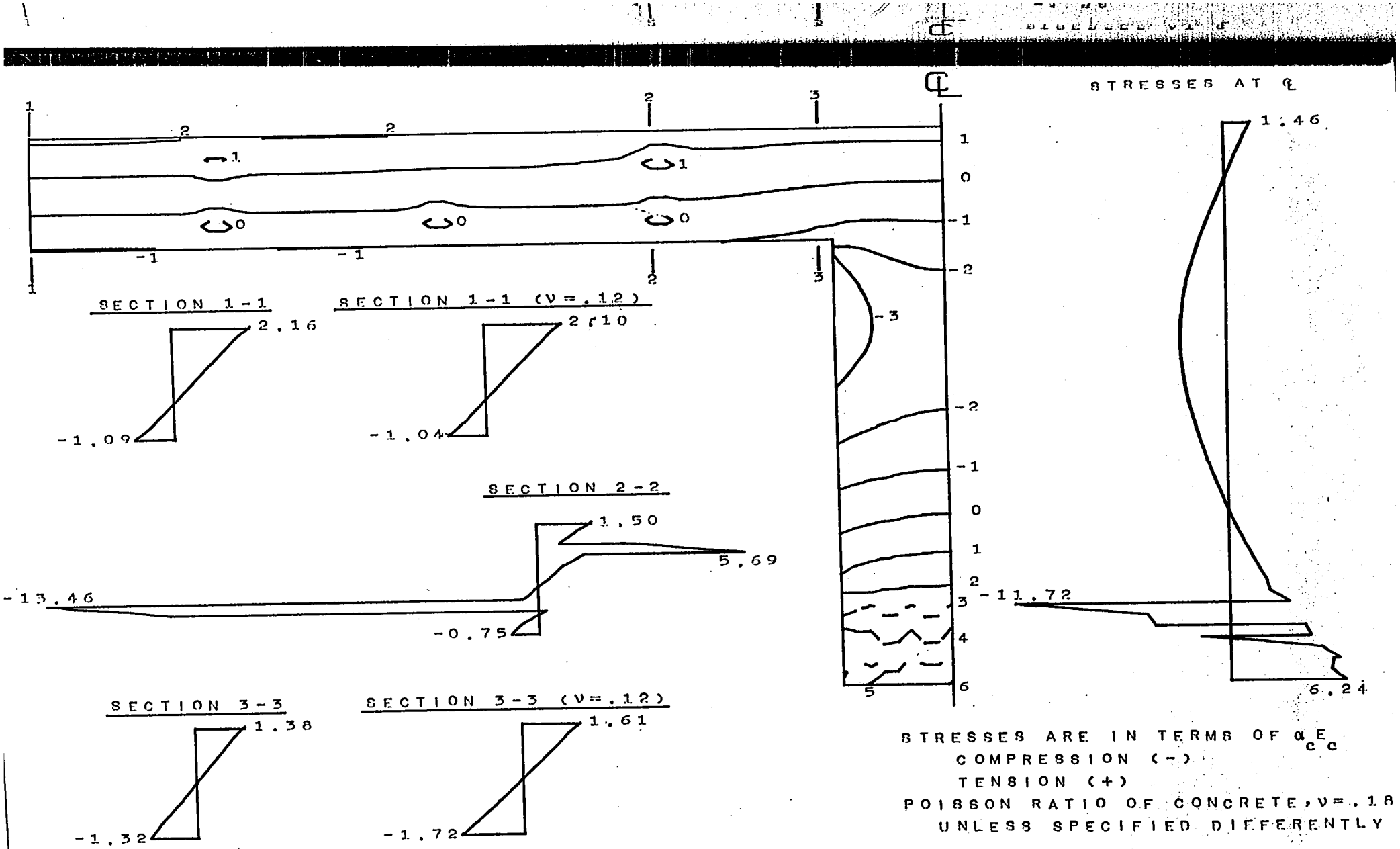

FIG. 28 STRESS DISTRIBUTION DUE TO TEMPERATURE VARITION T-3
T-BEAM

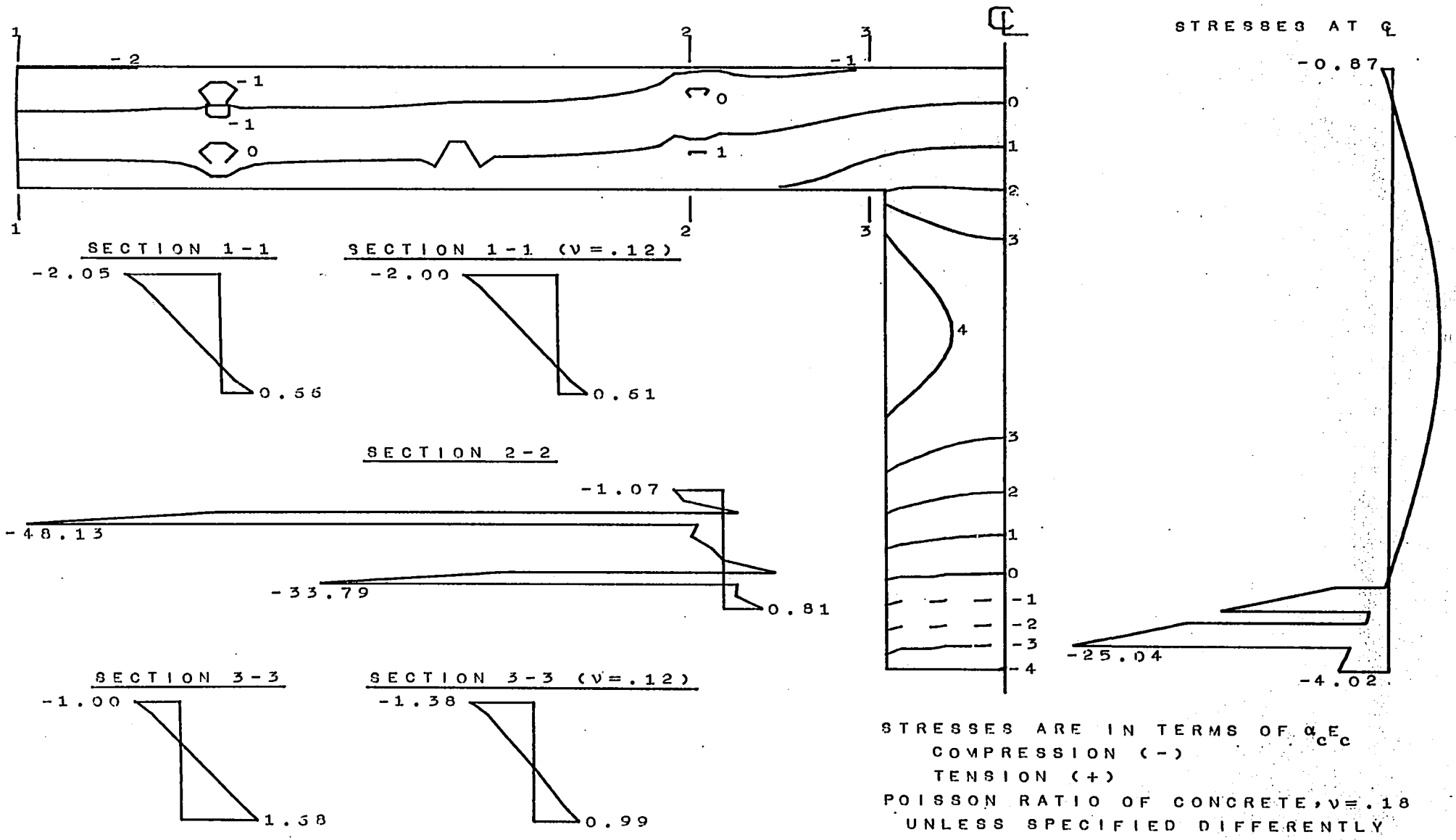

FIG. 29 STRESS DISTRIBUTION DUE TO TEMPERATURE VARIATION T-7
T-BEAM

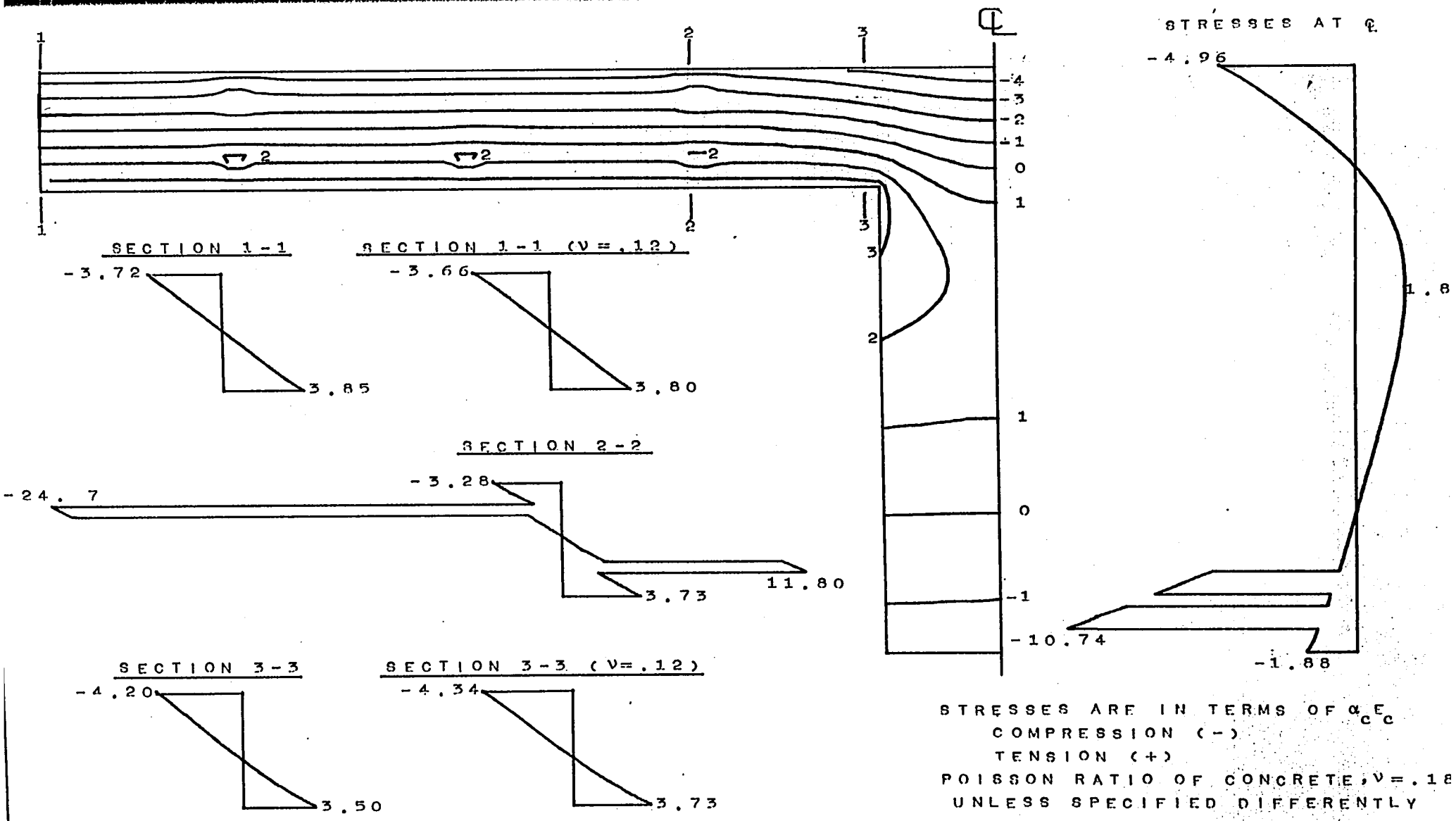

FIG. 30 STRESS DISTRIBUTION DUE TO TEMPERATURE VARITION T-8
T-BEAM

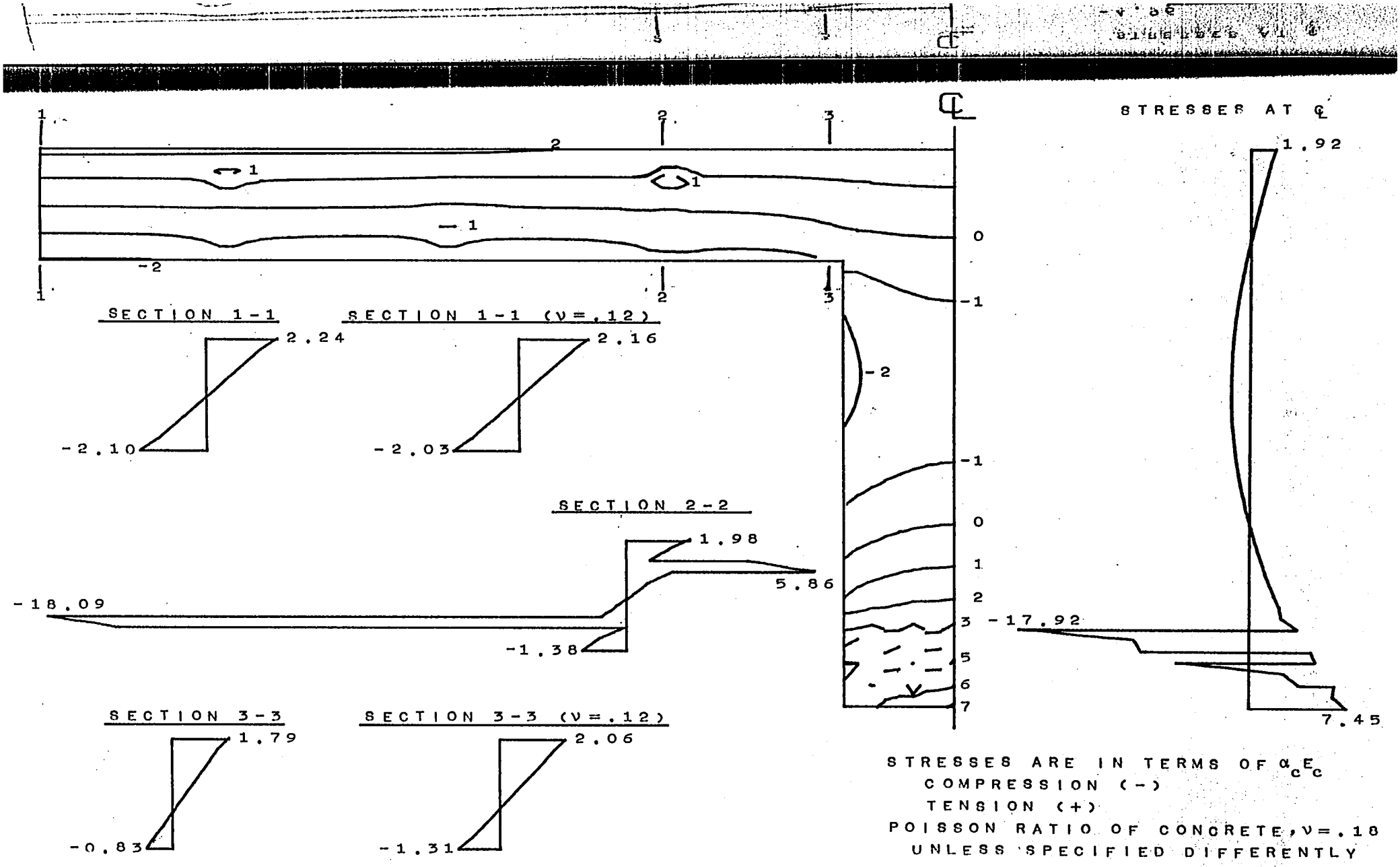

FIG. 31 STRESS DISTRIBUTION DUE TO TEMPERATURE VARITION T-9
T-BEAM

APPENDIX C - TABLES

TABLE 1 - EXPERIMENTAL AND F.E. TEMPERATURES IN COMPOSITE SECTION
LOWER SURFACE HEATED ELECTRICALLY

		CS - 1		CS - 2		CS - 3		CS - 4		CS - 5	
		EXP.	F.E.	EXP.	F.E.	EXP.	F.E.	EXP.	F.E.	EXP.	F.E.
TTG -F		84.3		84.1		87.6		76.6		73.25	
TBG -F		115.0		117.8		132.7		123.0		121.2	
Q BTU/FT-HR-F		37.85	35.98	45.06	43.454	65.01	64.177	66.88	64.804	66.88	66.248
HT BTU/HR-FT-IN-F		0.124		0.146		0.177		0.171		0.167	
HB BTU/HR-FT-IN-F		0.183		0.184		0.185		0.185		0.185	
HV BTU/HR-FT-IN-F		0.016		0.027		0.035		0.031		0.031	
AT CENTER LINE											
	TT	101.0	101.46	101.7	102.05	109.9	109.87	99.7	99.78	97.3	97.49
	TC	105.6	105.29	107.0	106.93	117.25	117.27	107.4	107.18	105.6	105.05
	TM	107.8	107.23	110.1	110.05	122.1	122.43	112.2	112.15	110.3	110.14
	TB	109.1	108.40	111.9	111.86	124.7	125.33	114.8	114.99	112.9	113.03
	T1	-		116.5		130.8		121.0		119.5	
	T2	114.2		117.5		131.8		122.2		120.4	
	T3	114.8		117.7		132.5		122.8		121.1	
AT 2 IN. FROM C.L.											
	T1	-		87.4		91.1		80.6		78.3	
	T2	-		89.3		94.1		82.9		79.9	
	TT	101.0	101.28	101.5	101.77	109.1	109.42	98.8	99.35	96.5	97.04
AT 4.375 IN. FROM C.L.											
	TT	100.7	100.91	101.1	101.17	108.7	108.46	98.6	98.42	96.0	96.08
	TB	104.3	104.55	105.5	105.53	115.3	114.88	105.2	104.91	103.3	102.72
AT 6.8125 IN FROM C.L.								80.6			
	T1	-		86.9		92.2		82.0		77.1	
	T2	-		88.4		93.7				78.5	
	TT	100.1	100.68	100.6	100.79	107.2	107.87	97.4	97.85	95.1	95.50
	TB	104.5	104.32	105.8	105.16	115.0	114.28	104.9	104.34	102.6	102.13
	T1	112.6		116.1		129.5		120.75		118.8	
	T2	113.25		177.1		131.4		121.7		120.2	
	T3	113.8		117.5		131.5		121.8		120.4	
	T4	114.5		117.8		132.7		123.0		121.2	
AT 10.375 FROM F.L.											
	TT	100.1	100.52	100.5	100.56	107.6	107.51	97.2	97.49	94.9	95.13
	TB	103.7	104.15	104.9	104.90	114.1	113.89	104.2	103.95	102.3	101.74
AT 14.6875 FROM C.L.											
	TT	99.7	100.50	100.0	100.52	107.5	107.47	97.6	97.46	94.5	95.08
	TB	103.6	104.08	104.7	104.80	114.0	113.76	104.0	103.82	102.1	101.60
BEHIND INSULATION		101.1	102.28	100.9	102.65	109.1	110.59	98.9	100.62	97.0	98.32

TABLE 1A - EXPERIMENTAL AND F.E. TEMPERATURES IN COMPOSITE SECTION
LOWER SURFACES HEATED AND UPPER SURFACE COOLED BY FORCED CONVECTION

		CS - 6		CS - 7		CS - 8		CS - 9	
		EXP.	F.E.	EXP.	F.E.	EXP.	F.E.	EXP.	F.E.
TTG -F		75.1		75.3		75.1		75.0	
TBG -F		120.6		110.0		129.0		118.0	
Q BTU/FT-HR-F		67.95	65.204	67.95	66.89	84.40	81.589	81.589	83.333
HT BTU/HR-FT-IN-F		0.182		0.510		0.202		0.580	
HB BTU/HR-FT-IN-F		0.184		0.165		0.186		0.160	
HV BTU/HR-FT-IN-F		0.030		0.055		0.040		0.048	
AT CENTER LINE									
	TT	96.6	97.04	83.5	84.39	100.0	100.26	84.1	85.01
	TC	104.9	104.48	93.7	93.15	110.3	109.84	96.4	95.92
	TM	109.5	109.44	100.2	100.31	116.5	116.74	104.3	104.71
	TB	112.6	112.27	103.4	104.06	119.6	120.57	107.9	109.44
	T1	119.0		108.4		127.8		115.7	
	T2	120.3		109.5		128.4		116.2	
	T3	120.6		109.8		128.9		117.9	
AT 2 IN. FROM C.L.									
	T1	78.3		75.7		78.9		75.0	
	T2	80.6		76.2		82.2		75.3	
	TT	96.0	96.61	83.2	83.92	99.0	99.68	83.7	84.47
AT 4.375 IN. FROM C.L.									
	TT	95.4	95.70	82.6	82.96	98.0	98.41	82.9	83.38
	TB	102.7	102.25	90.7	89.67	107.6	106.57	92.7	91.75
AT 6.8125 IN. FROM C.L.									
	T1	80.0		75.7		78.8		75.0	
	T2	80.6		76.0		80.9		75.2	
	TT	94.9	95.16	82.2	82.49	97.4	97.67	82.6	82.85
	TB	102.6	101.68	90.0	89.02	106.8	105.8	91.8	90.99
	T1	118.4		106.3		125.9		114.2	
	T2	119.4		107.9		127.7		116.1	
	T3	119.6		109.2		128.1		117.1	
	T4	120.6		109.6		128.5		117.9	
AT 10.375 FROM F.L.									
	TT	94.3	94.82	82.1	82.26	97.7	97.22	72.2	82.61
	TB	101.6	101.32	89.0	88.69	106.2	105.30	91.4	90.62
AT 14.6875 FROM C.L.									
	TT	94.2	94.78	81.2	82.26	97.3	97.17	81.8	82.62
	TB	101.5	101.18	88.9	88.60	106.0	105.13	91.1	90.52
BEHIND INSULATION		96.0	97.97	87.7	85.45	99.1	101.13	87.2	86.59

TABLE 2 - EXPERIMENTAL AND F.E. TEMPERATURES IN COMPOSITE SECTION
UPPER SURFACE HEATED ELECTRICALLY

		CS - 10		CS - 11		CS - 12		CS - 13	
		EXP.	F.E.	EXP.	F.E.	EXP.	F.E.	EXP.	F.E.
TTG -F		118.9		124.7		139.6		153.2	
TBG -F		79.2		81.0		79.0		76.0	
Q BTU/FT-HR-F		37.85	38.025	44.30	43.919	66.67	63.236	84.4	84.851
HT BTU/HR-FT-IN-F		0.096		0.100		0.103		0.117	
HB BTU/HR-FT-IN-F		0.141		0.152		0.162		0.153	
HV BTU/HR-FT-IN-F		0.061		0.068		0.076		0.073	
AT CENTER LINE									
	TT	94.3	94.27	97.5	97.45	101.7	101.55	107.8	107.60
	TC	89.7	89.51	92.0	91.08	93.9	93.69	97.2	96.88
	TM	85.4	85.14	87.0	86.06	86.9	86.76	87.8	87.22
	TB	83.6	83.09	85.4	84.81	83.8	83.67	84.1	82.86
	T1	79.3		82.2		79.3		76.7	
	T2	79.3		81.5		79.2		76.6	
	T3	79.2		81.4		79.2		76.3	
AT 2 IN. FROM C.L.									
	T1	105.25		110.0		120.1		129.7	
	T2	100.4		104.7		113.0		122.6	
	TT	94.6	94.75	98.0	97.99	102.6	102.30	109.1	108.63
AT 4.375 IN. FROM C.L.									
	TT	95.5	95.88	99.0	99.24	104.0	104.05	110.8	111.02
	TB	92.1	92.16	95.1	94.95	98.1	97.87	102.8	102.72
AT 6.8125 IN FROM C.L.									
	T1	103.6		108.3		118.1		127.6	
	T2	100.6		105.0		113.5		122.5	
	TT	95.9	96.61	99.4	100.04	105.1	105.16	112.4	112.54
	TB	-	92.90	-	95.74	-	98.96	-	104.24
	T1	-		-		-		-	
	T2	80.5		82.7		80.9		84.3	
	T3	80.2		82.2		80.4		78.8	
	T4	-		-		-		77.9	
AT 10.375 FROM F.L.									
	TT	96.4	97.15	100.2	100.62	106.8	105.95	113.1	113.59
	TB	92.8	93.43	96.1	96.31	99.4	99.73	104.8	105.29
AT 14.6875 FROM C.L.									
	TT	96.6	97.32	100.3	100.79	106.9	106.17	113.2	113.89
	TB	92.9	93.64	96.2	96.54	99.6	100.03	105.0	105.71
BEHIND INSULATION		-	95.57	96.2	98.69	101.0	102.41	107.3	109.85

TABLE 3 - EXPERIMENTAL AND F.E. TEMPERATURES IN COMPOSITE SECTION SURFACES COOLED AT MELTIG ICE TEMPERATURE

		CS - 14		CS - 15	
		EXP.	F.E.	EXP.	F.E.
TTG -F		77.6		32.66	
TBG -F		32.68		70.0	
Q BTU/FT-HR-F			196.01		192.01
HT BTU/HR-FT-IN-F		0.312			
HB BTU/HR-FT-IN-F				0.365	
HV BTU/HR-FT-IN-F				0.061	
AT CENTER LINE					
	TT	42.0	41.76	33.0	32.66
	TC	32.9	32.68	45.0	44.00
	TM	32.7	32.68	55.4	54.97
	TB	32.7	32.68	59.5	60.11
	T1	-		66.0	
	T2	-		68.2	
	T3	-		69.0	
AT 2 IN. FROM C.L.					
	T1	74.5		-	
	T2	61.5		-	
	TT	42.3	41.93	32.8	32.66
AT 4.375 IN. FROM C.L.					
	TT	42.6	42.12	32.8	32.66
	TB	32.7	32.68	42.2	41.84
AT 6.8125 IN FROM C.L.					
	T1	73.5		-	
	T2	62.3		-	
	TT	42.8	42.19	32.7	32.66
	TB	-	32.68	-	41.66
	T1	-		-	
	T2	-		68.6	
	T3	-		69.4	
	T4				
AT 10.375 FROM F.L.		42.9	42.23	32.7	32.66
	TT	32.8	32.68	42.0	41.59
	TB				
AT 14.6875 FROM C.L.		43.0	42.13	32.5	32.66
	TT	32.8	32.68	42.0	41.54
	TB				
		39.8	37.49	37.9	37.17

TABLE 4 - EXPERIMENTAL AND F.E. TEMPERATURES IN T-BEAM
LOWER SURFACE HEATED ELECTRICALLY

	T - 1		T - 2		T - 3		T - 4	
	EXP.	F.E.	EXP.	F.E.	EXP.	F.E.	EXP.	F.E.
TTG -F	74.5		72.5		73.0		72.5	
TBG -F	104.5		108.75		121.75		134.0	
Q . BTU/FT-HR-F	37.85	29.361	44.30	38.560	66.67	56.603	84.42	75.298
HT BTU/HR-FT-IN-F	0.120		0.130		0.150		0.165	
HB BTU/HR-FT-IN-F	0.130		0.140		0.155		0.165	
HV BTU/HR-FT-IN-F								
AT CENTER LINE								
TT	89.0	88.58	89.7	88.90	94.9	94.58	99.7	99.35
TB	97.7	98.00	101.2	101.08	112.5	112.06	123.0	122.26
T1	103.6		106.7		120.5		132.2	
T2	103.8		107.8		121.3		133.5	
T3	104.0		108.3		121.3		133.5	
AT 2 IN. FROM C.L.								
T1	78.4		76.0		77.1		77.2	
T2	78.7		77.0		78.0		79.6	
AT 2.144 IN FROM C.L.								
TC	92.4	92.69	94.3	94.29	101.9	102.48	109.1	109.82
AT 4.5	95.0	95.34	96.75	97.69	106.4	107.30	115.0	116.11
AT 9.5	96.7	97.62	100.1	100.59	110.6	111.37	121.0	121.37
AT 3.25 IN. FROM C.L.								
TT	89.0	88.49	89.1	88.81	101.8	94.51	98.9	99.29
AT 6.875 IN FROM C.L.								
T1	77.7		75.9		77.1		77.2	
T2	79.2		77.1		78.4		79.6	
TB	92.4	91.95	93.8	93.40	-	101.31	108.8	108.40
T1	102.1		105.9		118.0		129.3	
T2	102.6		106.5		119.0		130.9	
T3	103.5		107.2		120.1		133.0	
AT 10.5 IN.FROM C.L.								
TT	88.9	88.23	88.9	88.54	94.4	94.20	98.6	98.96
TB	92.3	91.89	93.7	93.34	101.7	101.27	108.4	108.37
AT 14.75 IN FROM C.L.								
TT	88.1	88.25	88.6	88.57	93.8	94.26	98.7	99.05
TB	92.1	91.84	93.4	93.29	101.4	101.21	108.9	108.29

TABLE 5 - EXPERIMENTAL AND F.E. TEMPERATURES IN T-BEAM
UPPER SURFACE HEATED ELECTRICALLY

	T - 5		T - 6		T - 7	
	EXP.	F.E.	EXP.	F.E.	EXP.	F.E.
TTG -F	107.0		118.0		134.0	
TBG -F	71.5		72.0		72.0	
Q BTU/FT-HR-F	37.85	31.243	44.30	44.900	66.67	63.025
HT BTU/HR-FT-IN-F	0.090		0.105		0.115	
HB BTU/HR-FT-IN-F	0.140		0.150		0.150	
HV BTU/HR-FT-IN-F	0.095		0.095		0.075	
AT CENTER LINE						
TT	86.3	86.60	92.1	92.98	101.5	102.33
TB	74.4	73.78	75.0	75.14	77.9	77.82
T1	-		-		-	
T2	-		-		-	
T3	-		-		-	
AT 2 IN. FROM C.L.						
T1	96.5		106.0		118.1	
T2	-		-		-	
AT 2.144 IN FROM C.L.						
TC	82.5	82.22	86.5	86.74	93.0	93.73
AT 4.5	78.3	78.38	81.4	81.49	86.1	86.88
AT 9.5	73.5	74.29	75.5	75.86	79.2	78.88
AT 3.25 IN. FROM C.L.						
TT	87.5	86.95	93.4	93.37	102.6	102.64
AT 6.875 IN FROM C.L.						
T1	96.0		105.7		117.6	
T2	-		-		-	
TB	83.7	83.55	88.4	88.33	95.4	95.27
T1	-		-		-	
T2	-		-		-	
T3	-		-		-	
AT 10.5 IN.FROM C.L.						
TT	88.0	87.53	94.3	94.11	103.8	103.27
TB	84.2	83.78	88.8	88.56	96.0	95.43
AT 14.75 IN FROM C.L.						
TT	88.0	87.56	94.3	94.11	103.5	103.24
TB	83.8	83.87	88.9	88.66	95.7	95.54

TABLE 6 - EXPERIMENTAL AND F.E. TEMPERATURES IN T-BEAM SURFACES COOLED AT ICE TEMPERATURE

	T - 8		T - 9	
	EXP.	F.E.	EXP.	F.E.
TTG -F	72.0		32.5	
TBG -F	32.5		70.0	
Q BTU/FT-HR-F	-	168.45	-	180.37
HT BTU/HR-FT-IN-F	0.310		-	
HB BTU/HR-FT-IN-F	-		0.370	
HV BTU/HR-FT-IN-F	-		0.080	
AT CENTER LINE				
TT	42.3	42.55	32.9	32.50
TB	32.2	32.50	55.0	55.54
T1			-	
T2			-	
T3			-	
AT 2 IN. FROM C.L.				
T1				
T2				
AT 2.144 IN FROM C.L.				
TC	32.8	32.50	42.0	41.12
AT 4.5	32.7	32.50	47.8	46.42
AT 9.5	32.6	32.50	54.0	54.34
AT 3.25 IN. FROM C.L.				
TT	-	41.58	32.4	32.50
AT 6.875 IN FROM C.L.				
T1	-			
T2	-			
TB	32.8	32.50	42.0	41.60
T1	-		-	
T2	-		-	
T3	-		-	
AT 10.5 IN.FROM C.L.				
TT	41.0	41.07	32.7	32.50
TB	32.4	32.50	42.8	41.79
AT 14.75 IN FROM C.L.				
TT	41.5	40.97	33.6	32.50
TB	32.7	32.50	42.4	41.72

TABLE 7 - EXPERIMENTAL AND F.E. STRAINS (IN/IN X10<-6>) IN COMPOSITE SECTION

FOR STEEL, COEFFICIENT OF EXPANSION USED 6.5X<-6> AND POISSON'S RATIO 0.30
FOR CONCRETE, COEFFICIENT OF EXPANSION USED 5.5X<-6> AND POISSON'S RATIO FROM 0.12 TO 0.18

	TEMPERATURE REFERENCE TR = 76.25 F									TR = 79 F				TR = 75 F	
	CS-1	CS-2	CS-3	CS-4	CS-5	CS-6	CS-7	CS-8	CS-9	CS10	CS11	CS12	CS13	CS-14	CS-15
UPPER SURFACE OF SLAB FINITE ELEMENT	142	143	186	131	118	116	44	132	48	93	126	152	190	-213	-231
EXPERIMENTAL VALUES AT C.L.	105	100	170	92	88	93	48	116	61	83	114	146	178	-196	-262
4 IN. FROM C.L. LEFT SIDE	101	103	161	107	101	89	39	109	42	74	108	138	162	-203	-249
9.5 IN. FROM C.L. LEFT SIDE	115	105	144	96	98	102	22	127	36	89	119	147	173	-178	-256
	87	92	151	75	82	58	34	122	44	82	113	140	181	-183	-237
	95	101	138	88	91	82	19	124	40	78	120	153	169	-191	-253
LOWER SURFACE OF SLAB FINITE ELEMENT	158	164	217	158	146	143	75	168	86	78	110	129	157	-231	-203
EXPERIMENTAL VALUES 4 IN. FROM C.L. LEFT SIDE	137	137	181	124	109	114	50	167	110	80	104	133	160	-221	-234
9.5 IN. FROM C.L. LEFT SIDE	126	124	168	138	132	125	62	180	96	74	92	124	148	-223	-210
	120	128	188	147	129	110	64	177	78	65	86	131	144	-240	-222
	134	135	175	131	118	120	57	172	89	71	98	118	153	-226	-228
STEEL BEAM 3.375 ABOVE FINITE ELEMENT	164	171	227	168	156	153	86	180	99	73	105	120	145	-237	-194
EXPERIMENTAL VALUES RIGHT SIDE	171	186	192	173	164	176	79	140	118	67	101	115	150	-260	-207
LEFT SIDE	158	162	208	159	157	151	92	163	130	58	88	126	141	-247	-181
STEEL BEAM 3.375 BELOW FINITE ELEMENT	214	236	326	258	245	240	185	295	221	25	54	46	39	-296	-106
EXPERIMENTAL VALUES RIGHT SIDE	221	252	297	246	253	239	206	307	233	14	45	50	71	-331	-72
LEFT SIDE	228	239	276	222	241	232	212	316	210	22	37	43	53	-312	-88

TABLE 8 - EXPERIMENTAL AND F.E. STRAINS (IN/INX10<-6>) IN T-BEAM

FOR STELL BEAM, COEFFICIENT OF EXPANSION 6.5X<-6> AND POISSON'S RAIO 0.30
FOR CONCRETE, COEFFICIENT OF EXPANSION 5.5<-6>
AND POISSON'S RATIO (0.12 TO 0.18)

	TR = 71.5 F				TR = 71.5 F			TR = 70 F	
	T-1	T-2	T-3	T-4	T-5	T-6	T-7	T-8	T-9
UPPER SURFACE OF SLAB									
FINITE ELEMENT	97	100	135	155	83	116	165	-176	-193
EXPERIMENTAL VALUES									
AT C.L.	112	98	148	157	59	88	136	-149	-226
4 IN. FROM C.L.	119	117	133	174	67	81	147	-142	-203
LEFT SIDE	102	123	129	149	78	104	151	-153	-191
9.5 IN. FROM C.L.	129	106	144	155	62	91	142	-158	-218
LEFT SIDE	122	115	139	152	71	98	159	-135	-209
LOWER SURFACE OF SLAB									
FINITE ELEMENT	112	119	160	198	67	95	135	-189	-169
EXPERIMENTAL VALUES									
4 IN. FROM C.L.	131	130	162	189	48	64	96	-173	-151
LEFT SIDE	117	148	147	182	40	72	122	-154	-165
9.5 IN. FROM C.L.	138	139	157	208	54	87	129	-166	-147
LEFT SIDE	129	128	142	195	43	75	113	-180	-158
4 IN. FROM UPPER SLAB									
FINITE ELEMENT	121	130	176	218	57	89	117	-196	-154
EXPERIMENTAL VALUES									
RIGHT SIDE	147	159	173	220	29	42	68	-181	-145
LEFT SIDE	142	154	160	209	38	57	84	-201	-134
11.375 IN. FROM TOP									
FINITE ELEMENT	158	177	242	303	16	25	42	-228	-92
EXPERIMENTAL VALUES									
RIGHT SIDE	191	202	223	290	-10	6	24	-223	-117
LEFT SIDE	178	193	237	277	5	14	31	-208	-105

TABLE 9A - F.E. STRAINS (IN/INX10<-6>) DUE TO TEMPERATURE DIFFERENTIAL
LOWEST TEMPERATURE ON UPPER SURFACE IN COMPOSITE SECTION

	UPPER SURFACE		LOWER SURFACE		3.875 ABOVE NA		3.875 BELOW NA	
	5.5<-6>	4.5<-6>	5.5<-6>	4.5<-6>	5.5<-6>	4.5<-6>	5.5<-6>	4.5<-6>
CS-(10 F)								
ν =.12	55.42	45.86	57.67	50.45	58.45	52.04	65.62	56.70
ν =.15	55.40	45.83	57.75	50.53	58.57	52.16	66.05	67.18
ν =.18	55.39	45.82	57.84	50.61	58.67	52.27	66.40	67.54
CS - 1								
TU=100.44 F								
ν =.12	8.37		18.36		21.82		53.71	
ν =.15	8.36		18.47		21.98		54.27	
ν =.18	8.34		18.55		22.08		54.69	
CS - 2								
TU=100.44 F								
ν =.12	9.61	7.23	24.32	22.44	29.41	27.71	76.41	76.32
ν =.15	9.60	7.21	24.47	22.58	29.62	27.90	77.13	77.00
ν =.18	9.57	7.18	24.56	22.67	29.76	28.03	77.66	77.51
CS - 3								
TU=107.34 F								
ν =.12	13.65		37.06		45.06		120.13	
ν =.15	13.63		37.30		45.55		121.06	
ν =.18	13.59		37.44		45.71		121.93	
CS - 4								
TU= 97.33 F								
ν =.12	13.93		36.83		44.65		118.03	
ν =.15	13.92		37.06		44.96		119.14	
ν =.18	13.88		37.21		45.29		119.84	
CS - 5								
TU= 94.96 F								
ν =.12	14.28		37.71		45.84		120.71	
ν =.15	14.27		37.95		46.16		121.84	
ν =.18	14.23		38.10		46.38		122.67	
CS - 6								
TU= 94.66 F								
ν =.12	13.94		36.76		44.67		117.60	
ν =.15	13.92		36.99		44.93		118.77	
ν =.18	13.88		37.14		45.20		119.52	
CS - 7								
TU= 82.18 F								
ν =.12	11.05		40.54		50.76		145.00	
ν =.15	11.04		40.80		51.07		146.29	
ν =.18	10.99		40.97		51.36		147.16	
CS - 8								
TU= 97.02 F								
ν =.12	16.89		47.73		58.42		156.96	
ν =.15	16.87		48.03		58.83		158.38	
ν =.18	16.82		48.22		59.10		159.44	
CS - 9								
TU= 82.53 F								
ν =.12	13.47		49.71		62.28		178.09	
ν =.15	13.45		50.04		62.72		179.63	
ν =.18	13.40		50.24		63.02		180.76	

TABLE 9B - F.E. STRAINS (IN/INX10<-6>) DUE TO TEMPERUTURE DIFFERENTIAL
LOWEST TEMPERATURE AT LOWER SURFACE IN COMPOSITE SECTION

	UPPER SURFACE		LOWER SURFACE		3.875 ABOVE NA		3.875 BELOW NA	
	5.5<-6>	4.5<-6>	5.5<-6>	4.5<-6>	5.5<-6>	4.5<-6>	5.5<-6>	4.5<-6>
CS- 10								
TL= 83.00 F								
ν =.12	70.65		54.85		49.38		-1.08	
ν =.15	70.63		54.81		49.33		-1.22	
ν =.18	70.68		54.82		49.34		-1.31	
CS- 11								
TL= 84.71 F								
ν =.12	79.14	66.56	61.41	51.99	55.26	46.94	-1.39	0.38
ν =.15	79.12	66.53	62.36	51.95	55.20	46.90	-1.56	0.31
ν =.18	79.18	66.55	61.37	51.96	55.21	46.90	-1.67	0.27
CS- 12								
TL= 83.53 F								
ν =.12	111.20		86.23		77.57		-2.22	
ν =.15	111.17		86.15		77.48		-2.43	
ν =.18	111.25		86.18		77.48		-2.27	
CS- 13								
TL=82.67 F								
ν =.12	154.27		119.71		107.73		-2.72	
ν =.15	154.24		119.61		107.61		-3.04	
ν =.18	154.34		119.65		107.62		-3.25	

TABLE 9C - F.E. STRAINS (IN/INX10<-6>) DUE TO TEMPERUTJRE DIFFERENTIAL
COOLED COMPOSITE SECTION

	UPPER SURFACE		LOWER SURFACE		3.875 ABOVE NA		3.875 BELOW NA	
	5.5<-6>	4.5<-6>	5.5<-6>	4.5<-6>	5.5<-6>	4.5<-6>	5.5<-6>	4.5<-5>
CS- 14								
TL= 32.68 F								
ν =.12	28.40	23.55	20.49	17.01	17.75	14.73	-7.51	-6.19
ν =.15	28.41	23.56	20.34	16.87	17.54	14.56	-8.25	-6.80
ν =.18	28.48	23.61	20.28	16.82	17.43	14.47	-8.79	-7.24
CS- 15								
TU= 32.66 F								
ν =.12	10.68	6.59	48.07	44.82	61.04	58.07	180.52	180.23
ν =.15	10.67	6.57	48.40	45.12	61.48	58.49	182.05	181.67
ν =.18	10.61	6.51	48.61	45.31	61.78	58.76	183.19	182.75

TABLE 10A -F.E. STRESSES (PSI) FROM TEMPERATURE DIFFERENTIAL -COMPOSITE BEAM

	SECTION 1-1		SECTION 2-2				AL CENTER LINE			
	UPPER	LOWER	UPPER	1-BAR	2-BAR	LOWER	UPPER	INT-C	INT-S	LOWER
CS-(10 F)										
ν =.12	1.6	10.0	-0.4	-319	-270	16.3	-7.8	19.8	-268.	84
ν =.15	1.5	10.3	3.3	-302	-269	13.2	-3.9	19.7	-286.	67
ν =.18	1.6	10.6	6.4	-291	-267	9.2	-0.4	19.1	-295.	53
-- COEF. EXP.=4.5<-6>										
ν =.12	3.2	20.4	1.6	-607	-525	28.1	-8.9	33.6	-524.	152
ν =.15	3.1	20.7	6.0	-589	-525	24.9	-5.1	34.6	-546.	133
ν =.18	3.1	21.0	9.7	-578	-523	22.0	-1.8	35.2	-557.	119
CS - 1										
TU=100.44 F -- COEF. EXP.=5.5<-6>										
ν =.12	32.1	-8.2	17.6	65	-128	-5.8	2.1	-29.3	-434.	237
ν =.15	32.3	-8.0	23.0	70	-129	-10.6	8.4	-31.0	-461.	218
ν =.18	32.4	-7.9	27.8	73	-130	-15.2	14.4	-33.0	-477.	205
CS - 2										
TU=100.44 F -- COEF. EXP.=5.5<-6>										
ν =.12	36.8	-1.0	16.9	69	-133	0.1	-8.1	-40.5	-590.	319
ν =.15	37.1	-0.7	23.7	76	-135	-6.1	0.1	-42.7	-625.	294
ν =.18	37.3	-0.6	29.9	80	-136	-12.0	7.8	-45.5	-645.	277
-- COEF. EXP.=4.5<-6>										
ν =.12	27.7	8.7	10.6	-66	-199	11.1	-12.1	-20.8	-668.	321
ν =.15	27.9	9.0	17.1	-40	-201	5.4	-4.8	-21.9	-702.	297
ν =.18	28.0	9.1	22.9	-26	-202	-0.0	2.1	-23.6	-721.	280
CS - 3										
TU=107.34 F -- COEF. EXP.=5.5<-6>										
ν =.12	52.3	3.7	22.3	101	-178	5.3	-17.6	-62.9	-910.	495
ν =.15	52.7	4.2	32.8	112	-181	-4.2	-5.0	-66.2	-963.	456
ν =.18	52.9	4.4	42.2	118	-182	-13.2	6.8	-70.5	-994.	430
CS - 4										
TU= 97.33 F -- COEF. EXP.=5.5<-6>										
ν =.12	53.4	1.2	23.7	104	-187	3.2	-14.8	-61.9	-899.	489
ν =.15	53.8	1.7	34.2	115	-189	-6.2	-2.3	-65.2	-952.	451
ν =.18	54.1	1.8	43.5	121	-191	-15.2	9.5	-69.5	-982.	424
CS - 5										
TU= 94.96 F -- COEF. EXP.=5.5<-6>										
ν =.12	54.8	1.5	24.2	105	-217	-3.3	-15.5	-63.4	-920.	500
ν =.15	55.1	2.0	34.9	117	-194	-6.4	-2.8	-66.8	-975.	461
ν =.18	55.4	2.1	44.4	123	-196	-15.6	9.3	-71.2	-1007	434

CONT D TABLE 10A

CS - 6
TU= 94.66 F -- COEF. EXP.=5.5<-6>

ν=.12	53.4	0.2	24.4	107	-188	2.7	-13.3	-61.6	-895.	488
ν=.15	53.8	0.7	34.8	118	-191	-6.7	-0.8	-64.9	-948.	450
ν=.18	54.1	0.8	44.2	124	-192	-15.8	11.0	-69.2	-979.	423

CS - 7
TU= 82.18 F -- COEF. EXP.=5.5<-6>

ν=.12	42.6	16.2	17.2	127	-106	21.8	-22.6	-72.2	-1025	579
ν=.15	42.9	16.8	29.0	139	-109	11.2	-8.4	-76.1	-1085	535
ν=.18	43.2	17.0	39.4	146	-111	1.2	5.1	-81.1	-1119	504

CS - 8
TU= 97.02 F -- COEF. EXP.=5.5<-6>

ν=.12	64.8	7.8	27.0	131	-212	10.0	-25.0	-81.8	-1179	644
ν=.15	65.2	8.4	40.5	145	-215	-2.2	-8.8	-86.1	-1248	594
ν=.18	65.6	5.6	52.6	153	-217	-13.7	6.5	-91.7	-1287	560

CS - 9
TU= 82.53 F -- COEF. EXP.=5.5<-6>

ν=.12	52.0	17.3	22.3	161	-135	25.6	-23.0	-87.3	-1244	705
ν=.15	52.4	18.1	36.8	177	-139	12.5	-5.9	-92.2	-1318	650
ν=.18	52.7	18.3	49.7	185	-141	0.2	10.8	-98.3	-1361	613

TABLE 10B -F.E. STRESSES (PSI) FROM TEMPERATURE DIFFERENTIAL -COMPOSITE BEAM

	SECTION 1-1		SECTION 2-2				AT CENTER LINE			
	UPPER	LOWER	UPPER	1-BAR	2-BAR	LOWER	UPPER	INT-C	INT-S	LOWER
CS- 10										
TL= 83.00 F -- COEF. EXP.=5.5<-6>										
ν=.12	-33.3	-12.6	-3.4	-445	-352	7.4	31.1	83.5	378	-275
ν=.15	-33.6	-12.6	-5.3	-445	-345	9.4	27.9	85.6	389	-272
ν=.18	-33.7	-12.2	-7.3	-443	-338	11.4	24.7	87.7	397	-271
CS- 11										
TL= 84.71 F -- COEF. EXP.=5.5<-6>										
ν=.12	-37.9	-12.1	-5.4	-509	-394	8.9	32.6	93.8	427	-315
ν=.15	-38.3	-12.0	-7.7	-508	-385	11.2	28.9	96.2	440	-310
ν=.18	-38.4	-11.6	-10.1	-506	-378	13.7	25.2	98.6	449	-310
-- COEF. EXP.=4.5<-6>										
ν=.12	-24.3	-3.3	3.4	-876	-712	16.0	30.5	87.8	109	-211
ν=.15	-24.6	-3.2	2.6	-875	-706	17.8	27.6	90.6	115	-210
ν=.18	-24.8	-3.0	1.5	-872	-700	19.6	24.6	93.5	121	-211
CS- 12										
TL= 83.53 F -- COEF. EXP.=5.5<-6>										
ν=.12	-54.2	-14.7	-9.5	-727	-554	13.2	43.5	132.5	606	-451
ν=.15	-54.7	-14.6	-12.8	-726	-541	16.6	38.2	135.9	625	-444
ν=.18	-54.9	-14.1	-16.2	-723	-530	20.2	32.8	139.4	639	-443
CS- 13										
TL=82.67 F -- COEF. EXP.=5.5<-6>										
ν=.12	-71.1	-23.1	-10.8	-998	-781	15.6	61.6	182.0	821	-613
ν=.15	-71.8	-23.0	-15.1	-997	-764	20.2	54.5	186.6	847	-605
ν=.18	-72.0	-22.3	-19.8	-992	-749	24.9	47.3	191.4	865	-604

TABLE 10C -F.E. STRESSES (PSI) FROM TEMPERATURE DIFFERENTIAL -COMPOSITE BEAM

	SECTION 1-1		SECTION 2-2				AT CENTER LINE			
	UPPER	LOWER	UPPER	1-BAR	2-BAR	LOWER	UPPER	INT-C	INT-S	LOWER
CS- 14										
TL= 32.68 F -- COEF. EXP.=5.5<-6>										
ν =.12	-94.0	78.6	-77.1	-531	137	71.6	-73.2	77.8	602	-384
ν =.15	-94.6	78.5	-84.8	-554	165	78.9	-82.7	81.2	643	-364
ν =.18	-95.0	79.0	-92.2	-569	182	86.4	-91.8	85.0	669	-355
-- COEF. EXP.=4.5<-6>										
ν =.12	-75.7	65.2	-61.0	-682	31	59.7	-58.6	64.5	493	-317
ν =.15	-76.2	65.1	-67.1	-704	51	65.8	-66.5	67.4	498	-301
ν =.18	-76.5	65.5	-72.9	-716	65	72.0	-74.0	70.5	501	-293
CS- 15										
TU= 32.66 F -- COEF. EXP.=5.5<-6>										
ν =.12	41.7	-8.0	26.9	156	-176	13.2	18.3	-51.5	-853	686
ν =.15	42.1	-7.3	41.5	172	-180	-7.4	36.1	-56.7	-929	634
ν =.18	42.5	-7.1	54.7	180	-182	-12.6	53.2	-63.2	-972	597
-- COEF. EXP.=4.5<-6>										
ν =.12	26.0	14.1	12.2	-85	-291	34.3	1.2	-17.4	-985	689
ν =.15	26.4	14.8	16.0	-31	-295	22.1	17.2	-20.6	-1058	634
ν =.18	26.7	15.0	38.2	58	-297	10.6	32.4	-25.0	-1100	597

TABLE 11A -F.E. STRAINS (IN/INX10<-6>) DUE TO TEMPERATURE DIFFERENTIAL T-BEAM
LOWER SURFACE HEATED -- CONCRETE COEFFICIENT OF EXPANSION 5.5X10<-6>

	UPPER SURFACE	LOWER SLAB	4 FROM TOP	11.375 FORM TOP
T - (10 F)				
ν =.12	54.73	55.86	56.69	60.20
ν =.15	54.52	55.86	56.66	60.07
ν =.18	54.12	55.85	56.65	60.06
T - 1				
TU= 88.18 F				
ν =.12	5.81	18.45	26.03	58.25
ν =.15	5.85	18.44	25.99	58.09
ν =.18	5.83	18.43	25.99	58.12
T - 2				
TU= 88.48 F				
ν =.12	7.62	23.81	33.52	74.75
ν =.15	7.67	23.80	33.47	75.48
ν =.18	7.65	23.79	33.47	74.62
T - 3				
TU= 94.13 F				
ν =.12	11.23	34.18	47.95	106.47
ν =.15	11.30	34.16	47.88	106.16
ν =.18	11.27	34.15	47.88	106.21
T - 4				
TU= 98.88 F				
ν =.12	15.00	44.87	62.79	138.97
ν =.15	15.10	44.85	62.69	138.55
ν =.18	15.06	44.83	62.69	138.62

TABLE 11B -F.E. STRAINS (IN/INX10<-6>) DUE TO TEMPERATURE DIFFERENTIAL T-BEAM
UPPER SURFACE HEATED & COOLED BEAM
CONCRETE COEFFIENT OF EXPANSION 5.5X10<-6>

	UPPER SURFACE	LOWER SLAB	4 FROM TOP	11.375 FORM TOP
T - 5				
TL= 73.64 F				
ν=.12	72.02	65.12	45.16	2.79
ν=.15	71.75	65.14	44.88	2.81
ν=.18	71.32	64.46	45.16	3.40
T - 6				
TL= 74.96 F				
ν=.12	98.30	75.23	61.63	3.83
ν=.15	97.92	75.25	61.66	3.87
ν=.18	97.31	75.25	61.64	3.82
T - 7				
TL= 77.54 F				
ν=.12	131.53	101.25	83.08	5.87
ν=.15	131.55	101.28	83.12	5.93
ν=.18	131.55	101.27	83.09	5.85
T - 8				
TL= 32.5 F				
ν=.12	27.81	20.48	16.08	-2.61
ν=.15	27.77	20.48	16.11	-2.47
ν=.18	27.80	20.48	16.09	-2.56
T - 9				
TU= 32.5 F				
ν=.12	11.46	40.97	58.68	133.93
ν=.15	11.55	40.95	58.58	133.54
ν=.18	11.51	40.93	58.58	133.60

TABLE 12A -F.E. STRESSES (PSI) FROM TEMPERATURE DIFFERENTIAL IN T-BEAM
LOWER SURFACE HEATED -- CONCRETE COEFFICIENT OF EXPANSION 5.5X10<-6>

	SECTION 1-1		SECTION 2-2				AT CENTER LINE			
	UPPER	LOWER	UPPER	1-BAR	2-BAR	LOWER	UPPER	1-BAR	2-BAR	LOWER
T - (10 F)										
ν=.12	-2.0	3.2	-0.8	-370	-347	4.9	-2.3	-191	-165	31.5
ν=.15	-1.8	3.2	-2.7	-371	-341	7.2	-4.4	-192	-167	38.6
ν=.18	-1.8	3.2	-1.5	-362	-338	6.3	-3.2	-188	-165	36.6
T - 1 TU= 88.18 F										
ν=.12	22.5	-8.2	16.1	53	-145	-8.0	13.6	-137	65	63.9
ν=.15	22.9	-8.5	12.2	51	-140	-4.0	9.9	-140	65	73.5
ν=.18	23.0	-8.8	14.6	54	-141	-6.2	12.1	-135	65	70.2
T - 2 TU= 88.48 F										
ν=.12	29.5	-12.5	22.0	74	-192	-11.3	19.9	-199	84	82.1
ν=.15	30.0	-12.8	17.0	71	-184	-6.2	15.1	-178	83	94.6
ν=.18	30.2	-13.2	20.1	75	-186	-9.2	18.0	-172	84	90.3
T - 3 TU= 94.13 F										
ν=.12	43.4	-21.4	33.7	117	-285	-18.2	32.9	-246	121	117.0
ν=.15	44.1	-21.9	26.5	112	-275	-11.0	26.0	-251	120	135.0
ν=.18	44.5	-22.4	31.0	117	-277	-15.5	30.2	-242	122	129.1
T - 4 TU= 98.88 F										
ν=.12	58.0	-30.9	46.0	161	-383	-26.1	46.7	-319	160	152.7
ν=.15	59.0	-31.6	37.0	154	-369	-16.2	37.4	-356	158	176.5
ν=.18	59.5	-32.3	42.5	161	-373	-22.0	43.1	-313	160	168.2

TABLE 12B -F.E. STRESSES (PSI) FROM TEMPERATURE DIFFERENTIAL IN T-BEAM
UPPER SURFACE HEATED & COOLED BEAM

CONCRETE COEFFICIENT OF EXPANSION 5.5X10<-6>

	SECTION 1-1		SECTION 2-2				AT CENTER LINE			
	UPPER	LOWER	UPPER	1-BAR	2-BAR	LOWER	UPPER	1-BAR	2-BAR	LOWER
T - 5										
TL= 73.64 F										
ν =.12	-22.4	-2.4	-9.1	-540	-366	4.3	1.4	-54	-309	-45.4
ν =.15	-22.7	-2.1	-7.0	-526	-362	2.7	2.9	-53	-310	-47.4
ν =.18	-22.9	-1.9	-7.9	-521	-355	4.2	2.0	-54	-309	-46.6
T - 6										
TL= 74.96 F										
ν =.12	-31.4	2.2	-15.4	-754	-487	6.6	-5.3	-74	-422	-61.9
ν =.15	-31.7	2.7	-12.6	-749	-482	6.4	-3.1	-72	-424	-65.4
ν =.18	-32.0	3.0	-14.2	-738	-473	5.0	-4.6	-74	-421	-63.6
T - 7										
TL= 77.54 F										
ν =.12	-41.3	12.6	-23.9	-956	-712	16.8	-18.9	-274	-515	-80.4
ν =.15	-41.7	13.2	-20.0	-1002	-714	13.9	-15.8	-272	-515	-85.3
ν =.18	-42.2	13.7	-22.2	-993	-697	16.7	-17.9	-274	-516	-82.9
T - 8										
TL= 32.5 F										
ν =.12	-75.6	78.3	-69.4	-523	248	78.2	-99.9	-112	-222	-34.4
ν =.15	-76.2	78.9	-64.5	-504	232	73.3	-99.2	-107	-221	-42.8
ν =.18	-76.7	79.5	-67.7	-511	243	76.9	-99.8	-110	-222	-38.8
T - 9										
TU= 32.5 F										
ν =.12	44.6	-41.9	44.0	121	-382	-32.0	43.0	-375	78	140.2
ν =.15	45.6	-42.6	35.3	114	-370	-22.9	34.4	-381	76	161.2
ν =.18	46.1	-43.3	40.8	121	-373	-28.4	39.5	-370	78	153.7

APPENDIX D - FLOW CHARTS

1 - HEAT CONDUCTION PROBLEM

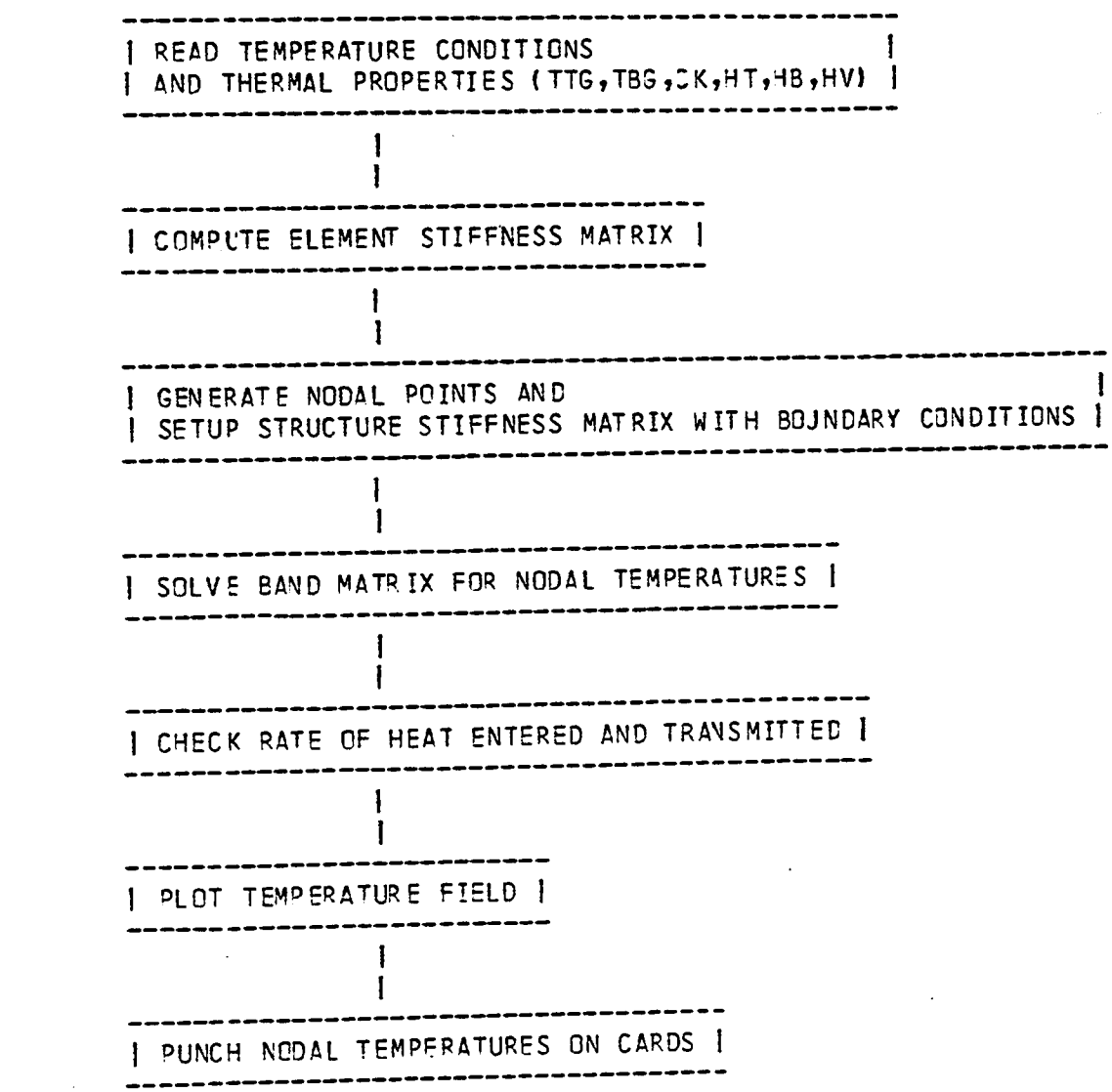

2 - NONTHERMAL ELASTICITY PROBLEMS

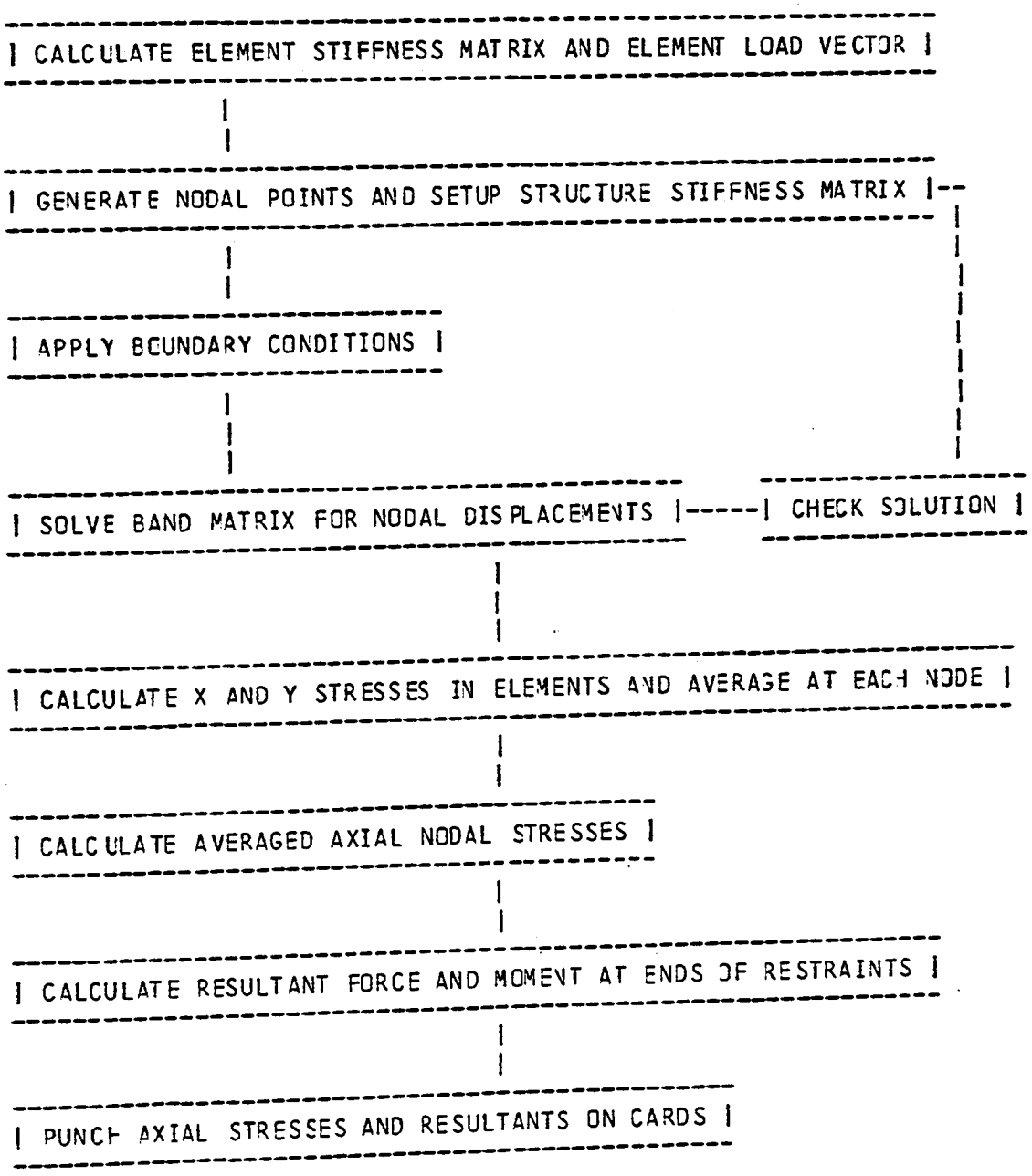

3 - THERMAL STRESS PROBLEM

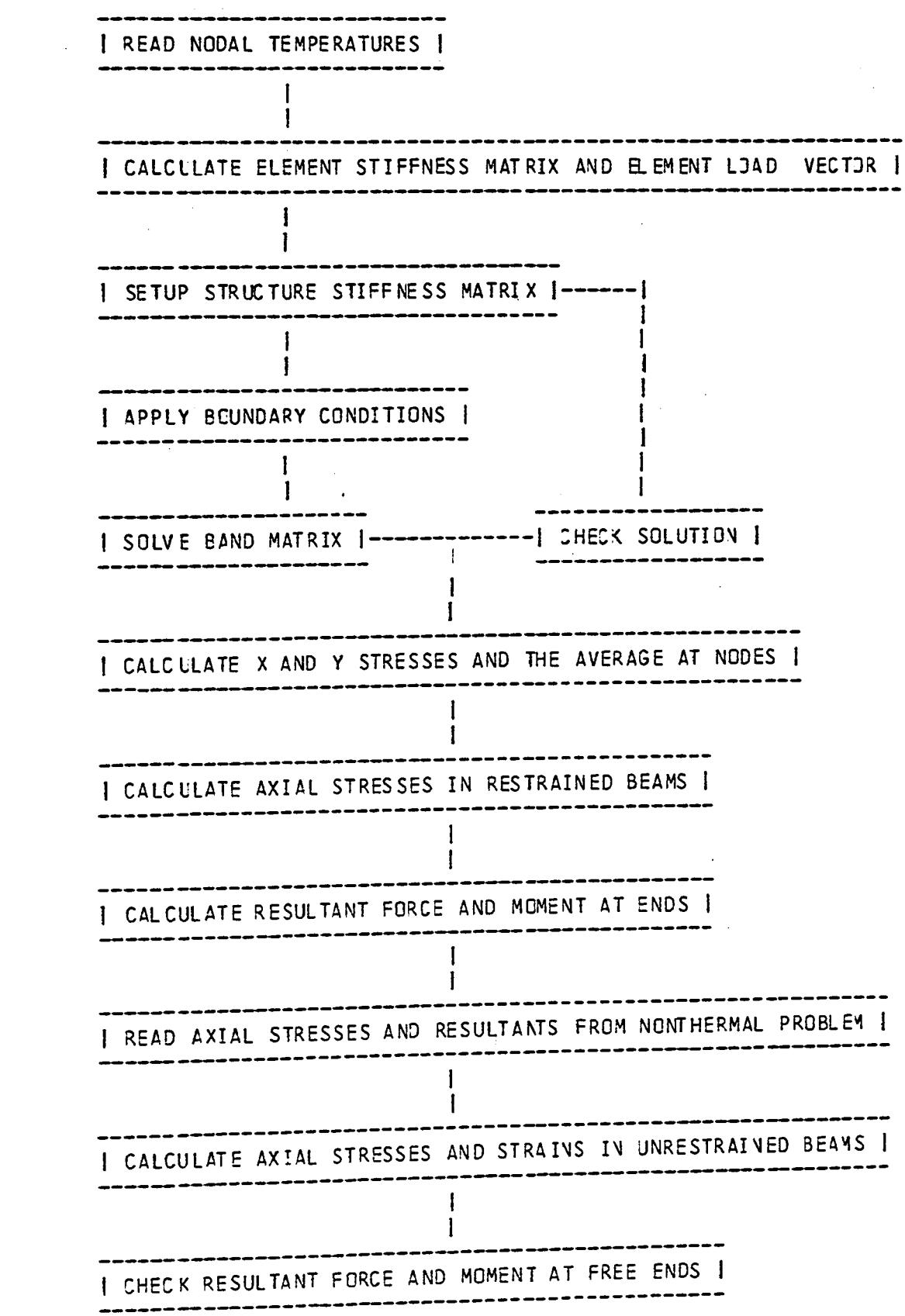

```
      SUBROUTINE LTT(X,Y,CK,SK)

C*****************************************************************
C PURPOSE
C    TO CALCULATE THE STIFFNESS MATRIX SK OF THE LINEAR TEMPERATURE
C    TRIANGULAR ELEMENT WHOSE THERMAL CONDUCTIVITY IS DENOTED BY G.  THE
C    COORDINATES OF THE NODES ARE X,Y .
C*****************************************************************

      IMPLICIT REAL*8(A-H,O-Z)
      DIMENSION T(3,3),SKO(3,3),SK(3,3),X(3),Y(3)
      SR=(X(2)-X(1))**2+(Y(2)-Y(1))**2
      SR=DSQRT(SR)
      AL=((X(2)-X(3))*(X(2)-X(1))+(Y(2)-Y(3))*(Y(2)-Y(1)))/SR
      BL=((X(3)-X(1))*(X(2)-X(1))+(Y(3)-Y(1))*(Y(2)-Y(1)))/SR
      CL=((X(2)-X(1))*(Y(3)-Y(1))-(X(3)-X(1))*(Y(2)-Y(1)))/SR
      DO 5 I=1,3
      DO 5 J=1,3
      SKO(I,J)=0.DO
      T(I,J)=0.DO
      SK(I,J)=0.DO
    5 CONTINUE
      T(1,1)=AL/(AL+BL)
      T(1,2)=BL/(AL+BL)
      T(2,1)=-1.DO/(AL+BL)
      T(2,2)=1.0DO/(AL+BL)
      T(3,1)=-AL/((AL+BL)*CL)
      T(3,2)=-BL/((AL+BL)*CL)
      T(3,3)=1.0DO/CL
      SKO(2,2)=CK*(AL+BL)*CL/2.0DO
      SKO(3,3)=CK*(AL+BL)*CL/2.0DO
      DO 15 I=1,3
      DO 15 J=1,3
      SUM=0.DO
      DO 10 K=1,3
      DO 10 L=1,3
   10 SUM=SUM+T(K,I)*SKO(K,L)*T(L,J)
   15 SK(I,J)=SUM
      RETURN
      END
```

```
      SUBROUTINE SETUP(I,J,K,A,NW,NUBW,B,VL,II,JJ,XL,H)

C.....................................................................
C PURPOSE
C    THE COEFFICIENTS OF THE ELEMENT STIFFNESS MATRIX B HAVING NODES I,
C    J,K ARE PLACED IN ITS LOCATION IN THE STRUCTURE MATRIX A.
C    CONVECTIVE CONDITIONS ARE TAKEN IN ACCOUNT WHEN BOTH II AND JJ ARE
C    NOT EQUAL TO ZERO.  THE SURFACE CONDUCTANCE IS REFERRED TO AS H .
C.....................................................................

      IMPLICIT REAL*8(A-H,O-Z), INTEGER(I-N)
      DIMENSION A(NW,NUBW),B(3,3),VL(NW)
      A(I,1)=A(I,1)+B(1,1)
      IF(I.LT.J) A(I,J-I+1)=A(I,J-I+1)+B(1,2)
      IF(I.LT.K) A(I,K-I+1)=A(I,K-I+1)+B(1,3)
      IF(J.LT.I) A(J,I-J+1)=A(J,I-J+1)+B(2,1)
      A(J,1)=A(J,1)+B(2,2)
      IF(J.LT.K) A(J,K-J+1)=A(J,K-J+1)+B(2,3)
      IF(K.LT.I) A(K,I-K+1)=A(K,I-K+1)+B(3,1)
      IF(K.LT.J) A(K,J-K+1)=A(K,J-K+1)+B(3,2)
      A(K,1)=A(K,1)+B(3,3)
      IF(II.EQ.0 .OR. JJ.EQ.0) GO TO 20
      A(II,1)=A(II,1)+XL*H/3.0D0
      IF(II.LT.JJ) A(II,JJ-II+1)=A(II,JJ-II+1)+XL*H/6.0D0
      A(JJ,1)=A(JJ,1)+XL*H/3.0D0
      IF(JJ.LT.II) A(JJ,II-JJ+1)=A(JJ,II-JJ+1)+XL*H/6.0D0
      VL(II)=VL(II)+XL*H/2.0D0
      VL(JJ)=VL(JJ)+XL*H/2.0D0
   20 CONTINUE
      RETURN
      END
```

```
      SUBROUTINE BSOLVE(A,NW,NUBW,B,C)

C.....................................................................
C PURPOSE
C    TO SOLVE A SYSTEM OF NW LINEAR EQUATIONS USING CHOLESKY'S SQUARE
C    ROOT METHOD.  THE SYMMETRIC COEFFICIENT MATRIX A HAS A HALF BAND
C    WIDTH OF NUBW.  THE KNOWN COLUMN MATRIX AND THE UNKNOWN COLUMN
C    MATRIX ARE DENOTED BY B AND C RESPECTIVELY
C.....................................................................

      IMPLICIT REAL*8(A-H,O-Z), INTEGER(I-N)
      DIMENSION A(NW,NUBW),B(NW),C(NW)
      DO 140 I=1,NW
      L=NW-I+1
      IF(NUBW .LT. L) L=NUBW
      DO 140 J=1,L
      L1=NUBW-J
      IF(L1 .GT. (I-1)) L1=I-1
      SUM=A(I,J)
      IF(L1 .EQ. 0) GO TO 110
      DO 100 K=1,L1
  100 SUM=SUM-A(I-K,1+K)*A(I-K,J+K)
  110 IF(J.EQ.1) GO TO 120
      A(I,J)=SUM*TEMP
      GO TO 140
  120 IF(SUM.GT.0.D0) GO TO 130
      WRITE(3,1) I,J,SUM
    1 FORMAT(1H0,2I3,E25.15,'DIAGONAL COEFF.  IS ZERO OR NEG.')
      GO TO 140
  130 SUM=SUM*100.D0
      TEMP=10.D0/DSQRT(SUM)
      A(I,J)=TEMP
  140 CONTINUE
      DO 150 I=1,NW
      J=I-NUBW+1
      IF((I+1) .LE. NUBW) J=1
      SUM=B(I)
      B(I)=C(I)
      IP1=I-1
      IF( IP1 .EQ. 0 ) GO TO 150
      DO 145 K=J,IP1
  145 SUM=SUM-A(K,I-K+1)*C(K)
  150 C(I)=SUM*A(I,1)
      DO 160 I1=1,NW
      I=NW-I1+1
      J=I+NUBW-1
      IF(J.GT.NW) J=NW
      SUM=C(I)
      IP1=I+1
      DO 155 K=IP1,J
  155 SUM=SUM-A(I,K-I+1)*C(K)
  160 C(I)=SUM*A(I,1)
      RETURN
      END
```

```
      SUBROUTINE LST(X,Y,CEX,EMR,ANU,T,XT,S,AL,BL,CL,SI,CO)

C*****************************************************************
C PURPOSE
C    TO CALCULATE THE STIFFNESS MATRIX FOR A LINEAR STRAIN TRIANGULAR
C    ELEMENT HAVING 6 NODES.  THERMAL LOAD MATRIX XT OF THE ELEMENT ARE
C    COMPUTED AS WELL.  MODULAR RATIO , POISSON'S RATIO, AND COEFFICIENT
C    OF EXPANSION ARE DESIGNATED BY EMR, ANU, CEX RESPECTIVELY.
C    X,Y, ARE THE GLOBAL COORDINATES OF THE NODES AT THE VERTICES.
C*****************************************************************

      IMPLICIT REAL*8(A-H,O-Z), INTEGER(I-N)
      DIMENSION K(3),L(3),M(12),N(12),MP(12),NQ(12),XT(12,3),SKO(12,12),
     1X(3),Y(3),T(12,12),T1(3,3),S(12,12)
      DATA K/0,1,0/,L/0,0,1/,M/0,1,0,2,1,0,0,0,0,0,0,0/,N/0,0,1,0,1,2,0,
     &0,0,0,0,0/,MP/0,0,0,0,0,0,0,1,0,2,1,0/,NQ/0,0,0,0,0,0,0,0,1,0,1,2/
      DO 5 I=1,12
      DO 5 J=1,12
      IF(I.LE.3 .AND. J.LE.3) T1(I,J)=0.0
      IF(J.LE.3) XT(I,J)=0.0
    5 T(I,J)=0.0
      SR=DSQRT((X(2)-X(1))**2+(Y(2)-Y(1))**2)
      AL=((X(2)-X(3))*(X(2)-X(1))+(Y(2)-Y(3))*(Y(2)-Y(1)))/SR
      BL=((X(3)-X(1))*(X(2)-X(1))+(Y(3)-Y(1))*(Y(2)-Y(1)))/SR
      CL=((X(2)-X(1))*(Y(3)-Y(1))-(X(3)-X(1))*(Y(2)-Y(1)))/SR
      CO=(X(2)-X(1))/SR
      SI=(Y(2)-Y(1))/SR
C                                   FORMATION OF ROTATION MATRIX
      SKO(1,1)=CO
      SKO(1,2)=SI
      SKO(2,1)=-SI
      SKO(2,2)=CO
      DO 10 II=2,10,2
      DO 10 I=1,2
      DO 10 J=1,2
   10 SKO(I+II,J+II)=SKO(I,J)
C                  FORMATION OF DISPLACEMENT TRANSFORMATION MATRIX T
      T(1,1)=1.0
      T(1,2)=-BL
      T(1,4)=BL*BL
      T(2,7)=1.0
      T(2,8)=-BL
      T(2,10)=BL*BL
      T(3,1)=1.0
      T(3,2)=AL
      T(3,4)=AL*AL
      T(4,7)=1.0
      T(4,8)=AL
      T(4,10)=AL*AL
      T(5,1)=1.0
      T(5,3)=CL
      T(5,6)=CL*CL
      T(6,7)=1.0
      T(6,9)=CL
      T(6,12)=CL*CL
```

```
      T(7,1)=1.0
      T(7,2)=(AL-BL)/2.0
      T(7,4)=(AL-BL)**2/4.0
      T(8,7)=1.0
      T(8,8)=(AL-BL)/2.0
      T(8,10)=T(7,4)
      T(9,1)=1.0
      T(9,2)=AL/2.0
      T(9,3)=CL/2.0
      T(9,4)=AL*AL/4.0
      T(9,5)=AL*CL/4.0
      T(9,6)=CL*CL/4.0
      T(10,7)=1.0
      T(10,8)=AL/2.0
      T(10,9)=CL/2.0
      T(10,10)=AL*AL/4.0
      T(10,11)=AL*CL/4.0
      T(10,12)=CL*CL/4.0
      T(11,1)=1.0
      T(11,2)=-BL/2.0
      T(11,3)=CL/2.0
      T(11,4)=BL*BL/4.0
      T(11,5)=-CL*BL/4.0
      T(11,6)=CL*CL/4.0
      T(12,7)=1.0
      T(12,8)=-BL/2.0
      T(12,9)=CL/2.0
      T(12,10)=BL*BL/4.0
      T(12,11)=-CL*BL/4.0
      T(12,12)=CL*CL/4.0
C                     FORMATION OF INVERTED TRANSFORMATION MATRIX T1
      T1(1,1)=AL/(AL+BL)
      T1(1,2)=BL/(AL+BL)
      T1(2,1)=-1.0/(AL+BL)
      T1(2,2)=1.0/(AL+BL)
      T1(3,1)=-AL/((AL+BL)*CL)
      T1(3,2)=-BL/((AL+BL)*CL)
      T1(3,3)=1.0/CL
C                          INVERT DISPLACEMENT TRANSFORMATION MATRIX T
      CALL MATINV(T,12)
      DO 15 I=1,12
      DO 15 J=1,12
      SUM=0.0
      DO 14 II=1,12
   14 SUM=SUM+T(I,II)*SKO(II,J)
   15 S(I,J)=SUM
C                                DEVELOPMENT OF THERMAL LOAD MATRIX XT
      DO 30 I=1,12
      DO 30 J=1,3
      IF(M(I).EQ.0) GO TO 20
      MF=K(J)+M(I)-1
      NF=L(J)+N(I)
      IF(MF.LT.0 .OR. NF.LT.0) GO TO 20
C                           CALCULATE THE MODIFIED EULER'S BETA FUNCTION
      CALL FACT(F,MF,NF,AL,BL,CL)
      XT(I,J)=M(I)*F
   20 CONTINUE
```

```
      IF(NQ(I).EQ.0) GO TO 30
      MF=K(J)+MP(I)
      NF=L(J)+NQ(I)-1
      IF(MF.LT.0 .OR. NF.LT.0) GO TO 30
      CALL FACT(F,MF,NF,AL,BL,CL)
      XT(I,J)=XT(I,J)+NQ(I)*F
   30 CONTINUE
      DO 32 I=1,12
      DO 32 J=1,3
      SUM=0.0
      DO 31 II=1,12
      DO 31 JJ=1,3
   31 SUM=SUM+S(II,I)*XT(II,JJ)*T1(JJ,J)
   32 T(I,J)=SUM
      DO 34 I=1,12
      DO 34 J=1,3
   34 XT(I,J)=T(I,J)*EMR*CEX/(1.0-2.0*ANU)
      DO 37 I=1,12
   37 WRITE(3,36) (XT(I,J),J=1,3)
   36 FORMAT(1H0,3E12.6)
C                              DEVELOPMENT OF ELEMENT STFFNESS MATRIX T
      SUM=ANU/(1.0-ANU)
      DO 70 I=1,12
      DO 70 J=1,12
      SKO(I,J)=0.0
      IF(M(I).EQ.0 .OR.M(J).EQ.0) GO TO 40
      MF=M(I)+M(J)-2
      NF=N(I)+N(J)
      IF(MF.LT.0 .OR. NF.LT.0) GO TO 40
      CALL FACT(F,MF,NF,AL,BL,CL)
      SKO(I,J)=M(I)*M(J)*F
   40 CONTINUE
      IF(NQ(I).EQ.0 .OR. NQ(J).EQ.0) GO TO 45
      MF=MP(I)+MP(J)
      NF=NQ(I)+NQ(J)-2
      IF(MF.LT.0 .OR.NF.LT.0) GO TO 45
      CALL FACT(F,MF,NF,AL,BL,CL)
      SKO(I,J)=SKO(I,J)+NQ(I)*NQ(J)*F
   45 CONTINUE
      IF(N(I).EQ.0 .OR.N(J).LT.0) GO TO 50
      MF=M(I)+M(J)
      NF=N(I)+N(J)-2
      IF(MF.LT.0 .OR. NF.LT.0) GO TO 50
      CALL FACT(F,MF,NF,AL,BL,CL)
      SKO(I,J)=SKO(I,J)+(1-SUM)*N(I)*N(J)*F/2.0
   50 CONTINUE
      IF(MP(I).LT.0 .OR. MP(J).LT.0) GO TO 55
      MF=MP(I)+MP(J)-2
      NF=NQ(I)+NQ(J)
      IF(MF.LT.0 .OR.NF.LT.0) GO TO 55
      CALL FACT(F,MF,NF,AL,BL,CL)
      SKO(I,J)=SKO(I,J)+(1-SUM)*MP(I)*MP(J)*F/2.0
   55 MF=M(J)+MP(I)-1
      NF=N(J)+NQ(I)-1
      IF(MF.LT.0 .OR. NF.LT.0) GO TO 60
      CALL FACT(F,MF,NF,AL,BL,CL)
      SKO(I,J)=SKO(I,J)+((1-SUM)*N(J)*MP(I)/2.0+SUM*M(J)*NQ(I))*F
```

```
60 MF=M(I)+MP(J)-1
   NF=N(I)+NQ(J)-1
   IF(MF.LT.0 .OR. NF.LT.0) GO TO 70
   CALL FACT(F,MF,NF,AL,BL,CL)
   SKO(I,J)=SKO(I,J)+((1-SUM)*N(I)*MP(J)/2.0+SJM*M(I)*NQ(J))*F
70 CONTINUE
   DO 85 I=1,12
   DO 85 J=1,12
   SUM=0.0
   DO 80 II=1,12
   DO 80 JJ=1,12
80 SUM=SUM+S(II,I)*SKO(II,JJ)*S(JJ,J)
85 T(I,J)=SUM*EMR*(1.0-ANU)/((1.0-2.0*ANJ)*(1.0+ANU))
   DO 86 I=1,12
86 WRITE(3,72) (T(I,J),J=1,12)
72 FORMAT(1HO,12F10.4)
   RETURN
   END
```

```
   SUBROUTINE FACT(F,MF,NF,AL,BL,CL)
```

```
C.....................................................................
C PURPOSE
C    TO CALCULATE THE MODIFIED EULER'S BETA FUNCTION.  THE TRIANGJLAR
C    DIMENSIONS ARE DENOTED BY AL,BL,CL .
C.....................................................................

   IMPLICIT REAL*8(A-H,O-Z), INTEGER(I-N)
   F=CL**(NF+1)*(AL**(MF+1)-(-BL)**(MF+1))
   J=MF+NF+2
   DO 10 I=1,J
   M=I
   IF(I.GT.MF) M=1
   N=I
   IF(I.GT.NF) N=1
   F=F*M*N/I
10 CONTINUE
   RETURN
   END
```

```
      SUBROUTINE SETUP(IO,A,B,VL,V,NW,NUBW)

C.....................................................................
C PURPOSE
C    COEFFICIENTS OF THE LINEAR STRAIN TRIANGULAR ELEMENT V, WHOSE NODES
C    ARE REFERRED TO AS IO, ARE ASSIGNED TO THE STRUCTURE STIFFNESS
C    MATRIX A.  THE THERMAL LOAD VECTOR VL OF THE STRUCTURE IS ALSO
C    FORMED FROM THE LOAD VECTORS V OF THE ELEMENTS.
C.....................................................................

      DIMENSION A(NW,NUBW),B(12,12),VL(NW),V(12),IO(6)
      DO 10 K=1,6
      DO 10 M=1,2
      MM=K*2-2+M
      I1=2*IO(K)-2+M
      VL(I1)=VL(I1)+V(MM)
      DO 10 L=1,6
      DO 10 N=1,2
      NN=L*2-2+N
      I2=2*IO(L)-2+N
      IF(I1.LE.I2) A(I1,I2-I1+1)=A(I1,I2-I1+1)+B(MM,NN)
   10 CONTINUE
      RETURN
      END
```